Gapless Color Superconductivity

by

Christoforos N. Kouvaris

Submitted to the Department of Physics
in partial fulfillment of the requirements for the degree of

Doctor of Philosophy

at the

MASSACHUSETTS INSTITUTE OF TECHNOLOGY

April 2005 [June 2005]

Author .....

Department of Physics
April 15, 2005

Certified by .....

Krishna Rajagopal
Professor
Thesis Supervisor

Accepted by .....

Thomas Greytak
Chairman, Department Committee on Graduate Students

Gapless Color Superconductivity

by

Christoforos N. Kouvaris

Submitted to the Department of Physics
on April 15, 2005, in partial fulfillment of the
requirements for the degree of
Doctor of Philosophy

Abstract

In this thesis, we propose and investigate the "Gapless Color-Flavor Locked" (gCFL) phase, a possible new phase of dense and cold quark matter. At high enough densities, quarks interact with each other and form pairs similarly to electrons in superconductors. This phenomenon in the case of quark matter is called Color Superconductivity. Color superconducting matter must be electrically and color neutral, because otherwise there are huge energy costs, due to the charges. At asymptotically high densities, equal numbers of up, down, and strange quarks make the system neutral, all the quarks pair, and the quark matter is in the Color-Flavor-Locked phase. At intermediate densities however, the strange quark mass changes the number densities of the quarks and this makes the CFL phase unstable. The gCFL phase emerges as a result of the strange quark mass effect and the neutrality conditions. The gCFL phase has gapless modes and non-zero electron density, unlike CFL. These new properties of gCFL have significant astrophysical implications. The interior of neutron stars might have densities at the regime where gCFL dominates. If this is the case, we argue that gCFL will change significantly the cooling of such a star, keeping it hot, even for late times. Also in this thesis we explore the rest of the phase diagram of neutral quark matter at high density as a function of temperature and strange quark mass. We investigate how zero temperature superconducting phases evolve if we heat the system. We derive the phase diagram of dense quark matter using a Nambu–Jona-Lasinio (NJL) model, that might be a good guide for understanding the QCD phase diagram.

Thesis Supervisor: Krishna Rajagopal
Title: Professor

Acknowledgments

The completion of this thesis would not be possible without the guidance, support, and help of two people. First of all, I would like to thank my advisor and friend Krishna Rajagopal. He was an inspiring figure for me all these five years in MIT. He introduced me to the field of active research, worked closely with me, and patiently answered countless questions. It was an honor for me to be one of his students and I would like to thank him.

The second person I would like to thank is Mark Alford. It was a pleasure to collaborate with him. I have benefitted from his knowledge, and from his experience. I am very grateful for his willingness to patiently discuss with me even the smallest technical detail.

I would like also to thank Frank Wilczek for his valuable comments, and for sparing the time to be a member of my thesis committee. My thanks also goes to Eric Hudson for his kindness to be member of my thesis committee and for carefully reading my thesis.

It was a pleasure to collaborate with Kenji Fukushima. I learned a lot from our discussions and I thank him for that. Furthermore, many thanks go to three physicists that although they are not directly related with this thesis, they taught me a lot of physics. I want to thank Prof. Costas Stassis for his wonderful course in Quantum Mechanics, Prof. Jianwei Qiu who taught me quantum field theory and Dr. Werner Vogelsang for teaching me spin physics.

I am grateful to my friend and officemate Michael Forbes for numerous long physics conversations and his help with computers. Many thanks also to my colleagues Jeff Bowers, Joydip Kundu, Andreas Schmitt, Rishi Sharma and Elena Gubankova.

Thanks go to my friends Lefteris Lidorikis, Theofilos Poutahidis and Costas Konistis for all the pleasant coffee breaks we had, discussing everything but physics.

I wish to thank my parents, Anastasia and Nikolao, and my sister Dimitra for their unconditional love. They support every step of my life. I would like also to thank my uncle Dyonisis and Melina for making my life in Boston easier and pleasant.

Finally, I would like to thank Dora for her love and her support all these years.

Contents

List of Figures

List of Tables

Chapter 1

Introduction

Ancient greek philosophers believed that matter is made of four elements: γαῖα (earth), ὕδωρ (water), ἀήρ (air) and πῦρ (fire). This was the first attempt to answer the question of what matter is made of. Ever since, the same question has intrigued natural scientists for thousands of years. Our understanding of matter has increased dramatically as physics progressed. In the last hundred years both theoretical and experimental developments have brought us closer to an answer of this question.

Nowadays we know that there are four fundamental forces in nature: the strong force (responsible for keeping the nucleus of the atoms bound), the weak force (responsible for the radiation of radioactive elements), the electromagnetic force and the gravitational force. A huge effort has been put in from physicists in order to describe all the fundamental forces in a unified way. Currently, the strong, the weak, and the electromagnetic forces are described by the Standard Model. In this picture, the strong force is of vital importance for our understanding of matter. We know that an atom is composed of a nucleus and electrons. The nucleus is composed of hadrons, which consist of quarks. The strong force is a short range force applied among the quarks and is responsible for keeping the nucleus bound. The modern theory that describes the strong force is called Quantum Chromodynamics (QCD). QCD describes the interactions among quarks mediated by the so-called gluons.

The acceptance of QCD as the proper theory for the description of the strong

interactions was not easy. There was a revolution of experimental discoveries as well as theoretical progress that gave some insight into this difficult problem. Experiments showed that although it is very hard to break the bonds among the quarks in the nucleus, in high energy collisions between hadrons, quarks interact as almost free particles. This is related to the most important feature of QCD, asymptotic freedom [1, 2]. In contrast with all the other forces and everyday experience, the strong coupling gets stronger at large distances, rather than short distances. Equivalently, as the energy of the interaction increases, the coupling of the force decreases. On the other hand if we decrease the energy the strength of the interaction becomes large and this is the reason why the quarks are tightly bound inside hadrons and why free quarks have not been observed so far.

This thesis will focus on the study of QCD at high density and low temperature. It addresses the question of what happens to nuclear matter if it is placed under extreme pressure. Although this is to date impossible to achieve in a laboratory, nature has provided the arena for a study like this. The "physical" laboratory is called neutron stars which are extremely dense and compact objects. They are formed during supernova explosions and have attracted interest from a large community among astrophysicists.

Because dense matter corresponds to high baryon chemical potential μ and the relevant energy is high, we are able to do calculations in high density QCD even at relatively low temperature. Due to asymptotic freedom the coupling in this regime is small and this suggests that perturbative methods can be used. However, this picture of QCD in high density turns out to be incorrect. The reason is that perturbation theory around the naive ground state (free quarks Fermi surfaces) encounters infrared divergences. As a result the naive ground state is not the true ground state of QCD in high density [3–6].

This type of instability has been faced before in the context of solid state physics. Particularly, similar problems were overcome before in the theory of superconductivity. In this case BCS (Bardeen, Cooper and Schrieffer) [7] showed that even weak attractive interactions between the electrons change the ground state drasti-

cally. These attractions are mediated by phonons and as a result the electrons form so-called Cooper pairs and the photons acquire a mass (Meissner effect). The charged excitations obtain energy gaps which are responsible for the removal of the infrared problems of perturbation theory.

In high density QCD, the phenomenon of Color Superconductivity is more complicated because instead of electrons we have quarks coming in different flavors and colors. However, in some sense it is simpler than the electron superconductivity. This is because the attractive channel between the electrons is a complicated force mediated by lattice vibrations (phonons). On the other hand in Color Superconductivity the attractive channel is a direct one gluon exchange antisymmetric in color ($\bar{3}$ channel).

In Section 1.1, we discuss the structure of the phase diagram of QCD. We show which regions can be explored by theory and experiments and how color superconductivity fits in the "big picture". Section 1.2 focuses on color superconductivity at asymptotically high density. In particular we review the basic aspects of the Color-Flavor-Locked phase (CFL). In Section 1.3 we give a preview of what follows in Chapters 2, 3 and 4. We indicate the problems of the CFL phase in lower densities and how a new phase, the Gapless Color-Flavor-Locked (gCFL) phase takes over. In Section 1.4 we mention alternatives to the gapless phase such as Crystalline Superconductivity (LOFF) and spin-1 superconductors.

1.1 Phase Diagram of QCD

In recent years a lot of effort has been devoted to the exploration of the phase diagram of QCD. Figure 1-1 shows the phase diagram of QCD as a function of temperature and baryon chemical potential. The hadronic gas phase lies at low baryonic chemical potential and low temperature. In this regime the coupling is very strong and the quarks are confined inside the hadrons. Let's focus now on the horizontal axis (chemical potential). If we increase the potential there is a first order phase transition between hadron gas and hadron liquid. The first order phase transition terminates at

a second order critical point at a temperature of about 10 MeV [8]. Nuclei are droplets of the hadron liquid phase and therefore lie on the right of the phase transition.

If we increase the chemical potential even more, we enter in the regime of color superconductivity [3–6, 9–15]. In this regime the nuclei have been squeezed together and a description in terms of quark degrees of freedom is needed. Although the phase transition between the hadron liquid phase and the superconducting phases is believed to be first order [5, 6, 16–19], it is very difficult to know exactly what phase takes over from the hadron liquid, because analytical, numerical and experimental methods to date fail to provide us with a reliable answer. It is hard to probe this regime of the phase diagram analytically because of the large coupling constant of the strong force that eliminates perturbative techniques. Similarly, a non-zero chemical potential creates problems for lattice QCD methods (the so called sign problem). Once the chemical potential is non-zero, the fermionic path integral measure is not positive definite due to explicit breaking of time reversal symmetry and the Monte Carlo methods used in lattice fail. Until now, lattice methods are only valid in regimes that have chemical potential much smaller than the temperature [20–22]. Moreover, this region is accessible to experiments only at very low densities (relative to the temperature). In RHIC (Relativistic Heavy Ion Collider) and CERN experiments, heavy ions and/or protons collide at very high energy. The system during the collision is in a high density, but the temperature of the system is much larger than the baryon chemical potential (there is no Fermi surface), and hence it would be extremely difficult, if not impossible, to probe the color superconducting phases. The only information about this part of the phase diagram might come from astrophysical observations. This is because neutron stars have low temperatures compared to their densities. Their temperature should be of the order 10-100 keV. Where exactly neutrons stars lie in the phase diagram is not known. The density of a neutron star varies as a function of its radius and it is still an open question if any part of the star is in a color superconducting phase [23].

At even higher densities the gapless color flavor locked phase (gCFL) takes over [24, 25]. However, as we shall see in Chapters 2 and 3, there is a possibility that

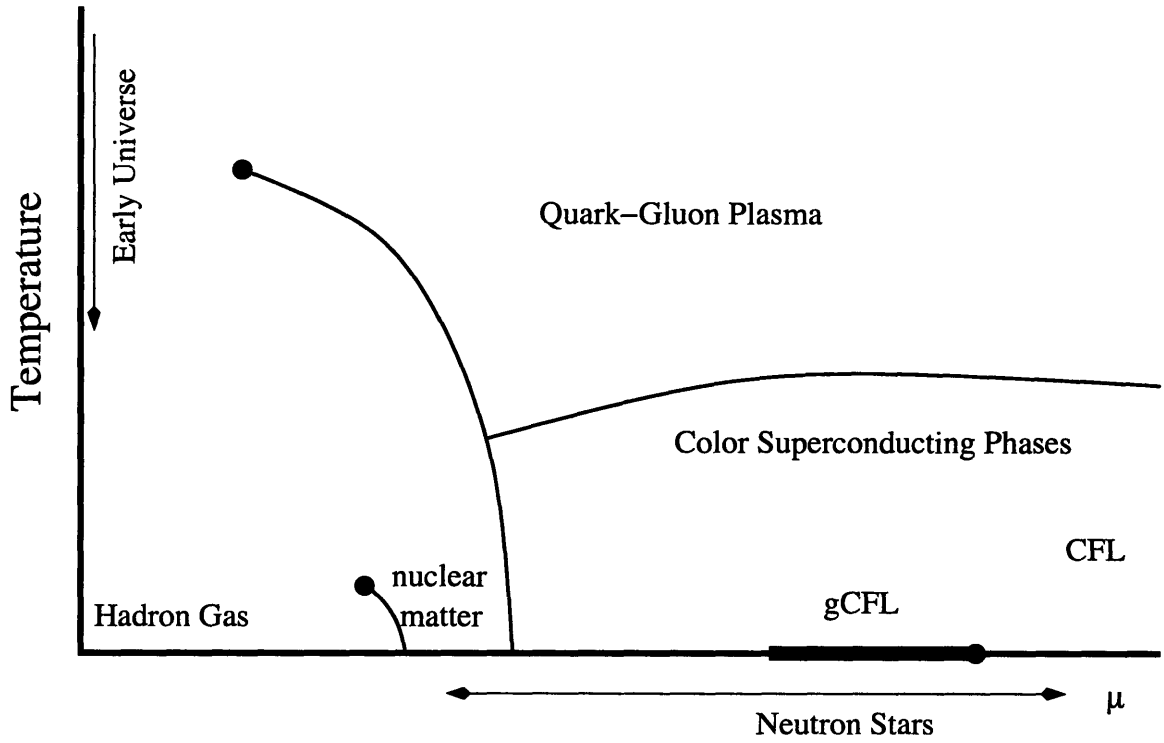

Figure 1-1: Schematic Phase Diagram of QCD: Temperature versus Baryon Chemical Potential μ.

the regime of gCFL may be extended to lower densities and therefore gCFL can be the phase that takes over from the hadronic liquid phase. The gCFL phase, and its astrophysical implications, will be the main subject of study of this thesis. Although perturbative QCD is still not reliable in densities where gCFL appears, analytical calculations with, for example, a Nambu–Jona-Lasinio (NJL) model are possible. At asymptotically high densities, the energetically favored phase is the Color-Flavor-Locked phase (CFL) [10]. The gCFL-CFL transition is a second order phase transition at zero temperature and a smooth cross over for non-zero temperature [26, 27].

Now consider moving along the vertical axis of the phase diagram. We start from the hadron gas phase again but we increase the temperature this time. At very high temperature the quarks are deconfined and form a quark-gluon plasma (QGP) [28–31]. Lattice simulations are applicable in this regime, and it has been shown that the transition between hadron gas and QGP takes place at a temperature of about 170 MeV [32, 33]. For low chemical potential, the transition is a smooth cross over,

but there are indications that at higher chemical potential the transition is of first order ending at a tricritical point [16, 17]. This part of the phase diagram is explored by RHIC. In this experiment heavy nuclei collide with large energies. During the collision the system enters the QGP phase and rapidly thermalizes. As the system expands, the temperature falls, and it re-enters the hadron gas phase. This part of the phase diagram is interesting from the point of view of particle physics and cosmology because the universe was created at very high temperature and as a function of time dropped vertically, going from QGP to the hadron gas phase.

1.2 Color-Flavor-Locked Phase

At asymptotically high densities the QCD coupling $g(\mu)$ is small. The masses of the up, down and strange quarks can be neglected, since they are much smaller than the baryon chemical potential μ. Actually, as we shall show in Chapter 2, the relevant quantity that must be small is $M_s^2/\mu\Delta << 1$, with Δ denoting the gap parameter. We have only three flavors (up, down and strange), because the other three quarks (charm, bottom and top) have very large masses so we can safely ignore them. As we mentioned earlier, in cold quark matter Fermi surfaces are unstable, if there is an attractive channel. In the case of QCD, single gluon exchange in the color antisymmetric $\bar{3}$ channel is attractive. Quarks that live on the Fermi surface can scatter with equal and opposite momenta (back to back) and as a result they can form Cooper pairs. Even if the coupling is arbitrarily weak, the infinite degeneracy of quarks with equal and opposite momenta in the Fermi surface renders the surface unstable to the formation of a condensate of quark Cooper pairs. The quark quasi-particles that interact with the condensate acquire an energy gap and all the gauge bosons that do not break the symmetry of the new ground state obtain effective Meisner masses [11, 34–36].

Since the attractive channel is the $\bar{3}$, we expect the dominant condensate to be antisymmetric in color. There are several renormalization group calculations done in QCD, starting from asymptotically high energies and running to lower energies

towards the Fermi surfaces [37]. Generally speaking, if a coupling goes to infinity before reaching the Fermi surface energy level, it implies that there is an infrared instability and a condensate in this channel is formed.

Although the renormalization group method is an appropriate and sophisticated way to determine possible condensates, it is not very difficult to guess the dominant condensate at high density with simple physical arguments. From the analysis above we expect the condensate to be antisymmetric in color. The diquark condensate is forced to be antisymmetric according to Pauli's principle. The above reasoning leaves us with two possibilities. We can have a condensate either antisymmetric in flavor and spin, or symmetric in flavor and spin. The latter case corresponds to a condensate with spin-1 and thus it breaks the rotational invariance. Heuristically, the favored ground state is the one that leaves a maximal symmetry group of the ground state. A zero spin condensate allows quarks from the whole Fermi surface to pair and therefore this condensate should be more favored. Finally, instantons favor a condensate that does not violate parity invariance. Using these simple arguments, we can write down the condensate

$$\langle \psi_a^\alpha C\gamma_5 \psi_b^\beta \rangle \sim \Delta_1 \epsilon^{\alpha\beta 1}\epsilon_{ab1} + \Delta_2 \epsilon^{\alpha\beta 2}\epsilon_{ab2} + \Delta_3 \epsilon^{\alpha\beta 3}\epsilon_{ab3} \tag{1.1}$$

The greek indices are color indices while the latin indices denote flavor. At asymptotically high density the three flavors (up, down and strange) are on equal footing and therefore $\Delta_1 = \Delta_2 = \Delta_3$. From the Lèvi-Civitá symbols it is easy to justify the name of the CFL phase. We can rewrite the symbols as

$$\epsilon^{\alpha\beta\Gamma}\epsilon_{ab\Gamma} = \delta_a^\alpha \delta_b^\beta - \delta_b^\alpha \delta_a^\beta \tag{1.2}$$

In this form it is apparent that flavor and color rotations are locked, because the Kronecker delta functions link color and flavor indices. These condensates transform nontrivially under separate color and flavor transformations. Neither color transformations nor flavor transformations separately are valid symmetries of the ground state. However, the delta functions do remain invariant if we simultaneously rotate

both color and flavor. Thus these symmetries are locked together. We can also see that a condensate like this corresponds to a phase with the lowest free energy because it allows pairing among all nine quarks, so the energy benefit from the formation of Cooper pairs is maximal [10]. However this is not the only condensate; it has been proven that the $\bar{3}$ channel induces a non-zero condensate in the color 6 channel. This channel is repulsive and does not break any new symmetry. Therefore, it is very small compared to the dominant $\bar{3}$ [38].

The type of condensate (1.1) is not new to physics. In the B phase of He_3, the ground state is not invariant under rotations of the spin or the orbital angular momentum. However, it is invariant under simultaneous rotations of spin and orbital angular momentum. In other words, spin and orbital angular momenta are locked. In the particle physics context, electroweak theory is another example of the same phenomenon. In this case, the Higgs bosons ϕ^a acquires a non zero vacuum expectation value $\langle \phi^a \rangle = u\delta_1^a$ and condenses, breaking spontaneously the original symmetry of the Lagrangian. The ground state is not invariant under $SU(2)$ and $U(1)$ hypercharge rotations separately. It is invariant under locked rotations, which represent rotations of the $U(1)$ electromagnetism. The example with the most striking similarity is chiral symmetry breaking in the QCD vacuum. The chiral group breaks spontaneously to a diagonal group where left and right rotations are locked. The Goldstone bosons of the theory are the pions, the kaons, and the η particles.

The symmetry breaking pattern in CFL is:

$$SU(3)_L \times SU(3)_R \times SU(3)_c \times U(1)_B \rightarrow SU(3)_{L+R+c} \times Z_2 \qquad (1.3)$$

Two condensates are formed, one involving left handed quarks and the other involving right handed quarks. In the first condensate left rotations are locked with color rotations and in the second condensate right rotations are locked with color rotations. This means that the ground state is invariant under simultaneous rotations of left, right and color. This is the meaning of the subscript $(L + R + c)$. The discrete group Z_2 just states the fact that the condensate is invariant if both quark fields

are multiplied by -1. The initial chiral, color and baryon group breaks down spontaneously to a diagonal $SU(3)$, where left, and color rotations as well as right and color rotations are locked. In addition the baryon number group is also spontaneously broken. This might seem strange, but it has been encountered in superfluidity where the atom number group is broken and superconductivity where the lepton number group is broken. This broken quantum symmetry has to do with the easy transport of quantum numbers inside the sample of superconducting matter. As in the vacuum, the $U(1)_A$ axial symmetry is explicitly broken by instantons. The instanton interaction is represented by a 6-fermion interaction in three flavor QCD. In high density a 6-fermion interaction is irrelevant as we approach the Fermi surface, suggesting that the instantons are suppressed. Practically, the η' is not going to be a massless Goldstone boson, but due to the smallness of the instanton contribution, the η' will be very light.

Consider now the spectrum of the CFL phase. What we have to remember is that the spontaneous symmetry breaking of a global symmetry gives rise to Goldstone bosons, but for a gauge symmetry that breaks down, the Goldstone bosons are "eaten", giving mass to the gauge bosons. This is the Higgs-Anderson mechanism. From (1.3) we can count the initial number of generators. In total we have 25 generators (16 for the chiral group, 8 for the color group and 1 for the $U(1)_B$). The CFL ground state has 8 unbroken generators (coming from the diagonal $SU(3)$ group). That means that we have 17 degrees of freedom. Eight of them are "eaten" by the gluons giving mass to them [10]. To be more accurate, there is one linear combination of a gluon and the photon that remains massless, whereas the 8 orthogonal combinations are massive. We shall talk about this in the next paragraph. The other 9 degrees of freedom correspond to the 8 Goldstone bosons: pions, kaons, and η. The CFL condensate may rotate within the manifold describing these mesons [39–41] and the true ground state might include condensed bosons. The superfluidity mode is due to the $U(1)_B$ spontaneous symmetry breaking and it remains massless even once quark masses are taken into account. Therefore this Goldstone boson plays a crucial role in many low energy properties of the CFL phase, for example in its viscosity

[42, 43], specific heat and neutrino opacity.

Now we return to the question of the massless gauge boson. The $U(1)_{EM}$ electromagnetism is a subgroup of the chiral $SU(3)_L \times SU(3)_R$, that is gauged. After the symmetry breaking there is a subgroup that respects the symmetry of the condensate and includes the generator of electromagnetism. Apparently, electromagnetism is spontaneously broken. This is because if we perform a $U(1)_{EM}$ rotation, the condensate does not remain invariant. We can see that the condensate has pairs between up and down as well as between down and strange. These two combinations have different overall electric charge. We can find what combination of electric and color charges is preserved by the condensate. It is the $\tilde{Q} = Q + T$, where Q is the electric charge and T is a color charge,

$$Q = diag(\frac{2}{3}, -\frac{1}{3}, -\frac{1}{3}) \quad \text{in flavor u, d, s space,} \tag{1.4}$$

$$T = diag(-\frac{2}{3}, \frac{1}{3}, \frac{1}{3}) \quad \text{in color r, g, b space.} \tag{1.5}$$

The $\tilde{Q}$ charge of all the Cooper pairs of the condensate is zero by construction. This means that $\tilde{Q}$ acting on the ground state gives zero. So, there is a a $U(1)_{\tilde{Q}}$ symmetry that leaves the ground state invariant, and thus this symmetry is unbroken. The gauge boson $A_{\tilde{Q}}$ that corresponds to this symmetry is massless. We can find the massless boson by considering the covariant derivative of the condensate

$$D_\mu \langle q_a^\alpha q_b^\beta \rangle = (\partial_\mu + eQA_\mu + gTG_\mu)\langle q_a^\alpha q_b^\beta \rangle, \tag{1.6}$$

where A_μ and G_μ are the photon and the relevant gluon. If we expand the kinetic term $|D\langle q_a^\alpha q_b^\beta \rangle|^2$ we can find the massive and massless bosons. The two bosons are the massive

$$A_\mu^X = \frac{-\eta e A_\mu + gG_\mu}{\sqrt{\eta^2 e^2 + g^2}} = -\sin\alpha_0 A_\mu + \cos\alpha_0 G_\mu, \tag{1.7}$$

and the massless

$$A_\mu^{\tilde{Q}} = \frac{gA_\mu + \eta e G_\mu}{\sqrt{\eta^2 e^2 + g^2}} = \cos\alpha_0 A_\mu + \sin\alpha_0 G_\mu. \tag{1.8}$$

This is analogous to the electroweak symmetry breaking where the $SU(2) \times U(1)_Y$ breaks spontaneously to the $U(1)_{EM}$. The photon remains massless and is a linear combination of the hypercharge boson and the W^3 boson, whereas the orthogonal combination corresponds to the massive Z particle. In this analogy, the Weinberg angle that denotes the mixing between the W^3 and Y is the analogue of the α_0 in CFL, that denotes the mixing between the gluon and the photon.

So far we mentioned only the renormalization group methods for doing calculations in color superconductivity. There are also other methods such as variational and diagrammatic [34]. Without trying to present them in detail,we shall mention the very basic principles. In the variational methods, first used in [7], we try to guess the ground state, meaning that we attempt to construct the wavefunction of the ground state and minimize the free energy with respect to the parameters of our model. This has been done successfully in the 2SC phase where the strange quark is ignored due to its large mass and there is pairing only between up and down quarks. The ground state is described by a wavefunction of quarks that fill the Fermi surface and Cooper pairs with equal and opposite momenta. The minimization of the free energy determines how many Cooper pairs we have. The diagrammatic method is in a sense a different form of the variational method. It was originally suggested by Bogoliubov [44] and Valatin [45] in a different context of physics and it involves making a mean-field theory ansatz for the form of the condensate with appropriate symmetries. The Hamiltonian is rewritten in a way that its dependence on the ansatz parameters is manifest, and finally from the minimization of the free energy, we obtain and solve a self-consistent gap equation for the free parameters of the ansatz. This approach is usually easier to implement technically when the ansatz is complicated, but it is not as transparent as the variational method. This is the method that we use in the calculations presented in Chapters 2 and 3.

1.3 Gapless Color-Flavor-Locked Phase

So far we discussed what happens in the case of asymptotically high density quark matter. However, neutron stars may or may not be at high enough densities to contain CFL matter. Therefore a very fundamental question that the reader might ask is what happens if we reduce the density. The first problem that we encounter is that it is not possible to rely on QCD weak coupling techniques. Once we start reducing the density, the quarks of the Fermi surface have energies that correspond to a coupling $g(\mu)$ close to one or larger than one, and it is meaningless to use weak coupling expansion. The other problem we face is that the mass of the strange quark becomes important. Although the masses of the up and down quarks can still be ignored since they are a few MeVs, the strange quark has a mass that should be around 90-150 MeV. At intermedate densities with a baryon chemical potential of order 500 MeV, having a strange quark mass M_s of order 150 MeV suggests that we cannot ignore the effect of M_s. As M_s is much larger than the masses of up and down quarks, it becomes more difficult to make strange quarks comparable to up and down. On the other hand, the electric charges of up, down and strange sum up to zero. If we want to have overall electric neutrality in the bulk matter, the net electric charge coming from the quarks and the electrons has to be zero.

It is instructive to talk first about what happens in the unpaired quark matter. At asymptotically high density, the masses of all the three quarks are negligible. Their number densities are the same and by having equal numbers of up, down and strange quarks we preserve electric neutrality and therefore there is no need for electrons. At intermediate densities however, we have fewer strange quarks, due to their large mass. In order to balance the excess positive charge coming from the up quarks, we need a non-zero electron density. The chemical potentials for the quarks are

$$\mu_u = \mu + \frac{2}{3}\mu_e, \qquad \mu_d = \mu_s = \mu - \frac{1}{3}\mu_e \tag{1.9}$$

where μ_e is the electron chemical potential having assumed weak equilibration. The

corresponding Fermi momenta are

$$p_F^{u,d,e} = \mu_{u,d,e}, \qquad p_F^s = \sqrt{\mu_s^2 - M_s^2}. \tag{1.10}$$

The number densities of the quarks and the electron is given by

$$N_{u,d} = \frac{1}{\pi^2}\mu_{u,d}^3, \qquad N_s = \frac{1}{\pi^2}(\mu_s^2 - M_s^2)^{3/2}, \qquad N_e = \frac{1}{3\pi^2}\mu_e^3. \tag{1.11}$$

Now we can impose electric neutrality. This means that the sum of all the charges should be zero

$$\frac{2}{3}N_u - \frac{1}{3}N_d - \frac{1}{3}N_s - N_e = 0. \tag{1.12}$$

If we combine the last two equations and expand to leading order in M_s, we can see that in order to have neutral matter on should have non-zero electron density with a $\mu_e = M_s^2/(4\mu)$. Finally we can rewrite the Fermi momenta of the quarks as

$$\begin{aligned} p_F^u &= \mu - \frac{M_s^2}{6\mu} \\ p_F^d &= \mu + \frac{M_s^2}{12\mu} = p_F^u + \frac{M_s^2}{4\mu} \\ p_F^s &= \mu - \frac{5M_s^2}{12\mu} = p_F^u - \frac{M_s^2}{4\mu}. \end{aligned} \tag{1.13}$$

Figure 1-2 shows the Fermi momenta of the quarks and the electrons as a function of M_s. The separation between up, down and strange is equidistant to leading order and equal to $M_s^2/4\mu$. As we increase M_s or equivalently as we decrease μ the split among the Fermi surfaces of the quarks becomes larger.

Now let's consider color superconducting matter. Again at asymptotically high densities, where we have CFL matter, the number densities of the three quarks are the same, since they are on an equal footing. As we reduce the density, or equivalently as we go to non-zero M_s, the main danger for the BCS pairing is to have quarks with different Fermi surfaces. As we explained previously, the Cooper pairs come from the degeneracy of quarks on the Fermi surface that scatter back to back with equal and

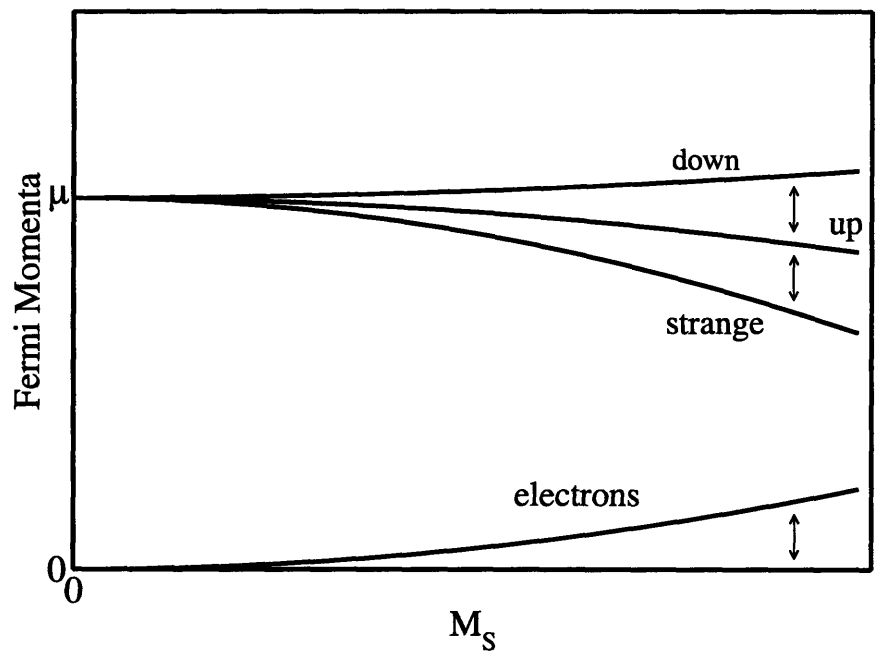

Figure 1-2: The Fermi momenta of the electrons and of the up, down and strange quarks, as a function of M_s, in electrically neutral unpaired quark matter.

opposite momenta. A non-zero M_s lowers the Fermi surface of the strange quarks, making it hard for the Cooper pairs to exist [46]. In the CFL we have pairings among ru-gd-bs, bu-rs, gs-bd and rd-gu, where the first letter denotes color and the second flavor. The pairing between rd-gu is not affected by the strange quark mass and therefore there are more red and green quarks, than blue. In order to maintain color neutrality, a negative μ_8 is needed, where μ_8 is a color electrostatic chemical potential coupled to the color charge $T_8 = diag(1, 1, -2)/3$ (in color space: red, green, blue) of the $SU(3)$ gauge group. This μ_8 decreases the difference between the Fermi surfaces of gs and bd as well of bu and rs, making the pairing more favorable. However, as we shall explain extensively in Chapter 2, this cannot continue for arbitrarily large values of M_s. There is a simple argument to see why CFL breaks down in lower densities. Consider the gs-bd pair. We shall see in Chapter 2 that at non-zero M_s the difference in their Fermi surfaces is $p_{bd} - p_{gs} = M_s^2/\mu$. A Cooper pair lowers the free energy of the system by 2Δ, where Δ is the energy gap. As long as 2Δ is larger than M_s^2/μ, the system can always give energy M_s^2/μ to a gs quark in order to be able to pair with a

bd and lowers the free energy by 2Δ. Therefore we expect that when $M_s^2/\mu > 2\Delta$, the BCS pairing is not energetically favored. This is exactly what we have found using an NJL model analysis. If we exceed the critical value of the inequality, we have a new phase at zero temperature, the Gapless Color-Flavor-Locked phase (gCFL).

The unique properties of this phase will be explored in the following chapters and will be the main focus of this thesis. The most important difference between CFL and gCFL is that in gCFL (unlike CFL) there are gapless dispersion relations. This has significant consequences for the phenomenological properties of the gCFL matter. In addition, a non-zero electron density makes the gCFL a conductor unlike CFL which is a insulator. In both the CFL phase and the gCFL phase, once we take into account the explicit breaking introduced by the strange quark mass and electromagnetism, the unbroken symmetry is reduced from the diagonal $SU(3)_{L+R+c}$ to $U(1)_{\tilde{Q}} \times U(1)$ [47]. The last $U(1)$ corresponds to "color + flavor hypercharge" and may be spontaneously broken by meson condensation [41]. The gapless CFL phase has the same symmetry as the CFL phase, and it will therefore be interesting to investigate the possibility of meson condensation in the gCFL phase. The effective theory for the Goldstone bosons alone will have the same form as in the CFL phase, albeit with new contributions to their masses coming from the differences between the values of the three Δ_i^2. And, furthermore, the gapless quasiparticles must be included in the low energy effective theory.

1.4 Phases at Lower Densities

From asymptotically high density, if we start reducing the chemical potential we go from CFL to gCFL. If we continue lowering the chemical potential, the strange quark mass separates the Fermi surfaces even further. There are several interesting possibilities of pairing in this case, provided the hadronic phase has not taken over. Until now, there is no definite answer about what exactly happens in this regime. This is because we are far from the regime where QCD perturbative techniques are applicable.

There are two most probable scenarios at lower densities. The first one is a spin-1 superconductor and the second is crystalline superconductivity (LOFF). Although we are not going to analyze these possibilities in this thesis, we shall mention their basic principles. As we decrease the chemical potential, M_s becomes more and more important. The effect of M_s is to split the Fermi surfaces of the different flavor quarks. If the difference of the Fermi surfaces is large, the only option of conventional pairing is to have Cooper pairs of the same flavor. The condensate is symmetric in flavor and antisymmetric in color because the attractive channel is the $\bar{3}$. This means that the condensate should be symmetric in spin. The condensate has spin one and therefore breaks rotational and Lorentz invariance. The relevant spin-1 condensates have been studied extensively [9, 48–53]. The phase with the lowest free energy among the spin-1 superconductors is the Color-Spin-Locked (CSL) phase [50]. Similarly to CFL, the CSL condensate locks the rotations of spin and color. The symmetry breaking pattern of CSL phase is

$$SU(3)_{color} \times SO(3)_J \to SO(3)_{color+J} \tag{1.14}$$

Weak coupling calculations showed that the gaps are of the order of keV, extrapolating to lower densities. The gaps are much smaller than the ones of the CFL phase.

The second possibility for lower densities is to have a LOFF phase. The crystalline phase (LOFF) was first proposed by Larkin, Ovchinnikov, Fulde and Ferrell as a mechanism for electron pairing in suprconductors with a Zeeman splitting between spin-up and spin-down Fermi surfaces [54, 55]. The idea of the LOFF phase is that when there is a mismatch in the Fermi surfaces, Cooper pairs may have non-zero total momentum. We mentioned that in BCS the Cooper pairs have zero total momentum and are formed from back-to-back scattering between quarks on the Fermi surface. However, in LOFF there is pairing between a quark with momentum p and a quark with momentum $-p+2q$. The direction of the momentum q is chosen spontaneously, and its magnitude has to be equal to the mismatch of the two Fermi surfaces. Of course it is expected that such a pairing cannot exploit the whole Fermi surface,

but has a restricted phase space. The pairing is forbidden in the so-called "blocking regions" and it exists only in ring type regions. Since the LOFF Cooper pairs have non-zero total momentum, we expect that the condensate varies in space like a plane wave

$$\langle \psi(x)\psi(x) \rangle \ \Delta e^{2iqx}. \tag{1.15}$$

Rotational symmetry is broken because we choose a direction for the momentum q. In addition translational invariance is also broken because of the space dependence of the condensate. Crystalline color superconductivity has been studied in simplified models with pairing between two quarks species whose Fermi momenta are pushed apart by a chemical potential difference or a mass difference [56–59]. A LOFF condensate does not have to be a monochromatic plane wave as in the last equation, but in the more general case, it could be a superposition of single plane waves with different $q's$. This has been investigated within the Landau-Ginzburg approximation in [60]. At this point only two flavor LOFF models have been studied. A three flavor LOFF phase remains to be constructed and compared with the other phases.

In Chapter 2, which follows Refs. [24, 25, 61], we analyze gCFL at length.We study the disruption of the CFL phase at intermediate densities due to the strange quark mass and how as a result of this, gCFL emerges. In Chapter 2 we work strictly at zero temperature, treating the effect of the strange quark mass as a shift in the chemical potential. We study extensively the most important properties of the gCFL phase: the non-zero electron density and the gapless modes. We also explain why the gapless modes appear naturally, once we impose neutrality. We compare the free energy of the gCFL phase with that of other phases (homogeneous and mixed) and we argue that gCFL is a strong candidate for moderate densities.

In Chapter 3, which follows Ref. [26], we derive a schematic phase diagram of dense matter, using the same model as in Chapter 2 (NJL). However in this chapter we allow the temperature to be non-zero and we do not make the chemical potential shift approximation for the strange quark mass effect. We find several superconducting phases as a function of the chemical potential and the temperature, and describe the

way they are connected in the phase diagram. In addition, we show how calculations done near the critical temperature at high densities, within the Ginzburg-Landau approximation, are consistent with our phase diagram.

In Chapter 4, which follows Ref. [62], we analyze probably the most important astrophysical implication of the gCFL phase. We show that if gCFL matter is present in the interior of a neutron star, it changes significantly the heat capacity and the neutrino emissivity of the star. We present how a toy star with gCFL matter cools and we argue that the effect of gCFL matter is to keep an old star warm, contrary to all other models of stars with quark matter. Therefore at the end of this thesis, we propose a unique and potentially observable signature of gCFL quark matter.

Chapter 2

Gapless Color-Flavor Locked Phase

2.1 Introduction

As mentioned in Chapter 1, we expect that matter at sufficiently high densities and/or temperatures will consist of almost-free quarks and gluons. However, over the last few years it has become clear that there is a rich and varied landscape of phases lying between these asymptotic regimes and the familiar hadronic phase at low temperature and density. In the region where the temperature is low and the density is high enough that hadrons are crushed into quark matter, there is a whole family of "color superconducting" phases [34–36, 63, 64]. The essence of color superconductivity is quark pairing, driven by the BCS mechanism, which operates when there exists an attractive interaction between fermions at a Fermi surface. The QCD quark-quark interaction is strong, and is attractive in many channels, so we expect cold dense quark matter to *generically* exhibit color superconductivity. Moreover, quarks, unlike electrons, have color and flavor as well as spin degrees of freedom, so many different patterns of pairing are possible. This leads us to expect a rich phase structure in matter beyond nuclear density.

In the previous chapter we argued that at asymptotic densities, where the up, down and strange quarks can be treated on an equal footing and the potentially disruptive strange quark mass can be neglected, quark matter is in the color-flavor locked (CFL) phase, in which quarks of all three colors and all three flavors form

Cooper pairs [10]. However, just as RHIC is teaching us about the properties of the hot but far from asymptotically hot quark-gluon plasma [65–68] we should expect that if neutron star cores are made of color superconducting quark matter, they may not reach the densities at which CFL predominates. In this chapter, we study the form of color superconducting quark matter that is the "next phase down in density". We begin in the CFL phase at asymptotic density, imagine reducing the density, and assume that CFL pairing is disrupted by the heaviness of the strange quark before color superconducting quark matter is superseded by the hadronic phase. Upon making this assumption, we ask what form the disruption takes and what are the properties of the resulting phase of dense, but not asymptotically dense, matter.

To describe quark matter as may exist in the cores of compact stars, we consider quark chemical potentials μ of order 500 MeV at most. The strange quark mass M_s must then be included: it is expected to be density dependent, lying between the current mass $\sim$ 100 MeV and the vacuum constituent quark mass $\sim$ 500 MeV. In bulk matter, as is relevant for compact stars where we are interested in kilometer-scale volumes, we must furthermore require electromagnetic and color neutrality [46, 69] (possibly via mixing of oppositely-charged phases) and allow for equilibration under the weak interaction. All these factors work to pull apart the Fermi momenta of the different quark species, imposing an energy cost on the cross-species pairing that characterizes color-flavor locking. At the highest densities we expect CFL pairing, but as the density decreases the combination of nonzero M_s and the constraints of neutrality put greater and greater stress on cross-species pairing, and we expect transitions to other pairing patterns.

In this chapter we study the first of these transitions, and work exclusively at zero temperature, which is a reasonable approximation in the interior of a neutron star that is more than a few seconds old. Nonzero temperature adds interesting new facets to the analysis. This will be the main scope of Chapter 3. We argue that the CFL phase will first give way, via a continuous phase transition, to a new phase with gapless fermions that we call gapless CFL (gCFL) [24, 25, 61]. The transition occurs when $M_s^2/\mu \simeq 2\Delta$, where Δ is the pairing gap parameter. We shall show that the

gCFL phase has two gapless modes and nonzero electron density. Although it has the same symmetries as the CFL phase, gapless CFL matter is a conductor whereas CFL quark matter is a dielectric insulator.

2.1.1 (Gapless) CFL Pairing Ansatz

To study the response of the CFL phase to a non-negligible strange quark mass, we use the pairing ansatz (1.1)

$$\langle \psi_a^\alpha C\gamma_5 \psi_b^\beta \rangle \sim \Delta_1 \epsilon^{\alpha\beta 1}\epsilon_{ab1} + \Delta_2 \epsilon^{\alpha\beta 2}\epsilon_{ab2} + \Delta_3 \epsilon^{\alpha\beta 3}\epsilon_{ab3} \tag{2.1}$$

Here ψ_a^α is a quark of color $\alpha = (r, g, b)$ and flavor $a = (u, d, s)$; the condensate is a Lorentz scalar, antisymmetric in Dirac indices, antisymmetric in color (the channel with the strongest attraction between quarks), and consequently antisymmetric in flavor. The gap parameters Δ_1, Δ_2 and Δ_3 describe down-strange, up-strange and up-down Cooper pairs, respectively. They describe a 9×9 matrix in color-flavor space that, in the basis $(ru, gd, bs, rd, gu, rs, bu, gs, bd)$, takes the form

$$\mathbf{\Delta} = \begin{pmatrix} 0 & \Delta_3 & \Delta_2 & 0 & 0 & 0 & 0 & 0 & 0 \\ \Delta_3 & 0 & \Delta_1 & 0 & 0 & 0 & 0 & 0 & 0 \\ \Delta_2 & \Delta_1 & 0 & 0 & 0 & 0 & 0 & 0 & 0 \\ 0 & 0 & 0 & 0 & -\Delta_3 & 0 & 0 & 0 & 0 \\ 0 & 0 & 0 & -\Delta_3 & 0 & 0 & 0 & 0 & 0 \\ 0 & 0 & 0 & 0 & 0 & 0 & -\Delta_2 & 0 & 0 \\ 0 & 0 & 0 & 0 & 0 & -\Delta_2 & 0 & 0 & 0 \\ 0 & 0 & 0 & 0 & 0 & 0 & 0 & 0 & -\Delta_1 \\ 0 & 0 & 0 & 0 & 0 & 0 & 0 & -\Delta_1 & 0 \end{pmatrix} \tag{2.2}$$

We see that (rd, gu), (bu, rs) and (gs, bd) quarks pair with gap parameters Δ_1, Δ_2 and Δ_3 respectively, while the (ru, gd, bs) quarks pair among each other involving all the Δ's. The most important physics that we are leaving out by making this ansatz is pairing in which the Cooper pairs are symmetric in color, and therefore also in

flavor. Diquark condensates of this form break no new symmetries, and therefore *must* arise in the CFL phase [10, 38]. However because the QCD interaction is repulsive between quarks that are symmetric in color, these condensates are numerically insignificant [10, 27, 38]. To find which phases occur in realistic quark matter, we must take into account the strange quark mass and equilibration under the weak interaction, and impose neutrality under the color and electromagnetic gauge symmetries. The arguments that favor (2.1) are unaffected by these considerations, but there is no reason for the gap parameters to be equal once $M_s \neq 0$. Much previous work [38, 46, 70–73] compared color-flavor-locked (CFL) phase (favored in the limit $M_s \to 0$ or $\mu \to \infty$), the two-flavor (2SC) phase (favored in the limit $M_s \to \infty$), and unpaired quark matter. We shall give a model-independent argument in Section 2.1.3, however, that when the CFL phase is disrupted, it cannot give way to either 2SC or unpaired quark matter. Above a critical M_s^2/μ, we shall show that the CFL phase is replaced by a new gapless CFL (gCFL) phase, not by 2SC quark matter. The defining (and eponymous) properties of the gapless CFL phase arise in its dispersion relations, not in its pattern of gap parameters. However, it is useful for orientation to list the patterns of gap parameters for all the phases we shall discuss:

$$\Delta_3 \simeq \Delta_2 = \Delta_1 = \Delta_{CFL} \qquad \text{CFL} \tag{2.3}$$

$$\Delta_3 > 0, \quad \Delta_1 = \Delta_2 = 0 \qquad \text{(gapless) 2SC} \tag{2.4}$$

$$\Delta_2 > 0, \quad \Delta_1 = \Delta_3 = 0 \qquad \text{2SCus} \tag{2.5}$$

$$\Delta_3 > \Delta_2 > \Delta_1 > 0 \qquad \text{gapless CFL .} \tag{2.6}$$

The 2SCus phase, which was introduced in Ref. [46], must be analyzed for completeness because it and the 2SC phase have the same free energy when $M_s = 0$, and to leading order in M_s if their respective nonzero gap parameters have the same value [46]. However, we shall show in Section 2.3.4 that the 2SCus phase is never favored, and never gapless.

In the remainder of this chapter we construct the free energies and solve the gap equations for the CFL, gapless CFL, 2SC, gapless 2SC [74, 75], and 2SCus phases

in an NJL model. We show in detail how the CFL→gCFL transition occurs and detail the properties of the gCFL phase. The gCFL phase is a $\tilde{Q}$-conductor with a nonzero electron density, and these electrons and the gapless quark quasiparticles make the low energy effective theory of the gapless CFL phase and, consequently, its astrophysical properties qualitatively different from that of the CFL phase, even though its $U(1)$ symmetries are the same. Both gapless quasiparticles have quadratic dispersion relations at the quantum critical point. For values of M_s^2/μ above the quantum critical point, one branch has conventional linear dispersion relations while the other branch remains quadratic, up to tiny corrections. In order to evaluate the range of M_s^2/μ above the critical point within which the gCFL phase remains favored, we construct the 2SC and 2SCus phases and reproduce the 2SC→g2SC transition of Refs.[74, 75], here in neutral 3-flavor quark matter, and show that in this context gCFL has a lower free energy than (g)2SC(us). We do not complete the study of mixed phase alternatives, but we do eliminate all the most straightforward possibilities everywhere in the gCFL regime in M_s^2/μ except very close to its upper end, where gCFL, g2SC and unpaired quark matter have comparable free energies. At such large values of M_s^2/μ, however, our pairing ansatz is not sufficiently general to describe all the possibilities, as we discuss in the concluding section of this chapter. Before turning to the model analysis, which we detail in Section 2.2 and whose results we present in Section 2.3, we conclude this introduction with a model-independent discussion of color and electric neutrality in QCD and with the model-independent argument of Ref. [24].

2.1.2 Color and Electric Neutrality in QCD

Stable bulk matter must be neutral under all gauged charges, whether they are spontaneously broken or not. Otherwise, the net charge density would create large electric fields, making the energy non-extensive. In the case of the electromagnetic gauge symmetry, this simply requires zero charge density. In the case of the color gauge symmetry, the formal requirement is that a chunk of quark matter should be a color singlet, i.e., its wavefunction should be invariant under a general color gauge trans-

formation. Color neutrality, meaning equality in the numbers of red, green, and blue quarks, is a less stringent constraint. A color singlet state is also color neutral, whereas the opposite is not necessarily true. However it has been shown that the projection of a color neutral state onto a color singlet state costs no extra free energy in the thermodynamic limit [76]. Analyzing the consequences of the requirement of color neutrality therefore suffices for our purposes.

In nature, electric and color neutrality are enforced by the dynamics of the electromagnetic and QCD gauge fields, whose zeroth components serve as chemical potentials which take on values that enforce neutrality [46, 77]. Since we are limiting ourselves to color neutrality and not color singletness we have to consider only the $U(1) \times U(1)$ diagonal subgroup of the color gauge group. This subgroup is generated by the diagonal generators $T_3 = \mathrm{diag}(\frac{1}{2}, -\frac{1}{2}, 0)$ and $T_8 = \mathrm{diag}(\frac{1}{3}, \frac{1}{3}, -\frac{2}{3})$ of the $SU(3)$ gauge group. Electromagnetism is generated by $Q = \mathrm{diag}(\frac{2}{3}, -\frac{1}{3}, -\frac{1}{3})$ in flavor space (u, d, s). The zeroth components of the respective gauge fields serve as chemical potentials μ_3 and μ_8 coupled to T_3 and T_8 charges, and as an electrostatic potential μ_e coupled to the *negative* electric charge Q. (We make this last choice so that $\mu_e > 0$ corresponds to a density of electrons, not positrons.) The dynamics of the gauge potentials then require that the charge densities, which are the derivatives of the free energy with respect to the chemical potentials, must vanish:

$$\begin{aligned} Q &= \frac{\partial \Omega}{\partial \mu_e} = 0 \\ T_3 &= -\frac{\partial \Omega}{\partial \mu_3} = 0 \\ T_8 &= -\frac{\partial \Omega}{\partial \mu_8} = 0 \,. \end{aligned} \tag{2.7}$$

A generic diquark condensate will be neither electrically nor color neutral, so it will spontaneously break these gauge symmetries. However it may be neutral under a linear combination of electromagnetism and color. Indeed, any condensate of the form (2.1) is neutral with respect to the "rotated electromagnetism" generated by $\tilde{Q} = Q - T_3 - \frac{1}{2}T_8$, so $U(1)_{\tilde{Q}}$ is never broken. This means that the corresponding gauge boson

(the "$\tilde{Q}$-photon"), a mixture of the ordinary photon and one of the gluons, remains massless. In both the CFL and gCFL phases, the rest of the $SU(3)_{\text{color}} \times U(1)_Q$ gauge group is spontaneously broken, meaning that the combination of the photon and gluons orthogonal to the $\tilde{Q}$-photon, and all the other gluons, become massive by the Higgs mechanism.

In an NJL model with fermions but no gauge fields, as we shall employ after pursuing model-independent arguments as far as we can, one has to introduce the chemical potentials μ_e, μ_3 and μ_8 "by hand" in order to enforce color and electric neutrality in the same way that gauge field dynamics does in QCD [46].

2.1.3 Where does CFL pairing become unstable?

We conclude this introduction with a model-independent argument that determines the density at which the CFL phase becomes unstable. The gap equations for the three Δ's will turn out to be coupled, but we can, for example, analyze the effect of a specified Δ_1 on the gs and bd quarks without reference to the other quarks. It turns out that gs-bd pairing is the first to break down, and this instability is what catalyzes the CFL$\rightarrow$gCFL transition.

The leading effect of M_s is like a shift in the chemical potential of the strange quarks, so the bd and gs quarks feel "effective chemical potentials" $\mu_{bd}^{\text{eff}} = \mu - \frac{2}{3}\mu_8$ and $\mu_{gs}^{\text{eff}} = \mu + \frac{1}{3}\mu_8 - \frac{M_s^2}{2\mu}$. In the CFL phase, color neutrality requires $\mu_8 = -M_s^2/2\mu$, a result that is model-independent to leading order in M_s^2/μ^2 [46, 72]. This result can be understood as arising because CFL pairing itself enforces equality in the number of rd and gu quarks, in the number of bu and rs quarks, and in the number of gs and bd quarks [78], but in order to achieve neutrality the number density of (rd, gu) quarks must be reduced relative to that of the (bu, rs) and (gs, bd) quarks, and this requires a negative μ_8. Because of the negative μ_8, $\mu_{bd}^{\text{eff}} - \mu_{gs}^{\text{eff}} = M_s^2/\mu$ in the CFL phase. The CFL phase will be stable as long as the pairing makes it energetically favorable to maintain equality of the bd and gs Fermi momenta, despite their differing effective chemical potentials [78]. It becomes unstable when the energy gained from turning a gs quark near the common Fermi momentum into a bd quark (namely M_s^2/μ) exceeds

the cost in lost pairing energy $2\Delta_1$. Hence, the CFL phase is stable when [24]

$$\frac{M_s^2}{\mu} < 2\Delta_{\rm CFL} \ . \tag{2.8}$$

For lower density, i.e. larger M_s^2/μ, the CFL phase must be replaced by some new phase with unpaired *bd* quarks. One might naively expect this phase to be either neutral unpaired quark matter or neutral 2SC quark matter, but it is known that these have higher free energy than CFL for $M_s^2/\mu < 4\Delta_{\rm CFL}$ [46, 72], so this new phase, which must have the same free energy as CFL at the critical $M_s^2/\mu = 2\Delta_{\rm CFL}$, must be something else. In view of its properties that are discussed in detail in Section 2.3, we call it gapless CFL (gCFL).

2.2 Model and Approximations

We are interested in physics at non-asymptotic densities, and therefore cannot use weak-coupling methods. We are interested in physics at zero temperature and high density, at which the fermion sign problem is acute and the current methods of lattice QCD can therefore not be employed. For this reason, we need to introduce a model in which the interaction between quarks is simplified, while still respecting the symmetries of QCD, and in which the effects of M_s, μ_e, μ_3 and μ_8 on CFL pairing can all be investigated. The natural choice is to model the interactions between quarks using a point-like four-fermion interaction, which we shall take to have the quantum numbers of single-gluon exchange. We work in Euclidean space. Our partition function $\mathcal{Z}$ and free energy density Ω are then defined by

$$\begin{aligned} \mathcal{Z} &= {\rm e}^{-\beta V\Omega} = \mathcal{N}\int \mathcal{D}\bar\psi\mathcal{D}\psi \exp\Big(\int \mathcal{L}(x)\, d^4x\Big) \\ \mathcal{L}(x) &= \bar\psi(i\partial\!\!\!/ + \mu\!\!\!/ - \boldsymbol{M})\psi - \frac{3}{8}G(\bar\psi\Gamma^A_\mu\psi)(\bar\psi\Gamma^\mu_A\psi) \end{aligned} \tag{2.9}$$

where the fields live in a box of volume V and Euclidean time length $\beta = 1/T$, and $\mu\!\!\!/ = \mu\gamma_4$. The interaction vertex has the color, flavor, and spin structure of the QCD

gluon-quark coupling, $\Gamma^A_\mu = \gamma_\mu T^A$. The mass matrix $\boldsymbol{M} = \mathrm{diag}(0, 0, M_s)$ in flavor space. The chemical potential $\boldsymbol{\mu}$ is a diagonal color-flavor matrix depending on μ, μ_e, μ_3 and μ_8. The normalization of the four-fermion coupling $3G/8$ is as in the first paper in Ref. [34–36, 63, 64]. In real QCD the ultraviolet modes decouple because of asymptotic freedom, but in the NJL model we have to add this feature by hand, through a UV momentum cutoff Λ in the momentum integrals. The model therefore has two parameters, the four-fermion coupling G and the three-momentum cutoff Λ, but it is more useful to parameterize the interaction in terms of a physical quantity, namely the CFL gap parameter at $M_s = 0$ at a reference chemical potential that we shall take to be 500 MeV. We shall call this reference gap Δ_0. We have checked that if we vary the cutoff Λ by 20% while simultaneously varying the bare coupling G so as to keep Δ_0 fixed, then our results change by a few percent at most. All the results that we present are for $\Lambda = 800$ MeV and for a coupling strength chosen such that $\Delta_0 = 25$ MeV.

We now sketch the derivation of the free energy Ω obtained from the Lagrangian (2.9) upon making the ansatz (2.1) for the diquark condensate and working in the mean field approximation. More sophisticated derivations exist in the literature [34–36, 63, 64], but since we are assuming that the only condensate is of the form (2.1) we simply Fierz transform the interaction to yield products of terms that appear in (2.1), and discard all the other terms that arise in the Fierz transformed interaction which would anyway vanish after making the mean field approximation. This yields

$$\mathcal{L}_{\rm int} = \frac{G}{4} \sum_\eta (\bar\psi P_\eta \bar\psi^T)(\psi^T \bar P_\eta \psi) \ , \tag{2.10}$$

where

$$(P_\eta)^{\alpha\beta}_{ij} = C\gamma_5 \epsilon^{\alpha\beta\eta} \epsilon_{ij\eta} \quad \text{(no sum over } \eta) \tag{2.11}$$

and $\bar P_\eta = \gamma_4 P_\eta^\dagger \gamma_4$. The index η labels the pairing channel: $\eta = 1, 2$, and 3 correspond to d-s pairing, u-s pairing, and u-d pairing. The overall coefficient in (2.10) is the product of the $3G/8$ in (2.9) and factors of -1, $4/3$, and $-1/2$ from Fierz transformations in Dirac, color and flavor space, respectively.

Next, for each channel we introduce a complex scalar field ϕ_η whose expectation value will be Δ_η, the strength of the pairing in the η channel, and bosonize the four-fermion interaction via a Hubbard-Stratonovich transformation. The interaction Lagrangian then becomes

$$\mathcal{L}_{\rm int} = \tfrac{1}{2}(\bar\psi P_\eta \bar\psi^T)\phi_\eta + \tfrac{1}{2}\phi_\eta^*(\psi^T \bar P_\eta \psi) - \frac{\phi_\eta^*\phi_\eta}{G}\ , \tag{2.12}$$

where here and henceforth repeated η's are summed and where it is understood that we are now integrating over the ϕ_η as well as ψ and $\bar\psi$ in the functional integral (2.9). The functional integral is now quadratic in the quark fields, so the fermionic function integral can be performed. Since there are terms in the action that can violate quark number, we must use Nambu-Gorkov spinors

$$\Psi = \begin{pmatrix} \psi(p) \\ \bar\psi^T(-p) \end{pmatrix}, \quad \bar\Psi = \left(\bar\psi(p)\ \psi^T(-p)\right) \tag{2.13}$$

and the full Lagrange density becomes

$$\mathcal{L} = \frac{1}{2}\bar\Psi \frac{S^{-1}}{T}\Psi - \frac{\phi_\eta^*\phi_\eta}{G} \tag{2.14}$$

where the inverse full propagator is

$$S^{-1}(p) = \begin{pmatrix} \not p + \not\mu - \boldsymbol{M} & P_\eta\phi_\eta \\ \bar P_\eta \phi_\eta^* & (\not p - \not\mu + \boldsymbol{M})^T \end{pmatrix}\ . \tag{2.15}$$

We now integrate over the fermionic fields to obtain the effective potential for the scalar fields. We also make the mean-field approximation, neglecting fluctuations in the scalar fields and setting ϕ_η to its expectation value Δ_η. The result is

$$\mathcal{Z} = \left[\mathrm{Det}\frac{S^{-1}(i\omega_n, p)}{T}\right]^{1/2} \exp\left(-\frac{V}{T}\frac{\Delta_\eta\Delta_\eta}{G}\right) \tag{2.16}$$

and hence

$$\Omega = -T\sum_n \int \frac{d^3p}{(2\pi)^3}\frac{1}{2}\mathrm{Tr}\log\Big(\frac{1}{T}S^{-1}(i\omega_n,p)\Big) + \frac{\Delta_\eta\Delta_\eta}{G}\ , \tag{2.17}$$

where $\omega_n = (2n-1)\pi T$ are the Matsubara frequencies. We do the Matsubara summation using the identity

$$T\sum_n \ln\Big(\frac{\omega_n^2+\varepsilon^2}{T^2}\Big) = |\varepsilon| + 2T\ln(1+e^{-|\varepsilon|/T})\ . \tag{2.18}$$

In the limit of zero temperature only the first term from the right hand side survives, leading to the result

$$\begin{aligned}\Omega &= -\frac{1}{4\pi^2}\int_0^\Lambda p^2 \sum_j |\varepsilon_j(p)|\,dp \\ &\quad +\frac{1}{G}(\Delta_1^2+\Delta_2^2+\Delta_3^2) - \frac{\mu_e^4}{12\pi^2}\ ,\end{aligned} \tag{2.19}$$

where the electron contribution is included, and $\varepsilon_j(p)$ are the dispersion relations of the quasiquarks, i.e. the values of the energy at which the propagator diverges:

$$\det S^{-1}(i\varepsilon_j(p),p) = 0\ . \tag{2.20}$$

S^{-1} is a 72×72 matrix, but because what occurs in the identity (2.18) is the combination $\omega^2+\varepsilon^2$, the sum in (2.19) is understood to run over 36 roots. (This can be seen as removing the doubling of degrees of freedom introduced by using the Nambu-Gorkov formalism.) In the specific cases where our general ansatz becomes 2SC or CFL pairing, our expression (2.19) for the free energy, and in particular the coefficient of the Δ^2 term, agrees with the expressions obtained by other methods [34–36, 63, 64] that do not involve Fierz transformations.

In our numerical evaluation, we omit the antiparticle modes (although in Chapter 3 we include them): exciting them costs of order 2μ and they therefore do not play an important role in the physics. This is discussed in more detail below. Neglecting the antiparticles leaves us with only 18 roots of (2.20) to sum over in (2.19). These correspond to 9 different dispersion relations describing the quasiparticles of differing

color and flavor, each doubly degenerate due to spin.

A stable, neutral phase must minimize the free energy (2.19) with respect to variation of the three gap parameters Δ_1, Δ_2, Δ_3, meaning it must satisfy

$$\frac{\partial\Omega}{\partial\Delta_1}=0, \qquad \frac{\partial\Omega}{\partial\Delta_2}=0, \qquad \frac{\partial\Omega}{\partial\Delta_3}=0\ , \tag{2.21}$$

and it must satisfy the three neutrality conditions (2.7). The gap equations (2.21) and neutrality equations (2.7) form a system of six coupled integral equations with unknowns the three gap parameters and μ_3, μ_8 and μ_e.

We must now find the dispersion relations $\varepsilon_j(p)$, determined by the zeroes of $\det S^{-1}$ which is specified by (2.20), (2.15) with ϕ_η replaced by Δ_η, and (2.11), then evaluate the free energy Ω using (2.19), and then solve the six simultaneous equations (2.7) and (2.21). Before carrying this calculation through, however, we first make a number of simplifying approximations within the expression for $\det S^{-1}$.

1. We neglect contributions to the condensate that are symmetric in color and flavor: these are known to be present and small [10, 27, 38].
2. We treat the up and down quarks as massless, which is a legitimate approximation in the high density regime, and we treat the constituent strange quark mass M_s as a parameter, rather than solving for an $\langle\bar{s}s\rangle$ condensate. The latter approximation should be improved upon, along the lines of Ref. [72].
3. We incorporate M_s only via its leading effect, namely as a shift $-M_s^2/2\mu$ in the chemical potential for the strange quarks. This approximation neglects the difference between the strange and light quark Fermi velocities, whose effects are known in other contexts to be small [79]. The approximation is controlled by the smallness of M_s^2/μ^2. For this reason, in all the results that we plot we shall work at $\mu = 500$ MeV and choose a coupling such that the CFL gap at $M_s = 0$ is $\Delta_0 = 25$ MeV. We expect the CFL pairing to break down near $M_s^2 \approx 2\mu\Delta_0$, and choosing $\Delta_0 = \mu/20$ ensures that this occurs where $M_s^2/\mu^2 \sim 1/10$, meaning that we can trust our results well into the gapless CFL phase. If, instead, we choose a larger Δ_0, as in Ref. [27], we find that our results become markedly

more Λ-dependent, which is a good diagnostic for model-dependence.

4. We work to leading nontrivial order in Δ_1, Δ_2, Δ_3, μ_e, μ_3 and μ_8. This should be a good approximation, as all these quantities are small compared to μ.
5. We neglect the anti-particles. This simplifies the numerics by discarding physically unimportant degrees of freedom, but one must be cautious with this truncation. It introduces cutoff-dependent terms in our free energy, including some that depend on the chemical potential and therefore introduce cutoff-dependence in the corresponding charges. For our purposes this is not important, firstly because we always present free energy differences relative to neutral unpaired quark matter, and secondly because we only care about electric and color charges that have zero trace over all fermion species, and for these the cutoff dependence cancels out. However, a non-traceless charge like baryon number would have an incorrect cutoff-dependent value when calculated in this approximation.
6. We ignore meson condensation in both the CFL and gCFL phases.

We expect that these approximations have quantitative effects, but none preclude a qualitative understanding of the new phase we shall describe.

We now give the explicit expression for $\det S^{-1}$, after having implemented the approximations above. As described in section 2.1.1 we use a color-flavor basis in which the gap matrix (2.2) is conveniently block-diagonal. Since the chemical potential and mass are diagonal in color and flavor, the full inverse propagator (2.15) is then also block-diagonal in color-flavor space. This means we can break the determinant in equation (2.20) into four more manageable pieces:

$$\det S^{-1}(p_0, p) = \left(D^{ru}_{\substack{gd \\ bs}} D^{rd}_{gu} D^{rs}_{bu} D^{gs}_{bd} \right)^2 . \tag{2.22}$$

We find that the 2×2 determinants are

$$\begin{aligned}
D^{rd}_{gu} &= 16\mu^4((\mu_{rd} - p - ip_0)(\mu_{gu} - p + ip_0) + \Delta_3^2) \\
&\quad ((\mu_{rd} - p + ip_0)(\mu_{gu} - p - ip_0) + \Delta_3^2), \\
D^{rs}_{bu} &= 16\mu^4((\mu_{rs} - p - ip_0)(\mu_{bu} - p + ip_0) + \Delta_2^2) \\
&\quad ((\mu_{rs} - p + ip_0)(\mu_{bu} - p - ip_0) + \Delta_2^2), \\
D^{gs}_{bd} &= 16\mu^4((\mu_{bd} - p - ip_0)(\mu_{gs} - p + ip_0) + \Delta_1^2) \\
&\quad ((\mu_{bd} - p + ip_0)(\mu_{gs} - p - ip_0) + \Delta_1^2),
\end{aligned} \tag{2.23}$$

and the 3×3 determinant is

$$\begin{aligned}
D^{ru}_{gd\,bs} = \quad & a(2\mu)^6\Big(\quad b(de - \Delta_1^2)(cf - \Delta_1^2) - cdf\Delta_2^2 \\
& \qquad +d\Delta_1^2\Delta_2^2 - def\Delta_3^2 + f\Delta_1^2\Delta_3^2 \Big) \\
+(2\mu)^6\Big(\quad & \Delta_3^2(de\Delta_2^2 - 4\Delta_1^2\Delta_2^2 + ef\Delta_3^2) \\
& +c(d\Delta_2^4 + f\Delta_2^2\Delta_3^2) \\
& +b(e\Delta_1^2\Delta_3^2 + c(\Delta_1^2\Delta_2^2 - de\Delta_2^2 - ef\Delta_3^2)) \Big)
\end{aligned} \tag{2.24}$$

where for compactness we assign

$$\begin{aligned}
a &= \mu_{ru} - p + ip_0 \\
b &= -\mu_{ru} + p + ip_0 \\
c &= \mu_{gd} - p + ip_0 \\
d &= -\mu_{gd} + p + ip_0 \\
e &= \mu_{bs} - p + ip_0 \\
f &= -\mu_{bs} + p + ip_0
\end{aligned} \tag{2.25}$$

and where we have dropped the superscript on the "effective quark chemical poten-

tials", given by

$$\begin{aligned}
\mu_{ru}^{\rm eff} &= \mu - \tfrac{2}{3}\mu_e + \tfrac{1}{2}\mu_3 + \tfrac{1}{3}\mu_8, \\
\mu_{gd}^{\rm eff} &= \mu + \tfrac{1}{3}\mu_e - \tfrac{1}{2}\mu_3 + \tfrac{1}{3}\mu_8, \\
\mu_{bs}^{\rm eff} &= \mu + \tfrac{1}{3}\mu_e - \tfrac{2}{3}\mu_8 - M_s^2/(2\mu), \\
\\
\mu_{rd}^{\rm eff} &= \mu + \tfrac{1}{3}\mu_e + \tfrac{1}{2}\mu_3 + \tfrac{1}{3}\mu_8, \\
\mu_{gu}^{\rm eff} &= \mu - \tfrac{2}{3}\mu_e - \tfrac{1}{2}\mu_3 + \tfrac{1}{3}\mu_8, \\
\\
\mu_{rs}^{\rm eff} &= \mu + \tfrac{1}{3}\mu_e + \tfrac{1}{2}\mu_3 + \tfrac{1}{3}\mu_8 - M_s^2/(2\mu), \\
\mu_{bu}^{\rm eff} &= \mu - \tfrac{2}{3}\mu_e - \tfrac{2}{3}\mu_8, \\
\\
\mu_{gs}^{\rm eff} &= \mu + \tfrac{1}{3}\mu_e - \tfrac{1}{2}\mu_3 + \tfrac{1}{3}\mu_8 - M_s^2/(2\mu), \\
\mu_{bd}^{\rm eff} &= \mu + \tfrac{1}{3}\mu_e - \tfrac{2}{3}\mu_8 \ .
\end{aligned} \tag{2.26}$$

These expressions explicitly show how we treat the strange quark mass as a shift in the chemical potential of the strange quarks. In evaluating these determinants, we have extensively used the identity

$$\det \begin{pmatrix} A & B \\ C & D \end{pmatrix} = \det(A)\det(D - CA^{-1}B)$$

for the determinant of a block matrix.

The numerical task is now explicit. We find the quasiparticle dispersion relations $\varepsilon(p)$ by finding the zeros of (2.22), viewed as a polynomial in p_0. We then perform the integral in (2.19) numerically, and obtain Ω. We evaluate the partial derivatives of the free energy required in the neutrality conditions (2.7) and the gap equations (2.21) numerically as finite differences, with differences 0.1 MeV in the relevant chemical potential or gap parameter.

As a check, we have also done the calculation of Ω and its partial derivatives by evaluating both the p and p_0 integrals numerically, never writing the latter as a Matsubara sum. In this alternative calculation, we were able to evaluate the partial

derivatives in (2.7) and (2.21) analytically.

The Ω that we obtain is cutoff dependent, but its partial derivatives (2.7) and (2.21) are insensitive to variations in Λ in the sense described above, namely as long as the coupling is changed to keep Δ_0 fixed upon variation in Λ, and as long as Λ is kept well above μ. Furthermore, we are only ever interested in free energy differences between phases. When we evaluate the differences between the Ω for unpaired, (g)CFL, and (g)2SC quark matter, we find that all such free energy differences are insensitive to the cutoff, as they should be since these differences all reflect physics near the Fermi surfaces. Because we are only interested in free energy differences, in evaluating Ω we make the numerical integral better behaved by subtracting the appropriate expression for neutral unpaired quark matter within the integrand.

The solutions of the system of gap and neutrality equations depend on three parameters: μ, M_s and Δ_0. Our purpose is to understand the effect of M_s on CFL pairing, and these effects are controlled by the relative size of M_s^2/μ and the gap parameters Δ_i, whose overall magnitude is set by Δ_0. It is therefore better to think of the three parameters in the problem as μ, M_s^2/μ and Δ_0. In compact stars, μ increases and M_s presumably decreases, meaning that M_s^2/μ decreases as one approaches the center of the star. For simplicity, we set the overall energy scale in our calculation by fixing $\mu = 500$ MeV, which is reasonable for the center of a neutron star, and vary M_s in order to vary M_s^2/μ. We have confirmed that as long as we choose a Δ_0 that is small enough that the transition (2.8) occurs where M_s^2/μ^2 corrections are under control, this transition occurs very close to $M_s^2/\mu \approx 2\Delta$, where Δ is gap parameter on the CFL side of the transition. The authors of Ref. [27] have confirmed that this result continues to be valid even for Δ_0 as large as 100 MeV, where the approximations are not as well controlled. We quote results only for $\Delta_0 = 25$ MeV, which is within the plausible range of values that Δ_0 may take in nature [34–36, 63, 64] and for which our calculation is clearly under control. Although we have obtained our results by varying M_s at fixed μ, we typically quote results in terms of the important combination M_s^2/μ.

2.3 Results

2.3.1 Domain where gCFL is favored

In Figs. 2-1 and 2-2, we show the gap parameters and chemical potentials as a function of M_s^2/μ, for $\Delta_0 = 25$ MeV. Fig. 2-3 shows the free energy. We see a continuous phase transition occurring at a critical M_s^c that, in our model calculation with $\mu = 500$ MeV, lies between $M_s = 153$ MeV and $M_s = 154$ MeV, i.e. at $(M_s^2/\mu)_c \approx 47.1$ MeV. This agrees exceedingly well with the expected value 2Δ from Eq. (2.8), since on the CFL side of the transition $\Delta_1 = \Delta_2 = \Delta_3 = 23.5$ MeV. For $M_s^2/\mu < (M_s^2/\mu)_c$, the CFL phase is favored, with all three gaps equal to each other within our approximations. If we improve upon our approximate treatment of M_s, we expect $\Delta_1 = \Delta_2$ with these gap parameters slightly smaller than Δ_3, because Δ_1 and Δ_2 describe pairing between quarks with differing Fermi velocities, an effect of M_s that we are neglecting because it is known to be small in other contexts [79]. (Indeed, it proves to be a few percent effect as we shall see in Chapter 3.)

For $M_s^2/\mu < (M_s^2/\mu)_c$ our results agree with the small-M_s expansion of Ref. [46], where $\mu_3 = \mu_e = 0$ and $\mu_8 = -M_s^2/(2\mu)$ and the free energy is

$$\begin{aligned}\Omega_{\substack{\text{neutral}\\\text{CFL}}} &= -\frac{3\mu^4}{4\pi^2} + \frac{3M_s^2\mu^2}{4\pi^2} - \frac{1-12\log(M_s/2\mu)}{32\pi^2}M_s^4 \\ &\quad - \frac{3\Delta^2\mu^2}{\pi^2} \\ &= \Omega_{\substack{\text{neutral}\\\text{unpaired}}} + \frac{3M_s^4 - 48\Delta^2\mu^2}{16\pi^2} \,. \end{aligned} \tag{2.27}$$

As the density decreases (i.e. as M_s^2/μ increases) through the CFL→gCFL transition, the gap parameters split apart, with Δ_3 increasing slightly and Δ_2 and Δ_1 dropping significantly, with Δ_1 dropping faster than Δ_2.

We have verified that $M_s^2/\mu\Delta$ is the relevant dimensionless quantity by changing the coupling strength, i.e. picking a different Δ_0 (gap at $M_s = 0$). The critical point $(M_s^2/\mu)_c$ changes as predicted by (2.8). Furthermore we checked the robustness of

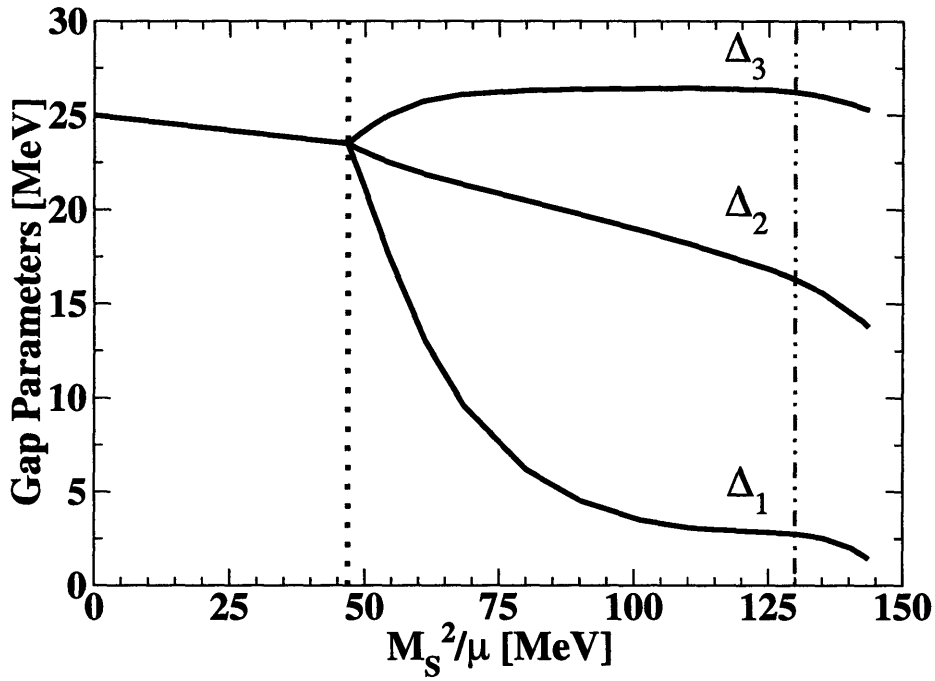

Figure 2-1: Gap parameters Δ_3, Δ_2, and Δ_1 as a function of M_s^2/μ for $\mu = 500$ MeV, in a model where $\Delta_0 = 25$ MeV (see text). At $M_s^2/\mu \approx 47.1$ MeV (vertical dotted line) there is a continuous phase transition between the CFL phase and a phase that we shall identify below as the gapless CFL phase. We find gapless CFL phase solutions up to $M_s^2/\mu \approx 144$ MeV. But, we shall see in Fig. 2-3 that above $M_s^2/\mu \approx 130$ MeV (which we denote here with a vertical dash-dotted line) unpaired quark matter has a lower free energy than the gapless CFL phase.

our results upon variation of the cutoff Λ, observing changes of only a few percent in the value of $M_s^2/\mu\Delta$ at the transition upon changing Λ by up to 20% while keeping Δ_0 fixed. However, if the CFL phase is augmented by a K^0-condensate [41, 80], the CFL→gCFL transition is delayed to a value of M_s^2/μ that is higher by a factor of 4/3 [81] or less [80].

Fig. 2-3 confirms that the slope of the free energy is continuous at the CFL/gCFL transition, indicating that it is not first order. We have not determined the order of the transition, because evaluating higher derivatives of the free energy with respect to M_s^2/μ is not numerically feasible. The most physically relevant order parameter is the electron density $n_e \sim \mu_e^3$, which is of course equal in magnitude to the electric charge density of the quarks. This increases above the transition like $n_e \sim [(M_s^2/\mu) - (M_s^2/\mu)_c]^3$, which would suggest a fourth order phase transition.

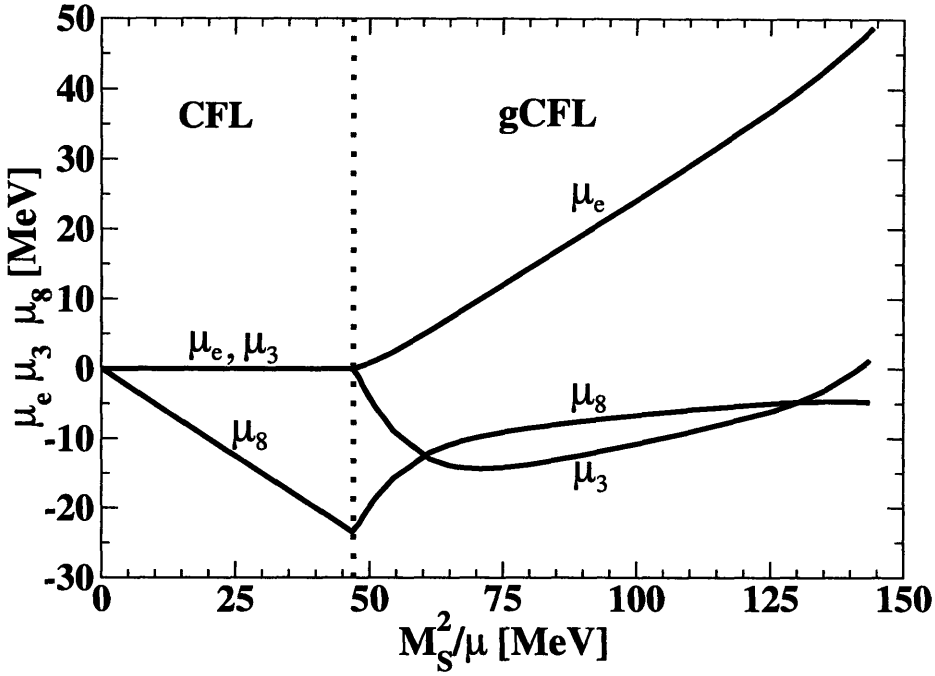

Figure 2-2: Chemical potentials μ_e, μ_3 and μ_8 as a function of M_s^2/μ in the CFL/gCFL phase for the same parameters as in Fig. 2-1. The effects of electrons on the free energy have been included in the calculation, as will be discussed in more detail below. We see that the gapless CFL phase has $\mu_e > 0$, meaning that it has a nonzero density of electrons. Perhaps the most physically relevant order parameter for the CFL/gCFL phase transition is the electron number density $n_e \sim \mu_e^3$.

This argument neglects the small electron mass and, furthermore, it neglects the fact that, as we shall see in Eq. (2.32), there is also a nonzero number density of neutral unpaired quark quasiparticles that grows like $[(M_s^2/\mu) - (M_s^2/\mu)_c]^{1/2}$. Although because these unpaired quasiparticles are neutral they are less important phenomenologically, this does suggest that the transition is second order, as in the analysis of Ref. [82].

If we had used a simpler ansatz in which the gap parameters were constrained to one value $\Delta \equiv \Delta_1 = \Delta_2 = \Delta_3$, then the CFL phase would have remained artificially stable above the critical value of M_s^2/μ. From Eq. (2.27), its free energy would be higher than that of gCFL, rising to equality with that of unpaired quark matter at a value of M_s^2/μ around 90 MeV. (The precise value depends on how the common Δ changes with M_s.)

Of course, we actually used the more general ansatz (2.1) that allows the Δ's

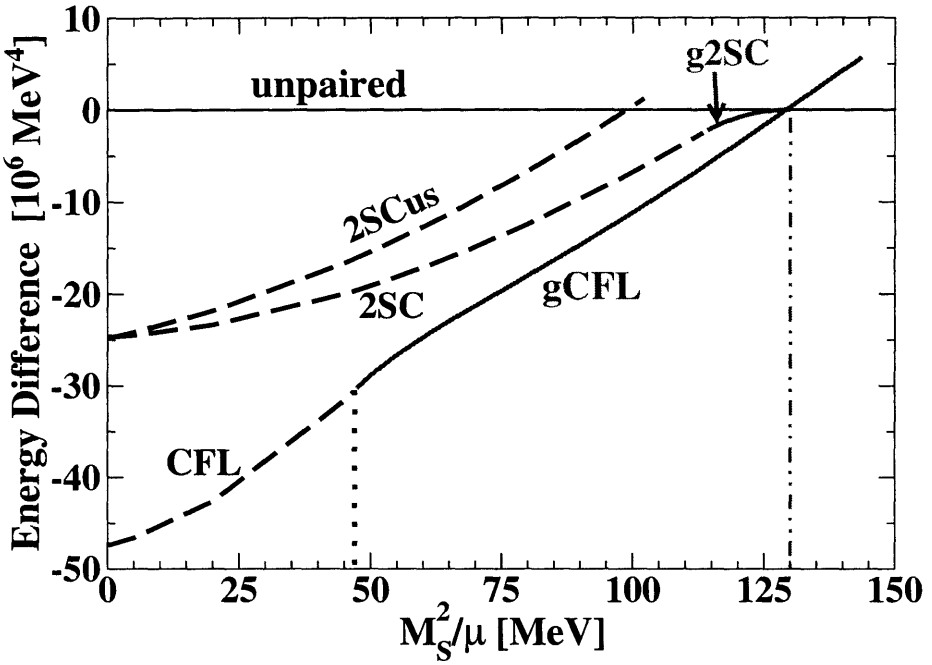

Figure 2-3: Free energy of the CFL/gCFL phase, relative to that of neutral noninteracting quark matter and that of the 2SC/g2SC and 2SCus phases, discussed in Section 2.3.4. There is a CFL→gCFL transition at $(M_s^2/\mu)_c \approx 47.1$ MeV, (vertical dotted line), at which the free energy and its slope are continuous, indicating that the transition is not first order. If we neglect the possibility of other phases (for example g2SC) we would conclude from this figure that there is a first order transition gCFL→unpaired at $M_s^2/\mu \approx 130$ MeV (vertical dash-dotted line).

to differ. We found that the CFL phase becomes unstable and is replaced by the gCFL phase, in which the gaps have very different values, so the simplified analysis of Ref. [46] does not apply. The free energy of the gCFL phase crosses that of unpaired quark matter at $M_s^2/\mu \approx 130$ MeV. This phase transition is first order, and we are able to follow the metastable gCFL phase up to $M_s^2/\mu = 144$ MeV where, as we shall explain below, it ceases to be a solution.

2.3.2 The nature of the gCFL phase

Up to this point we have not justified our use of the name "gapless CFL" for the new phase that replaces the CFL phase at $M_s^2/\mu \gtrsim 2\Delta$. We have given model-independent arguments to expect that it will contain unpaired *bd* quarks, but now we describe its properties in more detail. In calculating the free energy (2.19) of the Cooper-paired

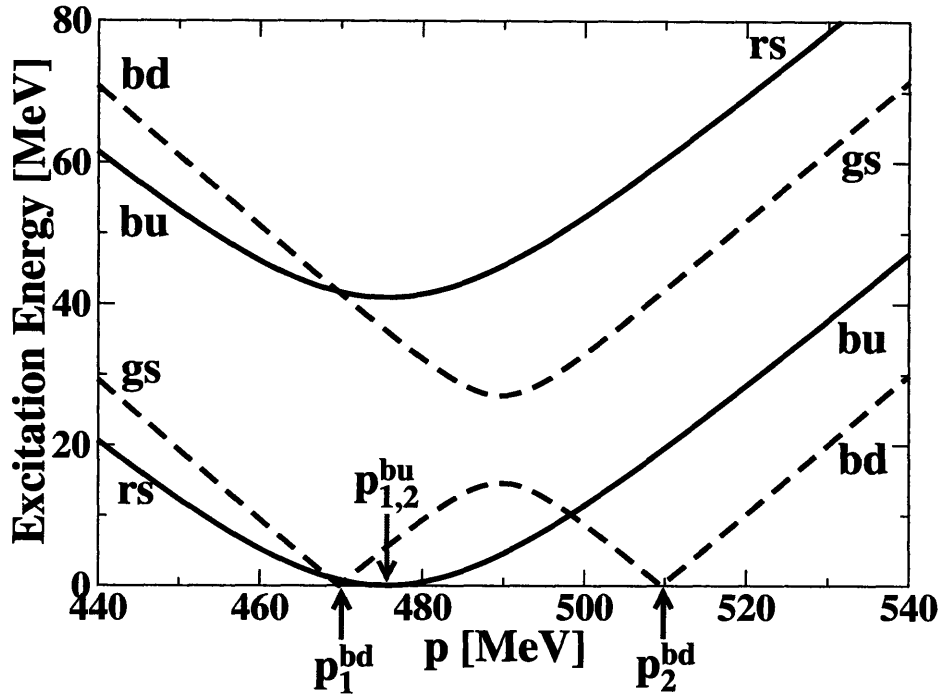

Figure 2-4: Dispersion relations at $M_s^2/\mu = 80$ MeV (with μ and Δ_0 as in previous figures) for the quasiparticles that are linear combinations of gs and bd quarks (dashed lines) and for the quasiparticles that are linear combinations of bu and rs quarks (solid lines). There are gapless gs-bd modes at $p_1^{bd} = 469.8$ MeV and $p_2^{bd} = 509.5$ MeV, which are the boundaries of the "blocking" [56, 57] or "breached pairing" [85] region wherein there are unpaired bd quarks and no gs quarks. One bu-rs mode is gapless at $p = 475.6$ MeV with an almost exactly quadratic dispersion relation that we shall discuss below.

quark matter we automatically obtain the quasiquark dispersion relations (2.20), so we can see what gapless modes exist. These modes are important because, at the temperatures $T \lesssim$ keV characteristic of neutron stars, only the lightest modes will contribute to transport properties.

In Fig. 2-4 we show the dispersion relations for the rs-bu and gs-bd 2×2 blocks in the quasiquark propagator, at $M_s^2/\mu = 80$ MeV. We see immediately that there are gapless modes in both blocks, justifying our name for this phase. Before moving on to a detailed discussion of the physical properties of the gCFL phase, we should note that the phenomenon of gapless superconductivity is well known, at least theoretically. It was first suggested by Sarma [83] who worked in a context much like our gs-bd block in isolation, and found that the gapless superconducting phase is never stable. Alford,

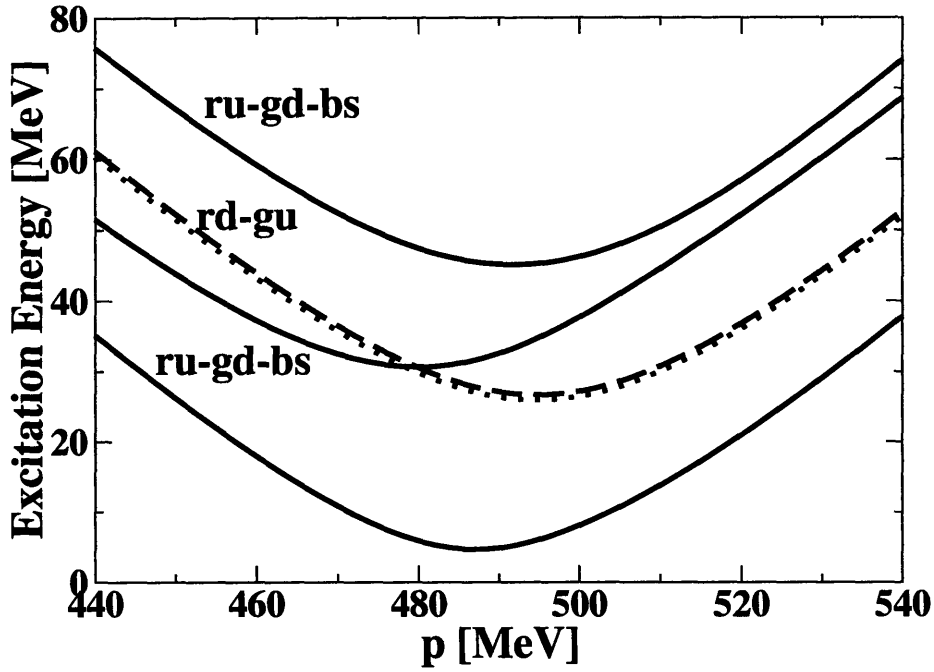

Figure 2-5: Dispersion relations at $M_s^2/\mu = 80$ MeV for the two quasiparticles that are linear combinations of rd and gu quarks (dashed and dotted), and for the three quasiparticles that are linear combinations of ru, gd and bs quarks (solid). These five quark quasiparticles all have gaps throughout the CFL and gCFL phases.

Berges and Rajagopal found a metastable gapless color superconducting phase in Ref. [84], but this phase was neither electrically nor color neutral. The key observation was made by Shovkovy and Huang [74], who discovered that when the constraints of electric and color neutrality are imposed on the 2SC phase in two-flavor QCD, there are regions of parameter space where a gapless color superconducting phase is stable. Following their nomenclature (they described a "gapless 2SC phase") we refer to the phase that we find above M_s^c as the "gapless color-flavor locked phase" [24].

Gapless two-flavor color superconductivity was also studied in Ref. [85], building upon prior work done in a cold atom context [86]. These authors analyzed pairing between a heavy and a light quark, akin to gs and bd, in the case in which the gs quarks are nonrelativistic. They find that a gapless phase (they describe the blocking region as a region in which pairing is "breached") is stable if the relative density of the two species is held fixed.

Note that in our three-flavor calculation, both the gap equations (2.21) and the

neutrality conditions (2.7) couple all nine quarks. Although the single particle dispersion relations can be analyzed for the gs and bd quarks in isolation, and are qualitatively similar to those obtained in Refs. [74, 85] in a two-flavor setting, the implications of neutrality are more subtle in our three-flavor context as we shall explain below.

Each of the dispersion relations in Figs. 2-4 and 2-5 describes an excitation with well-defined $\tilde{Q}$, although the sign of $\tilde{Q}$ changes at momenta where the dispersion relation is gapless. Beginning with an example with no gap, the upper solid curve in Fig. 2-4 describes excitations that are linear combinations of rs particles and bu holes, both with $\tilde{Q} = -1$. The lower dashed curve in Fig. 2-4 has clearly visible momenta p_1^{bd} and p_2^{bd} where it is gapless, so we use this as an example of "sign change" even though it describes $\tilde{Q} = 0$ quasiparticles: to the left of p_1^{bd}, it describes gs-holes with a very small admixture of bd particles; to the right of p_2^{bd}, it describes bd particles with a very small admixture of gs holes; but, between p_1^{bd} and p_2^{bd} it describes excitations that are superpositions of bd holes and gs particles.

In the CFL phase, once we take into account the explicit symmetry breaking introduced by the strange quark mass and electromagnetism, the unbroken symmetry is reduced from the diagonal $SU(3)_{L+R+c}$ to $U(1)_{\tilde{Q}} \times U(1)$ [47]. The last $U(1)$ corresponds to "color + flavor hypercharge" and may be spontaneously broken by meson condensation [41]. The gapless CFL phase has the same symmetry as the CFL phase, and it will therefore be interesting to investigate the possibility of meson condensation in the gCFL phase. The effective theory for the Goldstone bosons alone will have the same form as in the CFL phase, albeit with new contributions to their masses coming from the differences between the values of the three Δ_i^2. And, furthermore, the gapless quasiparticles must be included in the low energy effective theory.

Dispersion relations, gapless modes, and neutrality

As will soon become clear, the 3×3 block in the pairing pattern (2.2) plays a minor role: its quasiparticles are always gapped, so we mainly discuss the three 2×2 blocks. In general, when two species of massless quarks undergo s-wave pairing with gap

parameter Δ, the dispersion relations of the two resulting quasiparticles are

$$E(p) = \left| \delta\mu \pm \sqrt{(p-\bar{\mu})^2 + \Delta^2} \right| \tag{2.28}$$

where the individual chemical potentials of the quarks are $\bar{\mu} \pm \delta\mu$. As long as the chemical potentials pulling the two species apart are not too strong, Cooper pairing occurs at all momenta:

$$\text{pairing criterion:} \quad |\delta\mu| < \Delta \ . \tag{2.29}$$

However when this condition is violated there are gapless ($E = 0$) modes at momenta

$$p_{\text{gapless}} = \bar{\mu} \pm \sqrt{\delta\mu^2 - \Delta^2} \tag{2.30}$$

and there is no pairing in the "blocking" or "breached pairing" region between these momenta [56, 57, 74, 85, 86]. (The identification of the boundaries of a blocking region with locations in momentum space where a dispersion relation is gapless is discussed with considerable care in Ref. [57], which considers a more complicated setting in which rotational symmetry is spontaneously broken and the blocking regions are not spherically symmetric. Such blocking regions were analyzed previously in Ref. [56].) The pairing criterion (2.29) can be interpreted as saying that the free energy cost 2Δ of breaking a Cooper pair of two quarks a and b is greater than the free energy $2\delta\mu$ gained by emptying the a state and filling the b state (assuming that $\delta\mu$ pushes the energy of the a quark up and the b quark down) [78]. In the blocking region, we find unpaired b quarks and no a quarks.

We wish now to apply these ideas to the 2×2 pairing blocks in three-flavor quark matter, first in the CFL phase. As described above, neutrality is imposed via chemical potentials μ_e, μ_3, μ_8, and in the CFL phase the leading effect of the strange quark mass is an additional effective chemical potential $-M_s^2/2\mu$ for the strange quarks. The splittings of the various pairs are then as given in the middle column of Table 2.1.

Electrons will play a crucial role in understanding the gCFL phase, but it is

quark pair	$\delta\mu_{\rm eff}$	$\delta\mu_{\rm eff}$ in electronless CFL
rd-gu	$\frac{1}{2}(\mu_e+\mu_3)$	μ_e
rs-bu	$\frac{1}{2}(\mu_e+\frac{1}{2}\mu_3+\mu_8-\frac{1}{2}M_s^2/\mu)$	$\mu_e-\frac{1}{2}M_s^2/\mu$
gs-bd	$\frac{1}{2}(\frac{1}{2}\mu_3-\mu_8+\frac{1}{2}M_s^2/\mu)$	$M_s^2/2\mu$

Table 2.1: Chemical potential splittings for the 2×2 pairing blocks. ($\delta\mu_{\rm eff}$ and $\bar{\mu}$, which is not tabulated, are defined in each row such that the effective chemical potentials of the two quarks that pair are $\bar{\mu}\pm\delta\mu_{\rm eff}$.) The middle column gives $\delta\mu_{\rm eff}$ for general values of the chemical potentials μ_e, μ_3 and μ_8. In the last column, it is understood that as μ_e is varied, μ_3 and μ_8 "follow it" in such a way that varying μ_e corresponds to varying $\mu_{\tilde{Q}}$, tracking degenerate $\tilde{Q}$-neutral solutions for electron-less CFL quark matter.

fruitful initially to consider matter consisting only of quarks, which we can do by sending the electron mass to infinity. In the absence of electrons, at each M_s^2/μ there is a plateau in the free energy of neutral CFL (or gCFL) solutions: if we vary the chemical potential that couples to $\tilde{Q}$ charge,

$$\mu_{\tilde{Q}}=-\tfrac{4}{9}\left(\mu_e+\mu_3+\tfrac{1}{2}\mu_8\right)\ , \tag{2.31}$$

while keeping constant the gap parameters Δ_i and the two orthogonal combinations of chemical potentials, then over a range of $\mu_{\tilde{Q}}$ the free energy does not change and we have a family of neutral stable solutions to the gap equations. This indicates that, in the absence of electrons, both the CFL and gCFL phases are $\tilde{Q}$-insulators. On this plateau, all $\tilde{Q}$-charged quasiparticles remain gapped: (2.29) is obeyed for the (rd,gu) and (rs,bu) 2×2 quark pairing blocks. At the edges of the plateau, some $\tilde{Q}$-charged quasiparticles become gapless, the material ceases to be $\tilde{Q}$-neutral, $\partial\Omega/\partial\mu_{\tilde{Q}}\neq 0$, and the free energy is no longer independent of changes in $\mu_{\tilde{Q}}$. The range of $\mu_{\tilde{Q}}$ that defines the plateau is therefore the band gap for the CFL/gCFL insulator. In Fig. 2-6 we show the unpairing lines for each 2×2 quark pairing block. The rd-gu line and the rs-bu line bound the plateau region. Although the vertical axis is labelled "μ_e", it actually corresponds to variation in $\mu_{\tilde{Q}}$, since we varied (μ_e,μ_3,μ_8) by a multiple of $(1,1,\frac{1}{2})$. In the CFL phase, this corresponds to keeping $\mu_3=\mu_e$ and

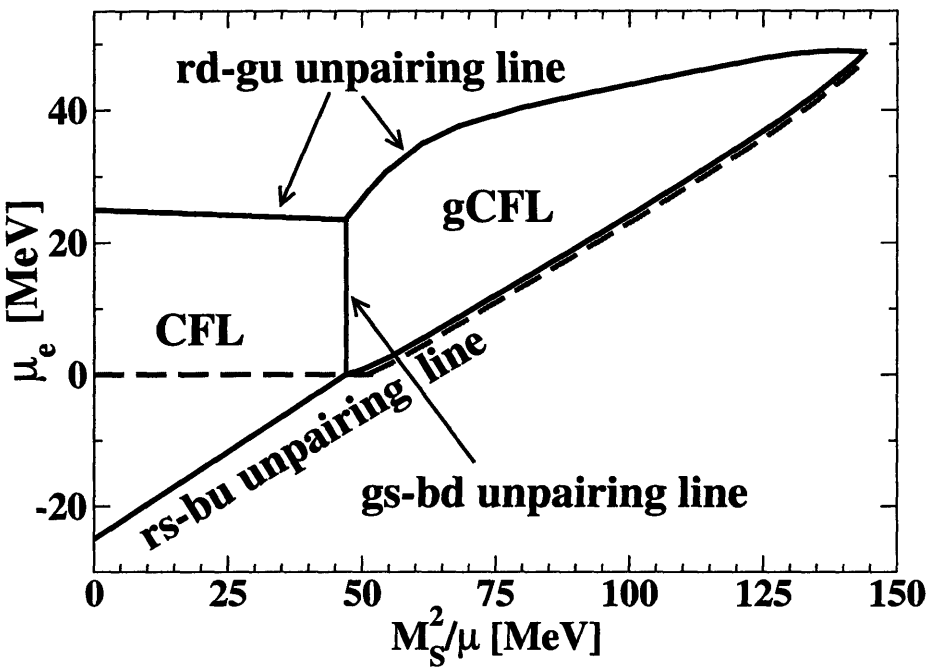

Figure 2-6: Unpairing lines for the same parameters as used in Fig. 2-1. If electrons are neglected, then the upper and lower curves bound the region of μ_e where neutral solutions to the gap equations are found. These solutions are all $\tilde{Q}$-insulators. Taking electrons into account, the correct solution is the dashed line: in the CFL phase $\mu_e = 0$, while the gCFL phase corresponds to values of μ_e below but very close to the *rs-bu* unpairing line. gCFL is a $\tilde{Q}$-conductor both because of the nonzero electron density and because of the ungapped $\tilde{Q}$-charged *rs-bu* quasiparticles.

$\mu_8 = \frac{1}{2}(\mu_e - M_s^2/\mu)$ while varying μ_e.

We see that (g)CFL matter exists in a wedge, between the *rd-gu* unpairing line and the *rs-bu* unpairing line. From Table 2.1 we can see that the *bd-gs*-unpairing line is vertical because the *bd* and *gs* quasiparticles are $\tilde{Q}$-neutral, so their splitting depends only on M_s^2/μ and not on μ_e. This unpairing line has a different character than the other two. Rather than bounding the band-gap within which solutions are found, it separates the CFL and gCFL phases. CFL is stable only up to a critical value of M_s^2/μ, where the the *gs-bd* pairs break.

At the lower (*rs-bu*-unpairing) line, $\mu_{\tilde{Q}}$ is large enough that the *bu* and *rs* quarks, which have $\tilde{Q} = +1$ and $\tilde{Q} = -1$ respectively and which pair with gap parameter Δ_2, no longer pair completely: it is energetically favorable to create a new blocking region of unpaired *bu* quarks. At this $\tilde{Q}$-electrostatic potential, the CFL $\tilde{Q}$-insulator breaks down, unpaired *bu* quarks with $\tilde{Q} = +1$ are created, the free energy is no

longer $\mu_{\tilde{Q}}$-independent, and in fact the neutrality conditions and gap equations are no longer satisfied.

At the upper (*rd-gu*-unpairing) line, $\mu_{\tilde{Q}}$ is so low that the *rd* and *gu* quarks, which have $\tilde{Q} = -1$ and $\tilde{Q} = +1$ respectively and which pair with gap parameter Δ_3, no longer pair completely, and it is energetically favorable to create a new blocking region of unpaired *rd* quarks, and once again no solution is found.

At $M_s^2/\mu = 143$ MeV, which is so large that the gapless CFL phase is anyway already metastable with respect to unpaired quark matter, the two boundaries cross, meaning that no gapless CFL solution can be found.

So, in the absence of electrons, we can find stable solutions of the gap and neutrality equations everywhere between the *rs-bu* and *rd-gu* curves in Fig. 2-6. To the left of the *gs-bd* unpairing line this is the CFL phase, a $\tilde{Q}$-insulator with no gapless quasiquark modes. To the right of that line we have the gCFL phase, again a $\tilde{Q}$-insulator, in which all $\tilde{Q}$-charged modes are gapped, but there are $\tilde{Q} = 0$ gapless quasiparticles.

We now restore the electrons, setting their mass to zero. In the CFL region, the system is forced to $\mu_e = 0$ (dashed line in Fig. 2-6) [78]. However, at the transition point to gCFL, where the *gs-bd* pairs break, we find that the neutrality requirement forces us over the line where *rs-bu* pairs also begin to break. The result is that as M_s^2/μ increases further, the system maintains neutrality by staying close to the *rs-bu*-unpairing line, where there is a narrow blocking region in which there are unpaired *bu* quarks. Their charge is cancelled by a small density of electrons. We analyze this quantitatively below.

We see that real-world gCFL quark matter is a conductor of $\tilde{Q}$ charge, since it has gapless $\tilde{Q}$-charged quark modes, as well as electrons. The *rd* and *gu* quarks, which are insensitive to the strange quark mass, remain robustly paired and the $\tilde{Q}$-neutral *bd* and *gs* quarks develop a large blocking region as the system moves far beyond their unpairing line. The neutrality requirement naturally keeps the system close to the *rs-bu*-unpairing line, following the dashed line in Fig. 2-6, so these quarks have a very narrow blocking region and an almost quadratic dispersion relation (see below).

Although $U(1)_{\tilde{Q}}$ is unbroken in the gapless CFL phase, the presence of electrons and unpaired bu quarks makes this phase a $\tilde{Q}$-conductor. This is in contrast to the CFL phase, which is a $\tilde{Q}$-insulator with no gapless quasiquarks and no electrons.

The gapless quark quasiparticles occur in the gs-bd and rs-bu sectors. Since these will have a dramatic effect on transport properties, we now discuss them in greater depth.

The gs-bd sector

In a typical part of the gCFL phase space, the $\tilde{Q}$-neutral gs-bd sector is well past its unpairing line, and there is a large blocking region between momenta p_1^{bd} and p_2^{bd} at which there are gapless excitations, as shown in Fig. 2-4. In the blocking region $p_1^{bd} < p < p_2^{bd}$ there are bd quarks but no gs quarks, and thus no pairing. We have confirmed this by direct evaluation of the difference between the number density of bd and gs quarks, showing this to be equal to the volume of the blocking region in momentum space.

Note that even though there is no pairing in the ground state in the blocking region, the dispersion relations are not trivial. Because the states obtained via the two different single particle excitations that are possible (adding a gs quark or removing a bd quark) mix via the Δ_1 condensate, the two dispersion relations exhibit an "avoided crossing" between p_1^{bd} and p_2^{bd}. If we neglect the mixing among the excitations introduced by Δ_1, the gapless excitations just above (below) p_2^{bd} are bd quarks (holes) and those just above (below) p_1^{bd} are gs quarks (holes).

It may seem coincidental that the value of M_s^2/μ at which the CFL phase becomes gapless is the same as the value at which Δ_1 and Δ_2 separate in Fig. 2-1. Although we do not see a profound reason for this, it is certainly not a coincidence. The CFL→gCFL transition is triggered by the instability of the CFL phase that occurs when a gs-bd quasiparticle dispersion relation goes gapless, indicating the instability towards gs-bd unpairing and the opening up of a blocking region in momentum space, filled with unpaired bd quarks and with no gs-bd pairing. Consequently, one of the terms in the Δ_1 gap equation — that corresponding to the gs-bd block — is reduced in

magnitude because its integrand vanishes within the blocking region. This reduction in the support of the Δ_1 gap equation integrand causes Δ_1 to drop.

The "thickness" of the *bd* blocking region can be considered an order parameter for gCFL: for M_s^2/μ below the critical value there is no blocking region. Just above the critical value we can use the results of table 2.1 and (2.30) to show that

$$p_2^{bd} - p_1^{bd} \sim \Delta_1^{1/2} \left(\frac{M_s^2}{\mu} - \frac{(M_s^c)^2}{\mu} \right)^{1/2} \sim (M_s - M_s^c)^{1/2} , \tag{2.32}$$

typical behavior for a second order phase transition. Because we are analyzing a zero temperature quantum phase transition, the long wavelength physics at the critical point is 4-dimensional rather than 3-dimensional as at a finite temperature transition.

The *rs-bu* sector

As discussed above, the gCFL phase remains neutral by crossing the *rs-bu* unpairing line, and developing enough unpaired *bu* quarks to cancel the $\tilde{Q}$ charge of the electrons. The electrons contribute $(-\mu_e^4/12\pi^2)$ to the free energy, so $\tilde{Q}$-neutrality can be maintained as long as

$$n_e = \frac{\mu_e^3}{3\pi^2} = n_{bu} = \frac{(p_2^{bu})^3 - (p_1^{bu})^3}{3\pi^2} , \tag{2.33}$$

where p_1^{bu} and p_2^{bu} bound the blocking region of unpaired *bu* quarks. The condition (2.33) implies that

$$(p_2^{bu} - p_1^{bu}) = \frac{\mu_e^3}{3\bar{p}^2} \tag{2.34}$$

where $\bar{p}$ is the average of p_1^{bu} and p_2^{bu}. At $M_s^2/\mu = 80$ MeV, where $\mu_e = 14.6$ MeV at the lower curve in Fig. 2-6, this implies $(p_2^{bu} - p_1^{bu}) = 0.0046$ MeV! Indeed, in Fig. 2-4 the separation between p_1^{bu} and p_2^{bu} is invisible, and the dispersion relation appears to be quadratic about a single gapless point. To resolve the separation between p_1^{bu} and p_2^{bu}, we did calculations assuming 200 and 500 "flavors" of massless electrons. In these cases, $(p_2^{bu} - p_1^{bu}) \sim 1$ MeV and ~ 3 MeV, in very good agreement with the above argument. Returning to our world with its single electron species, because

$(p_2^{bu} - p_1^{bu})$ is so small, the value of μ_e at the true $\tilde{Q}$-neutral solution is *very* close to that given by the lower curve in Fig. 2-6. And, the gaps are *very* close to those found in a calculation done in the absence of electrons.

From Eq. (2.28), the maximum in the quasiparticle energy between the two gapless momenta is $E_{\rm max} = |\delta\mu - \Delta|$, so from (2.30) we can express this in terms of the width of the blocking region: $4(|\delta\mu| + \Delta)E_{\rm max} = (p_2 - p_1)^2$. For the *rs-bu* quarks, the blocking region is always very narrow, so $E_{\rm max} \approx (p_2^{bu} - p_1^{bu})^2/(8\Delta_2)$ which from (2.34) is a small fraction of an electron volt at $M_s^2/\mu = 80$ MeV. Thus, at any astrophysically relevant temperature, the *rs-bu* dispersion relation can be treated as quadratic about a single momentum at which it is gapless. Indeed, even at $M_s^2/\mu = 130$ MeV where the gapless CFL phase ceases to be the ground state, $\mu_e = 40.3$ MeV, $(p_2^{bu} - p_1^{bu}) \sim 0.1$ MeV and the peak of the dispersion relation between p_1^{bu} and p_2^{bu} is at about 50 eV. The requirement of $\tilde{Q}$-neutrality naturally forces this dispersion relation to be *very* close to quadratic, without requiring fine tuning to a critical point.

The *rd-gu* sector and the 3×3 *ru-gd-bs* block

In Fig. 2-5 we show the dispersion relations for the quasiparticles in the *rd-gu* sector. One of these becomes gapless at the upper boundary of the wedge in Fig. 2-6, but we have seen that in the presence of electrons, the neutral gapless CFL solution is never near this upper boundary. Therefore, these dispersion relations are always gapped, as in the figure. In Fig. 2-5 we also show the dispersion relations for the three quasiparticles from the 3×3 block. These quasiparticles carry zero $\tilde{Q}$ charge and they always have nonzero gap. Their smallest gap becomes very small near the rightmost tip of the gCFL wedge region in Fig. 2-6, but is always greater than 1 MeV in the region in which gCFL is favored.

2.3.3 The gCFL Free Energy Function

In the previous subsection, we have used the dispersion relations to delineate the unpairing lines which bound the ranges in $\mu_{\tilde{Q}}$ where, in the absence of electrons,

$\tilde{Q}$-insulator solutions are to be found and which separate the CFL and gCFL phases. Here, we sketch the behavior of the free energy Ω in the vicinity of solutions to the gap and neutrality equations, and see how this behavior changes at the unpairing lines.

In Fig. 2-7 we study the free energy in the vicinity of a gapless CFL solution not far above the CFL→gCFL transition. We have neglected electrons in making this plot; the change from including them would be invisible on the scale of the plot. We plot the free energy upon variation of gap parameters while keeping μ's fixed (dashed curves in Fig. 2-7), and we also plot the "neutral free energy" (solid curves) obtained by varying gap parameters about the solution while solving the neutrality conditions anew for each value of the gap parameters. We see that the solution is a minimum of the neutral free energy, confirming that we have succeeded in finding a stable neutral solution. However, the solution is not at a minimum of the free energy upon variation of the gap parameters while keeping μ's fixed.

We see in the top panel of Fig. 2-7 that the solution is found at a local maximum of the dashed curve describing variation of Δ_1 at fixed μ's. Shovkovy and Huang described similar behavior in the gapless 2SC case in Refs. [74, 75], and suggested that this is a characteristic of gapless superconductivity. We find this *not* to be the case: deep in the gCFL phase, at $M_s^2/\mu = 80$ MeV rather than the $M_s^2/\mu = 51.2$ MeV of Fig. 2-7, we find that the gCFL solution is a local minimum of both the dashed and the solid curves in the analogue of the top panel of Fig. 2-7. That is, we find an onset of the behavior seen in the top panel of Fig. 2-7 as we cross the CFL→gCFL transition, namely the *gs-bd* unpairing line: as a *gs-bd* blocking region begins to open up, the solution goes from being a local minimum of the dashed curve to being a local maximum. However, we find that the dashed curve does not persist in this shape as the *gs-bd* blocking region expands. The *onset* of gaplessness is characterized by a dashed curve as in the top panel of Fig. 2-7, but gaplessness itself need not be.

In the middle panel of Fig. 2-7, we find that the solution is at a point of inflection with respect to variation of Δ_2 at fixed μ's. We find that the gCFL solutions at all values of M_s^2/μ above $(M_s^2/\mu)_c$ are at points of inflection of this sort. This arises

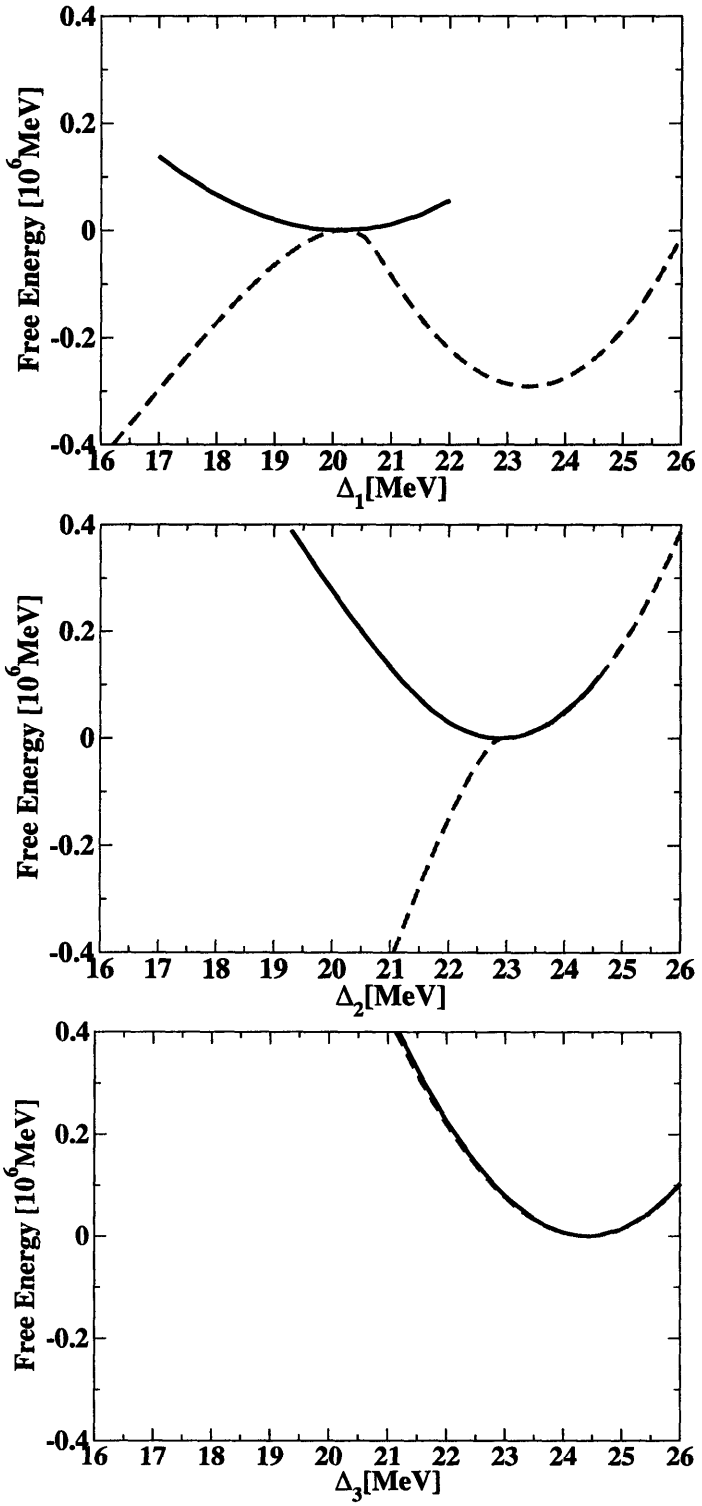

Figure 2-7: These figures show the free energy Ω in the vicinity of the gapless CFL solution for $M_s^2/\mu = 51.2$ MeV. In each panel, the dashed curve is obtained by varying one of the gap parameters (Δ_1 in the top panel, Δ_2 in the middle; Δ_3 in the bottom) while keeping the other parameters fixed. The free energies are measured relative to that of the solution. The solid curve in each panel depicts the "neutral free energy", obtained by varying one gap parameter, keeping the other gap parameters fixed, and solving the neutrality conditions anew for each point on the solid curve.

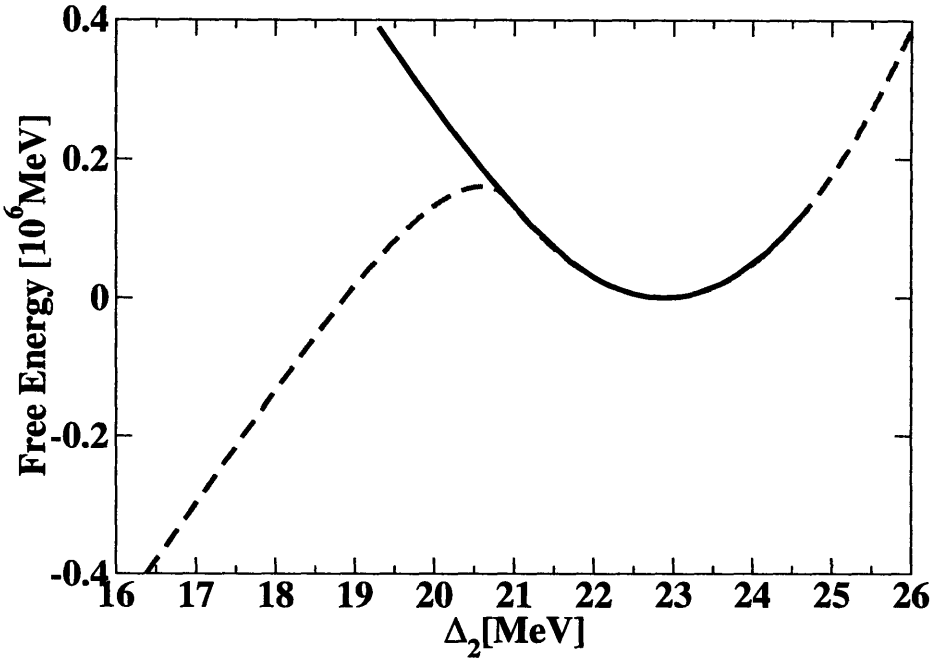

Figure 2-8: Same as the middle panel of Fig. 2-7, except that μ_e has been increased by 2 MeV while changing μ_3 and μ_8 so as to make this a shift in $\mu_{\tilde{Q}}$. This means that, neglecting electrons, we are now exploring the change of the free energy and the neutral free energy upon variation of Δ_2 about a gCFL solution that is in the interior of the wedge in Fig 2-6, rather than at its bottom boundary.

because a gCFL solution is forced by the neutrality constraint to be very close to the *bu-rs* unpairing line. In Fig. 2-8 we replot the middle panel of Fig. 2-7 after increasing μ_e by 2 MeV while varying μ_3 and μ_8 so that only $\mu_{\tilde{Q}}$ changes. This means that we have taken a 2 MeV step upwards in Fig. 2-6, away from the *bu-rs* unpairing line. And, we see that the solution is now a minimum with respect to variation of Δ_2 at fixed μ's. The point of inflection has resolved itself into a minimum and a maximum, with the solution at the minimum. Thus, the point of inflection in the dashed curve does indeed occur at the *bu-rs* unpairing line.

Note that at $M_s^2/\mu = 80$ MeV, once we have taken an upward step away from the *bu-rs* unpairing line in Fig. 2-6, obtaining the analogue of Fig. 2-8, the gapless CFL phase solution is now a local minimum of both the dashed and solid curves for variation in the Δ_1, Δ_2 and Δ_3 directions.

If we take a step in the "wrong direction" in Fig. 2-6, downwards from the *bu-rs* unpairing line, the point of inflection in the middle panel of Fig. 2-7 vanishes and the

dashed curve becomes monotonically increasing, indicating that there is no solution to the Δ_2 gap equation to be found at these values of the μ's. In the presence of electrons, the neutrality conditions are satisfied *just* below the *bu-rs* unpairing line in Fig. 2-6, and the dependence of the free energy on Δ_2 is slightly modified so that the point of inflection in the middle panel of Fig. 2-7 occurs where the neutrality conditions are satisfied. We have confirmed this in calculations done with 200 and 500 species of electrons; with a single species as in the real world, the changes in Fig. 2-7 are invisible on the scales of the plot.

Finally, with respect to variation of Δ_3, the solution is a local minimum of the dashed curve in the lower panel of Fig. 2-7. However, we have verified that if we move sufficiently upwards in Fig. 2-6 as to run into the *rd-gu* unpairing line, then the dashed curve in the lower panel exhibits a point of inflection (while that in the middle panel has a robust minimum.)

2.3.4 (Gapless) 2SC and 2SCus

In this subsection, we discuss the properties of phases in which only two of the three flavors pair. These cannot compete with the CFL and gCFL phases at low values of M_s^2/μ, but could conceivably become important at larger values (lower densities).

The Fermi momenta in cold unpaired quark matter are ordered $p_{Fd} > p_{Fu} > p_{Fs}$, since the strange quark mass tends to decrease the strange quark Fermi momentum, and the down quark Fermi momentum then increases to preserve neutrality. Thus, the likely two-flavor pairings in cold three-flavor quark matter are *u-d* pairing (i.e. 2SC, with gap parameter $\Delta_3 > 0$ and $\Delta_1 = \Delta_2 = 0$) and *u-s* pairing (i.e. 2SCus, with gap parameter $\Delta_2 > 0$ and $\Delta_1 = \Delta_3 = 0$).

Calculation

In order to find a two-flavor pairing solution, we need only solve four equations (one gap and the three neutrality equations). The other two gap equations are automatically satisfied upon setting the relevant gaps to zero. Using the same coupling

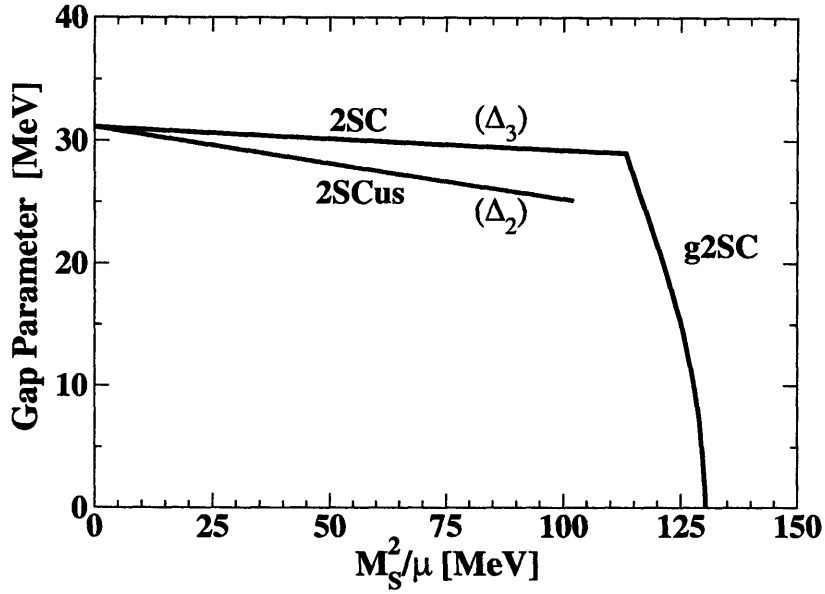

Figure 2-9: Gap parameters in 3-flavor quark matter for the 2SC phase (Δ_3) and the 2SCus phase (Δ_2). In each case the other two gaps are zero. The 2SC phase becomes gapless (g2SC) at $M_s^2/\mu > 113$ MeV and ceases to exist at $M_s^2/\mu \approx 130$ MeV, and its free energy is always lower than that of unpaired quark matter (Fig. 2-3). The 2SCus phase becomes unfavored relative to unpaired quark matter at $M_s^2/\mu > 99$ MeV, and ceases to exist at $M_s^2/\mu \approx 103$ MeV, without ever becoming gapless.

strength as in our investigation of the gCFL phase ($\Delta_0 = 25$ MeV) and working at the same value of $\mu = 500$ MeV, the nonzero gaps at $M_s^2/\mu = 0$ are $\Delta_3 = 31$ MeV in the 2SC phase and $\Delta_2 = 31$ MeV in the 2SCus phase. As we increase M_s^2/μ, as long as we do not enter a gapless phase the gaps decrease slowly and the simplified analysis of the 2SC and 2SCus phases in Ref. [46] should be a good guide. We do indeed find that our results are well approximated by $\mu_3 = \mu_8 = 0$ and $\mu_e = M_s^2/2\mu$ in the 2SC phase and $\mu_e = \mu_3 = \mu_8 = 0$ in the 2SCus phase, with a free energy given by

$$\Omega_{\substack{\text{neutral}\\ \text{2SC/2SCus}}} = \Omega_{\substack{\text{neutral}\\ \text{unpaired}}} + \frac{M_s^4 - 16\Delta_i^2\mu^2}{16\pi^2}\,, \tag{2.35}$$

with Δ_i given by Δ_3 in the 2SC phase and Δ_2 in the 2SCus phase, as predicted in Ref. [46]. The free energy of the 2SCus phase is higher than that of the 2SC phase because Δ_2 decreases more rapidly with M_s^2/μ in the 2SCus phase than Δ_3 does in

the 2SC phase. This cannot be discovered by the methods of Ref. [46], in which these two phases were treated as degenerate.

Our results for the gap parameters are shown in Fig. 2-9 and for the free energies in Fig. 2-3. As in our other figures, we vary M_s keeping μ fixed at 500 MeV.

2SC/g2SC Results

We find a neutral 2SC solution at low M_s^2/μ, with four gapped quasiparticles. At $M_s^2/\mu \approx 113$ MeV two of these quasiparticles become gapless, with blocking regions within which there are unpaired rd and gd quarks, and there is a continuous transition to the gapless 2SC (g2SC) phase. (Gapless 2SC was introduced in two-flavor quark matter in Refs. [74, 75].) The gap parameter then decreases rapidly until it reaches zero at $M_s^2/\mu \approx 130$ MeV and the solution ceases to exist.

As is clear from Fig. 2-3, 2SC/g2SC always has lower free energy than unpaired quark matter, and usually has higher free energy than CFL/gCFL. However, we find a tiny window of M_s^2/μ less than 1 MeV wide, very close to 130 MeV, in which the gapless 2SC phase has lower free energy than gCFL. In this regime, the one nonzero gap in the g2SC phase is almost zero whereas all three gaps are nonzero in the gCFL phase. This indicates that the fact that the gCFL free energy crosses that of unpaired quark matter almost at the same point where the g2SC and unpaired free energies come together is a nongeneric feature of our model. Taken literally, our calculation predicts that as M_s^2/μ increases, gCFL is supplanted by g2SC which is then almost immediately supplanted by unpaired quark matter. However, as we shall see in Chapter 3, treating the effects of M_s more accurately than we have may shut the tiny g2SC window completely. In contrast, treating M_s as a chemical potential shift, as we have in this chapter, but using $\Delta_0 = 100$ MeV appears to open a wide g2SC window [27], but this occurs in a regime where $M_s \sim \mu$ and so this result is not trustworthy. Also, as we discuss in the next section, a more general ansatz is required once one is at a sufficiently large M_s^2/μ that the free energy of the gCFL phase is close to that of unpaired quark matter, since there are other possible pairing patterns that likely become favorable.

Finally, it is interesting to note that the 2SC solution in three-flavor quark matter differs from its two-flavor version, which requires a large μ_e for neutrality given that there are no strange quarks present to carry negative charge. In three-flavor quark matter, we find that at $M_s = 0$ there is a small positive μ_e and a small negative $\mu_8 = -\mu_e$ in the 2SC phase. This happens because the pairing of ru, rd, gu and gd quarks increases their number density. This contributes a positive electric charge and excess redness/greenness, which is compensated by a small positive μ_e and a negative μ_8. As we increase M_s^2/μ, the small μ_8 remains approximately unaffected whereas the small μ_e due to pairing is rapidly swamped by the larger contribution of order $M_s^2/2\mu$ that compensates for the lack of strange quarks.

2SCus results

We find a neutral 2SCus solution, with a gap Δ_2 that decreases with increasing M_s^2/μ as shown in Fig. 2-9. This solution only exists for $M_s^2/\mu < 103$ MeV, and has a higher free energy than that of neutral unpaired quark matter for $M_s^2/\mu > 99$ MeV (see Fig. 2-3). It is always unfavored relative to the CFL/gCFL phase.

It is striking that two-flavor u-s pairing, unlike the two-flavor u-d pairing discussed above, has no gapless phase. In our calculations, we find that at $M_s^2/\mu > 103$ MeV, when the 2SCus phase becomes unstable to unpairing (i.e. when $\delta\mu_{\rm eff}$ in the u-s sector, line 2 of table 2.1, becomes as large as Δ_2), there is no neutral solution with a smaller value of Δ_2 (other than unpaired quark matter). We do find such a "gapless 2SCus" solution in a range of M_s^2/μ below 103 MeV, with Δ_2 smaller than that in the 2SC solution at the same M_s^2/μ, but the g2SCus solution is unstable: it is a local maximum of the neutral free energy as a function of Δ_2. (In a figure like Fig. 2-7 this g2SCus solution would be at a local maximum of the *solid* curve.) At $M_s^2/\mu = 103$ MeV, the g2SCus solution (local maximum) meets the 2SCus solution (local minimum) at an inflection point of the neutral free energy, and for $M_s^2/\mu > 103$ MeV neither 2SCus nor g2SCus solutions exist. Unlike the gapless 2SC phase [74, 75] and the gapless CFL phase [24], which are rendered stable by the constraint of neutrality, the gapless 2SCus phase remains unstable. This is presumably because u-s paired

phases are very close to being neutral anyway (only very small values of μ_e, μ_3, μ_8 are required to achieve neutrality [46]), so the constraint does not change the physics much. This can be summarized by saying that the 2SCus phase behaves analogously to that studied by Sarma [83], even after neutrality constraints are imposed.

2.3.5 Mixed Phase Alternatives

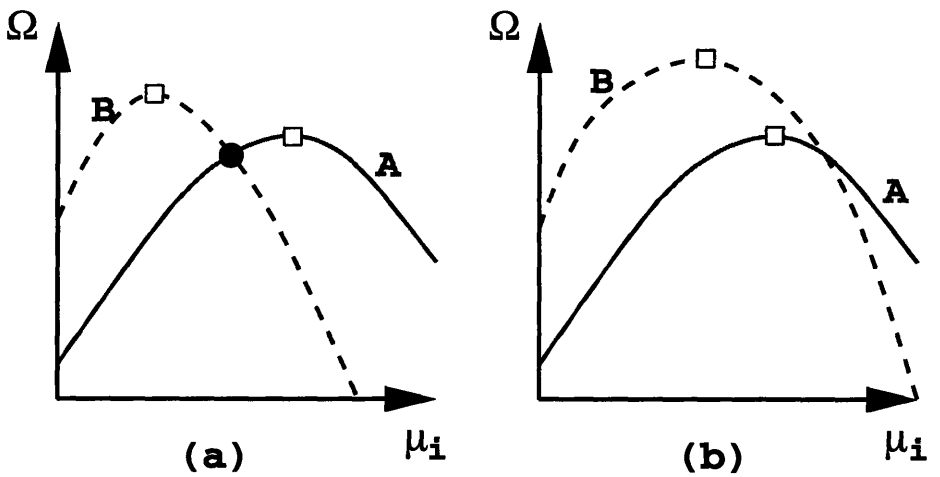

Figure 2-10: Schematic illustration of conditions for the occurrence of mixed phases. Free energy Ω for two phases A and B is shown as a function of some chemical potential μ_i. Charge $Q_i = -\partial\Omega/\partial\mu_i$ is given by the slope. Squares mark the neutral points. Panel (a): at the neutral point for each phase, the other phase has lower free energy, so there is a point (black dot) where the two phases can coexist with the same pressure and opposite charge, with lower free energy than either neutral phase. Depending on Coulomb and surface energy costs, a mixed phase may exist there. Panel (b): phase B has higher free energy than phase A at the point where A is neutral. At no point do the two phases coexist with opposite charge, so no mixed phase is possible.

Up to this point, the phases we have discussed have been locally neutral with respect to all gauge charges. However, it is well known that neutrality can also be achieved in an averaged sense, by charge separation into a mixture of two oppositely charged phases. This is shown schematically in Fig. 2-10, which shows generic free energy curves $\Omega(\mu_i)$ for two phases A and B. The free energy must be a concave function of the chemical potential, since increasing μ_i increases the charge $Q_i = -\partial\Omega/\partial\mu_i$. There are then two possible situations. In one Fig. 2-10(b) there is no

coexistence point and hence no mixed phase is possible. In the other Fig. 2-10(a) there is a coexistence point of oppositely-charged phases, and its free energy is lower than that of either neutral phase, so if Coulomb and surface energy costs are low enough then a neutral mixed phase will be free-energetically preferred over either homogeneous neutral phase.

We now consider possible gCFL+unpaired mixed phases. (Note that for $(M_s^2/\mu) > (M_s^2/\mu)_c$ a CFL+unpaired mixture is not possible because there is no CFL solution, charged or neutral.) For the unpaired and gCFL phases, the free energies are of the form shown in Fig. 2-10a. At the values of (μ_e, μ_3, μ_8) that make one phase neutral, the other phase has lower free energy. Thus there is a value of (μ_e, μ_3, μ_8) "between" that for neutral gCFL and that for neutral unpaired quark matter, where the two can coexist with opposite color and electric charge density. However, a mixed phase is not favored in this case because each component would have net color charge, and color is a gauge symmetry with a strong coupling constant, so this mixed phase would pay a huge price in color-Coulomb energy. (For similar arguments applied to systems with no gauge symmetries, where the initial conclusion that a mixed phase is favored is the correct one, see Refs. [87, 88].)

It is then natural to ask whether one could construct a gCFL+unpaired mixed phase whose components are electrically charged, but color neutral. This avoids the large color-Coulomb energy cost of mixed phases with colored components. Such mixed phases have recently been constructed in two-flavor quark matter, with unpaired and 2SC components [89]. There is still some color electric field (and color-charged boundary layers) at the interfaces where the color chemical potentials change rapidly as one travels from one component to the other, analogous to the charged boundary layers and ordinary electric field at the CFL/nuclear interface constructed in Ref. [90], but Ref. [89] finds that the 2SC + unpaired mixed phase does occur in two-flavor quark matter. However, for color neutral unpaired and gCFL phases, we have found that the situation is typically that of Fig. 2-10(b): the free energy of color neutral, but electrically charged, unpaired quark matter is typically *higher* than the free energy of color-neutral gCFL, at the value of μ_e where color-neutral gCFL is

electrically neutral. Hence there is no value of μ_e at which oppositely charged phases can coexist. We have found that this is true for all values of M_s^2/μ except for a range of a few MeV just below $M_s^2/\mu = 130$ MeV, where the neutral gCFL and neutral unpaired free energies cross. There, a mixed phase may arise, although it may be superseded by other more favorable possibilities.

We now examine some other possibilities for mixed phases. In the case of a possible 2SC+2SCus mixed phase, we find the situation of Fig 2-10(a): a neutral mixed phase exists. However, its free energy is higher than that of gCFL even before electrostatic and surface energy costs are included. At $M_s^2/\mu = 80$ MeV, it has $\Omega = -14.93 \times 10^6$ MeV^4, vs. $\Omega_{\rm gCFL} = -18.01 \times 10^6$ MeV^4. (These free energies are both measured relative to that of neutral unpaired quark matter.) We have checked that a neutral 2SC+2SCus mixed phase is also free-energetically unfavored relative to homogeneous gCFL at $M_s^2/\mu = 51.2$ MeV, which is just above the CFL→gCFL transition.

In the case of a gCFL+2SCus mixed phase, we find that the μ_e dependence of the free energies of these two phases is as in Fig 2-10(b), so a mixed phase is not possible. We have verified this at $M_s^2/\mu = 51.2$ MeV and 80 MeV.

Finally we investigate the possibility of a gCFL+2SC phase. At $M_s^2/\mu = 51.2$ MeV we find the situation of Fig. 2-10(b), so no mixed phase is possible. At $M_s^2/\mu = 80$ MeV, the free-energy dependence is of the type shown in Fig. 2-10(a), so a mixed phase is possible, and since gCFL itself is one of the components its free energy is necessarily lower than that of neutral gCFL. However, $\Omega_{gCFL}(\mu_e)$ depends *very* weakly on μ_e: the $\Omega_{gCFL}(\mu)$ parabola is very shallow. This suppresses the mixed phase in two ways. (i) the free energy of the mixed phase is only lower than that of neutral gCFL by a very small margin (0.0012×10^6 MeV^4 at $M_s^2/\mu = 80$ MeV), so there is very little chance that it will survive once electrostatic and surface costs are included; (ii) The charge density of gCFL, proportional to $\partial\Omega/\partial\mu_e$, is very small so the mixed phase must be dominantly gCFL, with a tiny admixture of 2SC, to achieve neutrality. It is known that such highly asymmetric mixed phases have the highest electrostatic energy costs[90].

We have not eliminated all conceivable mixed phase constructions, involving mixtures of all possible phases. However, over most of the gCFL regime there can be no mixed phase constructed from gCFL and unpaired quark matter, or gCFL and 2SC, or gCFL and 2SCus, or 2SC and 2SCus.

2.4 Concluding Remarks and Open Questions

The gapless CFL phase seems sufficiently well-motivated as a possible component of compact stars to warrant further study of its low energy properties and its phenomenological consequences: it is the phase that supplants the asymptotic CFL phase as a function of decreasing density, and compact stars are certainly far from asymptotically dense.

The low energy effective theory of the gCFL phase must incorporate the gapless fermionic quasiparticles with quadratic dispersion relations, which have number densities $\sim \mu^2\sqrt{\Delta_2 T}$ and dominate the low temperature specific heat, the gapless quarks with linear dispersion relations, with number densities $\sim \mu^2 T$, and the electron excitations, with number density $\sim \mu_e^2 T$. In contrast, the (pseudo-)Goldstone bosons present in both the CFL and gCFL phases have number densities at most $\sim T^3$. This means the gCFL phase has very different phenomenology from CFL. As we shall show in Chapter 4, the cooling of a compact star with a gCFL core is particularly interesting because neutrino emission requires conversion between quasiparticles with linear and quadratic dispersion relations. We shall argue that in a star with CFL, gCFL and nuclear volume fractions, the gCFL shell will dominate the total heat capacity and the total neutrino emissivity, and that the presence of gCFL matter in the star has phenomenological implications. It will be also interesting to work out the magnetic field response of the gCFL phase, since the gauge boson propagators will be affected both by the gapless quasiparticles (all nine gauge bosons) and by the condensate (Meissner effect for eight out of nine.) Finally, we have left the study of possible meson condensation in the gapless CFL phase to future work.

Although we have studied the gCFL phase in a model, all of the qualitative prop-

erties of this phase that we have focussed on appear robust. We have also offered a model-independent argument for the instability that causes the transition, and for the location of the transition. We have used our model to show that the gCFL phase is favored over the two-flavor-pairing phases (2SC, g2SC, and 2SCus) throughout almost all of the regime where the gCFL phase is favored over unpaired quark matter. It remains a possibility, however, that the CFL gap is large enough that baryonic matter supplants the CFL phase before $M_s^2/\mu > 2\Delta$. Assuming that the gCFL phase does replace the CFL phase, it is also possible that gaps are small enough that a third phase of quark matter could supplant the gCFL phase at still lower density, before the transition to baryonic matter. We do not trust our analysis to determine this third phase. Perhaps it is a mixed phase of some sort, although we have ruled out the straightforward possibilities. Perhaps it is the gapless 2SC phase [74, 75], as the literal application of our model would suggest. We should stress, in addition, that our model relies upon a pairing ansatz designed to study the instability of the CFL phase, and hence well-suited to the study of the gCFL phase. Determining what phase comes after gCFL almost certainly requires a more general ansatz. For example, perhaps weak pairing between quarks with the same flavor plays a role once gCFL is superseded [52], or perhaps it is the crystalline color superconducting phase [56, 57, 60, 79, 91] that takes over from gapless CFL at lower densities. (Other possibilities have also been suggested [92].)

Recent developments [91] make the crystalline color superconducting phase look like the most viable contender for the "third-from-densest phase". Previous work [60] had suggested that the face-centered-cubic crystal structure was sufficiently favorable that its free energy could be competitive with that of BCS pairing over a wide range of parameter space, but because these indications came from a Ginzburg-Landau calculation pushed beyond its regime of validity, quantitative results were not possible. The results of Ref. [91] suggest that a crystalline phase involving pairing of only two flavors is favored over the unpaired phase by $\approx 0.2\mu^2\Delta_{2SC}^2/\pi^2$ at $M_s^2/\mu \approx 4\Delta_{2SC}$. Here, Δ_{2SC} is the gap parameter in the 2SC phase at $M_s = 0$, which is 31 MeV with the parameter values we have used in all our figures. This suggests that if we were to

generalize our pairing ansatz to allow the crystalline phase as a possibility, it would take over from gCFL at $M_s^2/\mu \sim 120$ MeV, or even somewhat lower if the three-flavor crystalline phase, which no one has yet constructed, is more favorable than the two-flavor version. Furthermore, the authors of Ref. [91] find that the crystalline phase persists until a first order crystalline→unpaired transition at $M_s^2/\mu \approx 7.5\Delta_{2SC}$, hence over a very wide range of densities. If analysis of three-flavor crystalline color superconductivity supports these estimates, we will not have to worry about the resolution of the puzzles and possible mixed phases associated with the confluence of the free energies for the gCFL, g2SC and unpaired phases near $M_s^2/\mu \sim 130$ MeV in Fig. 2-3. By that density the crystalline phase will already be robustly ensconced on the phase diagram.

Chapter 3

Heating (Gapless) Color-Flavor Locked Quark Matter

3.1 Overview

In Chapter 2 we showed that at zero temperature the CFL phase breaks down as we reduce the density and a new phase (gCFL) emerges. In particular, we argued that as we go to lower densities and M_s becomes significant relatively to the baryon chemical potential, the CFL stops to exist. A mismatch in the Fermi surfaces of the different quarks drives this transition. The emergence of gCFL is dictated by the neutrality conditions and the minimazation of the free energy. However we treated the effect of the strange quark mass M_s as a shift in the chemical potential of the strange quarks. In this chapter we treat the effect of M_s without making this approximation. As we shall show, our approximation in Chapter 2 is fully justified. Furthermore, in the previous chapter we restricted our analysis to zero temperature. The main goal in this chapter is to map the phase diagram of neutral dense quark matter at nonzero temperature, answering the question of what phases and phase transitions result when CFL or gCFL quark matter is heated. In the case of CFL quark matter with strange quark mass $M_s = 0$, this question has been answered in Ref. [93]. In this most symmetric setting, there is a single phase transition at a temperature $T_c^{\rm CFL}$ below which there is CFL pairing and above which there is no pairing. In mean field

theory,

$$T_c^{\rm CFL} = 2^{\frac{1}{3}} \frac{e^\gamma}{\pi} \Delta_0 \ , \tag{3.1}$$

where Δ_0 is the CFL gap parameter at $T = 0$, estimated to be of order 10 to 100 MeV. [34–36, 63, 64] The enhancement of T_c/Δ_0 by a factor of $2^{1/3}$ over the standard BCS value (which our results confirm) originates in the fact that in the CFL phase with $M_s = 0$ there are eight fermionic quasiparticles with gap Δ_0 and one with gap $2\Delta_0$ [93]. As at any phase transition at which a superconducting order parameter melts, gauge field fluctuations that are neglected in mean field theory can elevate T_c and render the transition first order [94]. Because the gauge coupling in QCD is strong, these effects are significant [95, 96]. They have been evaluated to date only at $M_s = 0$ [95, 96]. Once $M_s \neq 0$, the mean field analysis alone becomes rather involved and we shall therefore leave the inclusion of fluctuations to future work.

To see why $M_s \neq 0$ results in an intricate phase diagram at nonzero temperature, we must recall the pairing ansatz that we used in the previous chapter

$$\langle \psi_a^\alpha C\gamma_5 \psi_b^\beta \rangle \sim \Delta_1 \epsilon^{\alpha\beta 1}\epsilon_{ab1} + \Delta_2 \epsilon^{\alpha\beta 2}\epsilon_{ab2} + \Delta_3 \epsilon^{\alpha\beta 3}\epsilon_{ab3} \tag{3.2}$$

As we mentioned before the gap parameters Δ_1, Δ_2 and Δ_3 describe down-strange, up-strange and up-down Cooper pairs, respectively. At $T = 0$, we argued that there is an insulator-metal transition at $M_s^2/\mu \simeq 2\Delta_1$, at which the CFL insulator with $\Delta_3 \simeq \Delta_2 = \Delta_1$ is replaced by the gapless CFL metal, which has $\Delta_3 > \Delta_2 > \Delta_1 > 0$ [24, 25]. (If the CFL phase is augmented by a K^0-condensate [41], the CFL→gCFL transition is delayed to $M_s^2/\mu \simeq 8\Delta_1/3$ [81]). An analogous zero temperature metal insulator transition has been analyzed in Ref. [82].

At $M_s = 0$, $\Delta_1 = \Delta_2 = \Delta_3 = \Delta_{\rm CFL}$, and $\Delta_{\rm CFL}$ decreases from Δ_0 at $T = 0$ to 0 at $T_c^{\rm CFL}$. As soon as $M_s \neq 0$, however, we can expect that Δ_1, Δ_2 and Δ_3 do not all vanish at the same temperature. This expectation is evident for the gCFL phase, which has $\Delta_3 > \Delta_2 > \Delta_1 > 0$ already at $T = 0$. We shall see that it also applies to the CFL phase with $M_s \neq 0$.

The distinction between an insulator and a metal is sharp only at $T = 0$. At

any nonzero temperature, there will be some nonzero density of thermally excited fermionic quasiparticles, some of which are charged. This means that the CFL→gCFL "transition" should be a crossover at any nonzero temperature [27]. The CFL phase at $T = 0$ with $M_s \neq 0$ has fermionic quasiparticles with opposite charges whose excitation energies differ. This means that upon heating this phase, the chemical potentials needed to maintain neutrality are not the same as at zero temperature. Adjusting the chemical potentials feeds back into the gap equations for Δ_1, Δ_2 and Δ_3 differently, and these gap parameters can therefore have different T-dependence. If we start in the CFL phase at $T = 0$, heat, then increase M_s^2/μ above that for the zero temperature CFL→gCFL transition, and then cool back to $T = 0$ we can go from CFL to gCFL without ever crossing a phase boundary. We illustrate this by showing an example phase diagram in Fig. 3-1.

The purpose of this chapter is to derive and understand the phase diagram of Fig. 3-1. We shall present the model and approximations that we use in Section 3.2. We follow the conventions for naming phases used in previous literature:

$\Delta_1, \Delta_2, \Delta_3 \neq 0$	(g)CFL
$\Delta_1 = 0, \quad \Delta_2, \Delta_3 \neq 0$	uSC
$\Delta_2 = 0, \quad \Delta_1, \Delta_3 \neq 0$	dSC
$\Delta_1 = \Delta_2 = 0, \quad \Delta_3 \neq 0$	(g)2SC
$\Delta_1 = \Delta_2 = \Delta_3 = 0$	UQM,

with "UQM" meaning unpaired quark matter. The origin of the remaining names is that in the 2SC phase, only quarks of two flavors and two colors pair, whereas in the uSC (or dSC) phase, all u (or all d) quarks pair [97]. All these phases except (g)CFL may be augmented by spin-1 condensates that pair quarks of the same flavor, but these inevitably lead to gaps that are much smaller than those we shall consider [52] and so we shall neglect these modifications to the 2SC, uSC and dSC phases. The phase diagram features three lines denoting second order phase transitions at which Δ_1, Δ_2 or Δ_3 vanish. At $M_s = 0$, all three gaps vanish at the same temperature

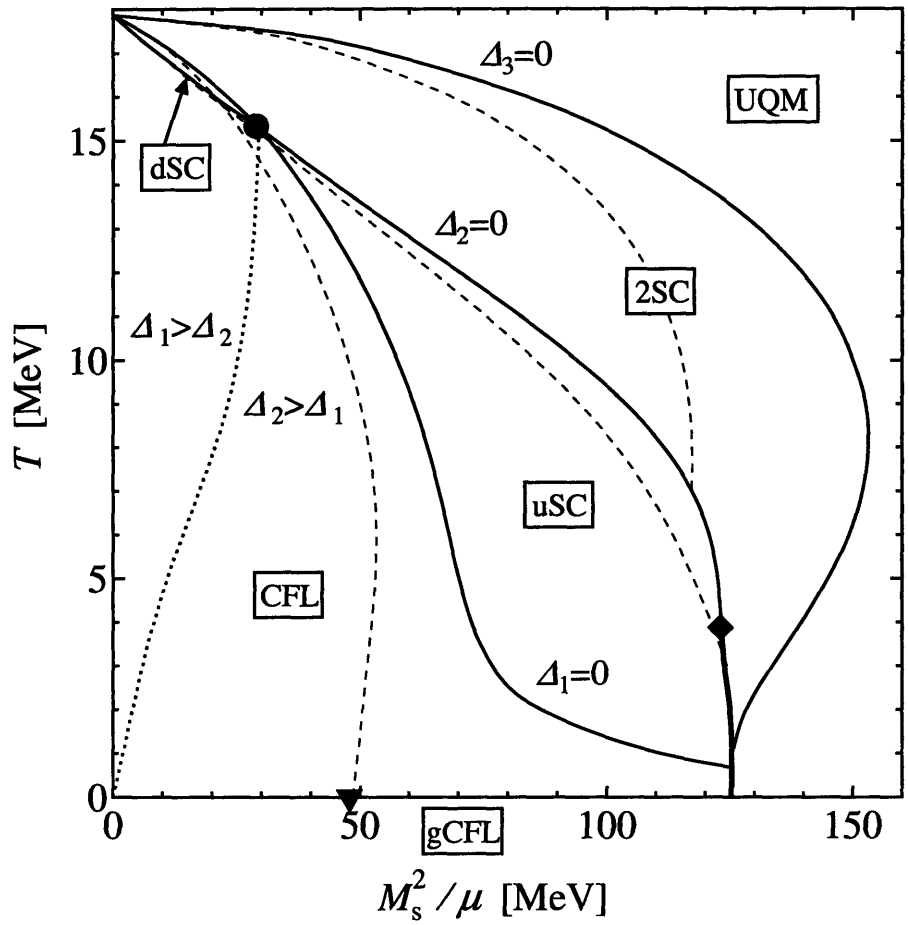

Figure 3-1: Phase diagram of dense neutral quark matter in the $(M_s^2/\mu, T)$ plane. Only the solid curves represent phase transitions. The thin solid curves denote mean field second order phase transitions at which Δ_1 or Δ_2 or Δ_3 vanish. Two of these lines cross at the circle, which we call a "doubly critical" point. The heavy solid line is a first order phase transition that ends at a tricritical point denoted by the diamond. The dashed curves indicate locations where, as M_s^2/μ is increased, new gapless modes appear. At any nonzero temperature, however, there is no physical distinction between a phase with truly gapless modes and one in which the same modes have excitation energies of order T. The dashed curves therefore have physical significance only where they cross $T = 0$. In this phase diagram, this occurs only at the triangle, which denotes the zero temperature CFL→gCFL transition, which is a quantum critical point. The dotted line separates the $\Delta_1 > \Delta_2$ and $\Delta_2 > \Delta_1$ regions. This phase diagram is drawn for $\mu = 500$ MeV, with M_s and T varying, and with the quark-quark interaction strength fixed and chosen such that the CFL gap is $\Delta_0 = 25$ MeV at $T = 0$. We shall describe the model and approximations within which this phase diagram has been obtained in Section 3.2, and describe the results summarized by this diagram in Sections 3.3 and 3.4.

but at generic values of M_s, there are three distinct transition temperatures. Two of these lines cross at a point denoted by the circle: at this "doubly critical point", Δ_1 and Δ_2 vanish at the same temperature. The phase diagram is intricate, and one natural question is to what extent its features are generic. We address this by varying parameters, as we shall discuss in Sections 3.3 and 3.4. We shall find that the physics at large M_s^2/μ, where we find a first order phase transition in Fig. 3-1, is not generic, changing qualitatively for larger values of Δ_0. We find that the shape of the second order phase boundaries separating the CFL, dSC, uSC and 2SC phases is generic, as is the existence of the doubly critical point.

Physics in the vicinity of any of these phase transitions can be analyzed using a Ginzburg-Landau approximation, in which the relevant Δ or Δ's are taken to be small. This analysis has been performed at $M_s = 0$ in Refs. [69, 95, 98] and at small but nonzero M_s in Ref. [97]. We shall show in Section 3.6 that our numerical results for the three phase transition lines at small $M_s^2/\mu\Delta_0$ are in quantitative agreement with the Ginzburg-Landau approximation, and shall show that the ratios of coefficients in the Ginzburg-Landau potential that we obtain in our model agree quite well with those obtained in full QCD at higher densities. At small $M_s^2/\mu\Delta_0$, the region of the phase diagram where the Ginzburg-Landau analysis applies near T_c, Δ_2 vanishes at a lower critical temperature than Δ_1. In heating gCFL quark matter, however, we expect Δ_1 to vanish first because it is already much smaller at $T = 0$. Our model analysis can be extended to larger M_s and smaller T than the Ginzburg-Landau analysis, allowing us to see how the phase diagram fits together, consistent with this expectation.

A phase diagram similar to ours was obtained previously in Ref. [27], but our results differ in a crucial, qualitative respect at low M_s^2/μ, where we believe that our results are robust: the authors of Ref. [27] found that Δ_1 always vanishes at a lower temperature than Δ_2, meaning that there is no dSC region on their phase diagram. This also disagrees with the Ginzburg-Landau analysis [1]. We shall detail our approximations in Section 3.2, but we note already here that whereas in Refs. [24, 25, 27]

[1] We have learned from them in private communications that the authors of Ref. [27] now find an ordering of phase transitions in agreement with our results and the Ginzburg-Landau analysis.

M_s was assumed to be much smaller than μ, we do not make such an approximation. This likely explains the differences between our results and those of Ref. [27] at large M_s^2/μ.

Although not associated with a phase transition, it is interesting to ask *how* the CFL phase ceases to be an insulator as it is heated. This must happen, given the phase diagram that we and the authors of Ref. [27] find, but how? At small T, the number density of charged quark quasiparticles in the CFL phase is exponentially small. Because of the interplay between $M_s \neq 0$ and the constraints of neutrality, the excitation energies of oppositely charged quasiparticles are not the same and these thermally excited quasiparticles have a net charge which must be balanced by a nonzero electron density of order μ_e^3, where μ_e is the electron chemical potential. Because the quasiparticle densities are proportional to the quark Fermi surface area $\sim \mu^2$, where $\mu \gg \mu_e$, we show that μ_e ceases to be exponentially suppressed – rising rapidly to $\mu_e \sim M_s^2/4\mu$ – in an insulator-metal crossover that occurs in a narrow, and quite low, range of temperatures. We describe this crossover analytically in Section 3.5. There are other charged excitations in the CFL phase, namely the pseudo-Nambu-Goldstone bosons, coming from the breaking of chiral symmetries. These bosons acquire masses [10, 34–36, 47, 63, 64, 99–101] and furthermore the CFL condensate may rotate in the K^0-direction within the manifold describing these mesons [41]. We neglect the possibility of K^0-condensation throughout. We shall see in Section 3.5.1 that this corresponds to assuming that the instanton contribution to the K^0 mass is comparable to Δ_0 [101, 102], which is likely the case for all but the largest Δ_0 that we consider. We must also consider the thermally excited pseudo-Nambu-Goldstone bosons, but we show in Section 3.5.1 that their effects are negligible.

In Section 3.2 we detail our model and approximations, stressing also those approximations used in Chapter 2 that we have not made. In Section 3.3, we review results at $T = 0$. In Section 3.4, we present our results at $T \neq 0$, analyzing the phase diagram in Fig. 3-1 and that for other values of Δ_0. In Section 3.5, we analyze the insulator-metal crossover that occurs when the CFL phase is heated. In Section 3.6, we make the connection between our work and the Ginzburg-Landau

analysis quantitative. We conclude in Section 3.7.

3.2 Model and Approximations

3.2.1 A Model for the Thermodynamic Potential

We are interested in physics at non-asymptotic densities, and we cannot use weak-coupling methods. Therefore, in this chapter we shall use the same Nambu–Jona-Lasinio (NJL) and the same pairing ansatz as in Chapter 2. The partition function and the free energy are defined by (2.9). The derivation of the free energy follows the steps from (2.9) to (2.18). However in this chapter we are going to consider non-zero temperature. In addition we make fewer approximations and we consider several coupling strengths for the 4-point interaction. If we denote the CFL gap at $M_s = T = 0$ by Δ_0, we consider three different coupling strengths that correspond to $\Delta_0 = 25, 40, 100$ MeV. If we perform the Matsubara summation in (2.17), using the identity (2.18), the free energy can be written as

$$\Omega = -\frac{1}{4\pi^2}\int_0^\Lambda dp\, p^2 \sum_j \Big\{ |\varepsilon_j(p)| + 2T \ln\big(1 + \mathrm{e}^{-|\varepsilon_j(p)|/T}\big) \Big\} + \frac{1}{G}\big(\Delta_1^2+\Delta_2^2+\Delta_3^2\big) - \frac{\mu_e^4}{12\pi^2} - \frac{\mu_e^2 T^2}{6} - \frac{7\pi^2 T^4}{180}\,, \tag{3.3}$$

where the electron contribution for $T \neq 0$ has been included. The functions $\varepsilon_j(p)$ are the dispersion relations for the fermionic quasiparticles. They are not explicitly T-dependent, but they do depend on the Δ's and μ's which are T-dependent. As we mentioned before the quasiquark dispersion relations $\varepsilon_j(p)$ are the values of the energy at which the propagator diverges,

$$\det S^{-1}(-i\varepsilon_j(p), p) = 0\,. \tag{3.4}$$

Here, the inverse propagator S^{-1} is the 72×72 matrix

$$S^{-1}(p) = \begin{pmatrix} \not{p} + \not{\mu} - \boldsymbol{M} & P_\eta \Delta_\eta \\ \bar{P}_\eta \Delta_\eta & (\not{p} - \not{\mu} + \boldsymbol{M})^T \end{pmatrix} \tag{3.5}$$

that acts on Nambu-Gor'kov spinors

$$\Psi = \begin{pmatrix} \psi(p) \\ \bar{\psi}^T(-p) \end{pmatrix}, \quad \bar{\Psi} = \begin{pmatrix} \bar{\psi}(p) & \psi^T(-p) \end{pmatrix} . \tag{3.6}$$

The sum in (3.3) is understood to run over 36 roots, because the Nambu-Gor'kov formalism has artificially made each $|\varepsilon_j|$ doubly degenerate. There is a further (physical) degeneracy coming from spin, meaning that there are only 18 distinct dispersion relations to be found. The free energy of any solution to the gap equations obtained from this mean field free energy is the same as that obtained from the Cornwall-Jackiw-Tomboulis effective potential [103], with the mean field approximation implemented via keeping the double bubble diagram and dropping all other 2PI diagrams.

We shall evaluate Ω numerically, meaning that at every value of the momentum p we must find the zeros of the inverse propagator. In order to do this numerically, we follow Ref. [72] and note that it is equivalent and faster to find the eigenvalues of the "Dirac Hamiltonian density" $\mathcal{H}(p)$, which is related to S^{-1} by

$$\det S^{-1}(p_4, p) = \det\left[\gamma^4 \left(i p_4 - \mathcal{H}(p)\right)\right] , \tag{3.7}$$

which makes it clear that eigenvalues of $\mathcal{H}(p)$ are zeros of S^{-1}. Like S^{-1}, the Dirac Hamiltonian $\mathcal{H}(p)$ is a 72×72 matrix in color, flavor, spin, and Nambu-Gor'kov space. This matrix can be decomposed into 4 blocks – three 16×16 matrices for the $(rd\text{-}gu)$, $(rs\text{-}bu)$ and $(gs\text{-}bd)$ pairing sectors, and one 24×24 matrix for the $(ru\text{-}gd\text{-}bs)$ sector. The absolute values of the eigenvalues are quadruply degenerate due to the Nambu-Gor'kov doubling and the spin degeneracy.

We have found considerably simpler expressions for the $(rd\text{-}gu)$, $(rs\text{-}bu)$ and $(gs\text{-}bd)$ sectors. The calculation becomes easier if one adopts a different choice of Nambu-

Gor'kov basis, i.e. $\Psi = (\psi(p), C\bar{\psi}^{\mathrm{T}}(-p))^{\mathrm{T}}$ as in Ref. [71]. Then the Nambu-Gor'kov and spin degeneracies are manifest, as the 16×16 matrix separates into 4×4 blocks with the form

$$\mathcal{H}_{(gs\text{-}bd)} = \begin{pmatrix} -\mu_{bd} & p & 0 & i\Delta_1 \\ p & -\mu_{bd} & -i\Delta_1 & 0 \\ 0 & i\Delta_1 & \mu_{gs}+M_s & p \\ -i\Delta_1 & 0 & p & \mu_{gs}-M_s \end{pmatrix} \tag{3.8}$$

for the (*gs-bd*) sector and likewise for other sectors. Each of the 4 eigenvalues of this matrix, and of its counterparts for the other sectors, contributes twice (for spin) in the sum in (3.3). The quark chemical potentials occurring in (3.8) and below are defined straightforwardly:

$$\begin{aligned} \mu_{ru} &= \mu - \tfrac{2}{3}\mu_e + \tfrac{1}{2}\mu_3 + \tfrac{1}{3}\mu_8, \\ \mu_{gd} &= \mu + \tfrac{1}{3}\mu_e - \tfrac{1}{2}\mu_3 + \tfrac{1}{3}\mu_8, \\ \mu_{bs} &= \mu + \tfrac{1}{3}\mu_e - \tfrac{2}{3}\mu_8, \\ \\ \mu_{rd} &= \mu + \tfrac{1}{3}\mu_e + \tfrac{1}{2}\mu_3 + \tfrac{1}{3}\mu_8, \\ \mu_{gu} &= \mu - \tfrac{2}{3}\mu_e - \tfrac{1}{2}\mu_3 + \tfrac{1}{3}\mu_8, \\ \\ \mu_{rs} &= \mu + \tfrac{1}{3}\mu_e + \tfrac{1}{2}\mu_3 + \tfrac{1}{3}\mu_8, \\ \mu_{bu} &= \mu - \tfrac{2}{3}\mu_e - \tfrac{2}{3}\mu_8, \\ \\ \mu_{gs} &= \mu + \tfrac{1}{3}\mu_e - \tfrac{1}{2}\mu_3 + \tfrac{1}{3}\mu_8, \\ \mu_{bd} &= \mu + \tfrac{1}{3}\mu_e - \tfrac{2}{3}\mu_8 \ . \end{aligned} \tag{3.9}$$

In the (*ru-gd-bs*) sector, we could not find any simple way to make the spin degeneracy manifest, but the Nambu-Gor'kov degeneracy is manifest as the 24×24 matrix separates into 12×12 blocks with the form

$$\mathcal{H}_{(ru\text{-}gd\text{-}bs)} = \begin{pmatrix}
-\mu_{ru} & p & 0 & -i\Delta_3 & 0 & -i\Delta_2 & 0 & 0 & 0 & 0 & 0 & 0 \\
p & -\mu_{ru} & i\Delta_3 & 0 & i\Delta_2 & 0 & 0 & 0 & 0 & 0 & 0 & 0 \\
0 & -i\Delta_3 & \mu_{gd} & p & 0 & 0 & 0 & -i\Delta_1 & 0 & 0 & 0 & 0 \\
i\Delta_3 & 0 & p & \mu_{gd} & 0 & 0 & i\Delta_1 & 0 & 0 & 0 & 0 & 0 \\
0 & -i\Delta_2 & 0 & 0 & \mu_{bs}+M_s & p & 0 & 0 & 0 & -i\Delta_1 & 0 & 0 \\
i\Delta_2 & 0 & 0 & 0 & p & \mu_{bs}-M_s & 0 & 0 & i\Delta_1 & 0 & 0 & 0 \\
0 & 0 & 0 & -i\Delta_1 & 0 & 0 & -\mu_{bs}+M_s & p & 0 & 0 & 0 & -i\Delta_2 \\
0 & 0 & i\Delta_1 & 0 & 0 & 0 & p & -\mu_{bs}-M_s & 0 & 0 & i\Delta_2 & 0 \\
0 & 0 & 0 & 0 & 0 & -i\Delta_1 & 0 & 0 & -\mu_{gd} & p & 0 & -i\Delta_3 \\
0 & 0 & 0 & 0 & i\Delta_1 & 0 & 0 & 0 & p & -\mu_{gd} & i\Delta_3 & 0 \\
0 & 0 & 0 & 0 & 0 & 0 & 0 & -i\Delta_2 & 0 & -i\Delta_3 & \mu_{ru} & p \\
0 & 0 & 0 & 0 & 0 & 0 & i\Delta_2 & 0 & i\Delta_3 & 0 & p & \mu_{ru}
\end{pmatrix} . \tag{3.10}$$

The 12 eigenvalues of this matrix each contribute once in the sum in (3.3). They occur in degenerate pairs due to spin.

A stable, neutral phase must minimize the free energy (3.3) with respect to variation of the three gap parameters Δ_1, Δ_2, Δ_3, meaning it must satisfy

$$\frac{\partial\Omega}{\partial\Delta_1} = 0, \qquad \frac{\partial\Omega}{\partial\Delta_2} = 0, \qquad \frac{\partial\Omega}{\partial\Delta_3} = 0 \ , \tag{3.11}$$

and it must satisfy the three neutrality conditions (2.7). The gap equations (3.11) and neutrality equations (2.7) form a system of six coupled integral equations with unknowns the three gap parameters and μ_e, μ_3 and μ_8. We have solved these equations numerically at a grid of values of T and M_s^2/μ. We evaluate Ω using (3.3), finding the ε_j by determining the eigenvalues of the matrices specified explicitly above. We evaluate partial derivatives of Ω using finite difference methods. (We used three and five point finite difference evaluations of derivatives, with the interval in the Δ or μ with respect to which Ω is being differentiated taken as 0.04 MeV.) We have worked entirely with $\mu = 500$ MeV, varying M_s^2/μ by varying M_s, and have worked at three values of the coupling G chosen so that Δ_0, the gap parameter at $M_s = T = 0$, takes on the values $\Delta_0 = 25$, 40 and 100 MeV.

3.2.2 Approximations made and not made

Having described our calculation in explicit detail, we close this section by enumerating the approximations that we are making, and stressing several that we have not made.

We have made the following approximations:

1. We work throughout in a mean field approximation. Gauge field fluctuations will surely be important, and must be included in future work.

2. We neglect contributions to the condensates that are symmetric in color and flavor: these are known to be present and small, smaller than the contributions that we include by at least an order of magnitude [10, 27, 38].

3. We choose light quark masses $M_u = M_d = 0$ and we treat the constituent strange quark mass M_s as a parameter, rather than solving for an $\langle \bar{s}s \rangle$ condensate. These approximations should be improved upon, along the lines of Refs. [71, 72]. In future studies in which the $\langle \bar{q}q \rangle$ condensates are solved for dynamically, the six-quark 't Hooft interaction induced by instantons must be included, since it introduces terms of the form $\langle \bar{s}s \rangle |\Delta_3|^2$, for example.

4. We ignore meson condensation in both the CFL phase and gCFL phases. We shall see in Section 3.5.1 that in the CFL phase this means that we are assuming that the instanton contribution to the K^0 mass is comparable to or larger than Δ_0 [101, 102]. Meson condensation in the gCFL phase has yet to be analyzed.

We expect that these approximations have quantitative effects, but none preclude a qualitative understanding of the phase diagram.

In Chapter 2, we made further simplifying assumptions. We worked only to leading nontrivial order in Δ_1, Δ_2, Δ_3, μ_e, μ_3 and μ_8. We neglected the effects of antiparticles. And, most serious, we incorporated M_s only via its leading effect, namely as an effective shift $-M_s^2/\mu$ in the chemical potentials of the strange quarks. This limits the regime of applicability of our results to $M_s \ll \mu$. For $\Delta_0 \sim 100$ MeV, there is pairing even at $M_s \gtrsim \mu$ and our calculation runs into no difficulties in this regime. (We shall show some results, even though this likely corresponds to such small μ that in reality the hadronic phase has taken over.) In the next section, we shall present our $T = 0$ results. Those with $\Delta_0 = 25$ MeV, as in Chapter 2, are in very good

agreement with the results of Chapter 2. This provides quantitative evidence for the validity of the approximations made in Chapter 2 at $\Delta_0 = 25$ MeV.

3.3 Zero temperature results

In this section we shall present the results of our model analysis at $T = 0$. Here as in Chapter 2, we set $\mu = 500$ MeV corresponding to a baryon density about ten times that in nuclear matter, which is within the range of expectations for the density at the center of compact stars. In reality, both M_s and Δ_0 vary with μ, and our knowledge of both is uncertain. Our model is by construction well-suited to study the disruptive effects of M_s on pairing but it is not adequate to fix the density-dependent values of either M_s or Δ_0 quantitatively. In this study, therefore, as in Refs. [27, 46] and Chapter 2 we treat both M_s and Δ_0 simply as parameters. We shall plot our results versus M_s^2/μ, rather than versus M_s itself, because the strength of the disruptive effects introduced by the strange quark mass are characterized by M_s^2/μ. For example, the splitting between Fermi surfaces in unpaired quark matter is of order $M_s^2/4\mu$, and the CFL→gCFL transition occurs where $M_s^2/\mu \simeq 2\Delta_1$. Although we only present results at a single value of μ, because the effects of M_s are controlled by M_s^2/μ, and because in reality M_s is itself a decreasing function of μ, one can think of our plots as giving a qualitative description of the effects of varying μ, with high density at small M_s^2/μ and low density at large M_s^2/μ. This description is only qualitative because our plots are each made with some fixed value of Δ_0, whereas in reality Δ_0 depends on μ.

We begin by choosing the four fermion coupling G so that $\Delta_0 = 25$ MeV, as in Chapter 2. The solid curves in Fig. 3-2 show the gap parameters as a function of M_s^2/μ, and those in Fig. 3-3 show the chemical potentials. These plots are in very good agreement with Figs. 2-1, and 2-2, indicating that the approximations made in Chapter 2 that we have dispensed with here, chiefly the small-M_s^2/μ^2 assumption, were good approximations for $\Delta_0 = 25$ MeV. For small M_s^2/μ, we see the CFL phase with $\Delta_1 = \Delta_2 \simeq \Delta_3$. The small difference between $\Delta_1 = \Delta_2$ and Δ_3, less than 2%

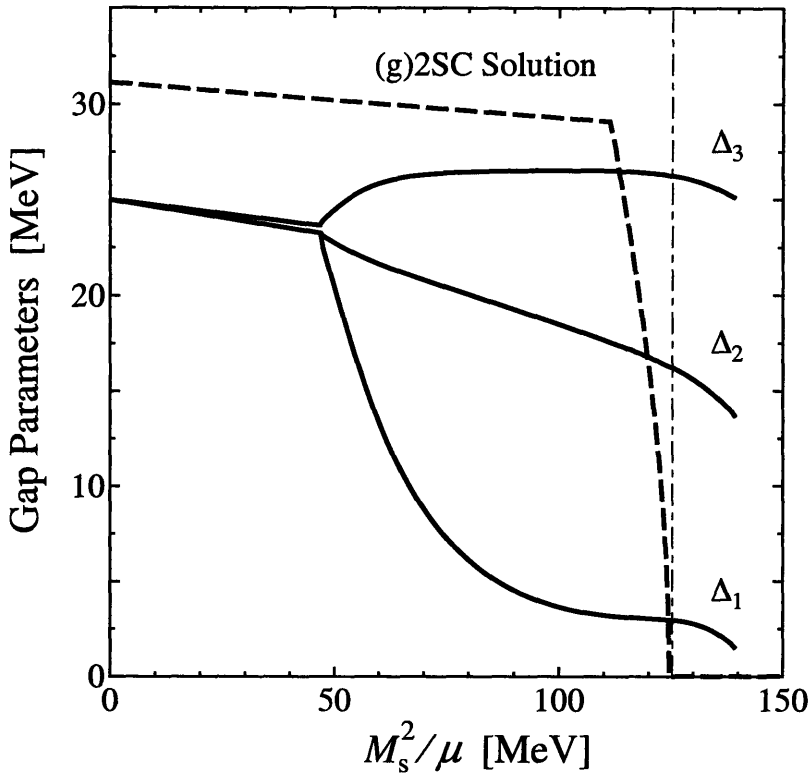

Figure 3-2: Gap parameters Δ_1, Δ_2 and Δ_3 as a function of M_s^2/μ at $T = 0$. The solid curves show the CFL/gCFL solution, with the CFL→gCFL transition occurring where $M_s^2/\mu \simeq 2\Delta_1$. There is a first order phase transition between the gCFL phase and unpaired quark matter at $M_s^2/\mu = 125.3$ MeV, denoted by the the thin vertical line. To the right of this line, the gCFL solution is metastable. We also find a neutral 2SC solution, with Δ_3 given by the dashed curve in the figure, which undergoes a transition to the gapless 2SC phase of Ref. [74] at $M_s^2/\mu = 112$ MeV. However, from Fig. 3-4 we see that the (g)2SC solution is everywhere metastable, having a larger free energy than the (g)CFL solution at the same M_s^2/μ.

everywhere within the CFL phase, is an example of an effect that we can see but that cannot be seen in the small-M_s^2/μ^2 approximation in which M_s is approximated as a shift in the chemical potential for the strange quarks [24, 25]. The CFL→gCFL transition occurs at $M_s^2/\mu = 46.8$ MeV, which is very close to $2\Delta_1$, since $\Delta_1 = 23.2$ MeV at $M_s^2/\mu = 46.8$ MeV. We see from Fig. 3-3 that $\mu_e \neq 0$ in the gCFL phase, indicating a nonzero electron density.

As discussed in detail in Chapter 2, the negative $\tilde{Q}$-charge of the electrons is balanced by that of unpaired *bu* quarks, which have $\tilde{Q} = +1$, occurring in a narrow

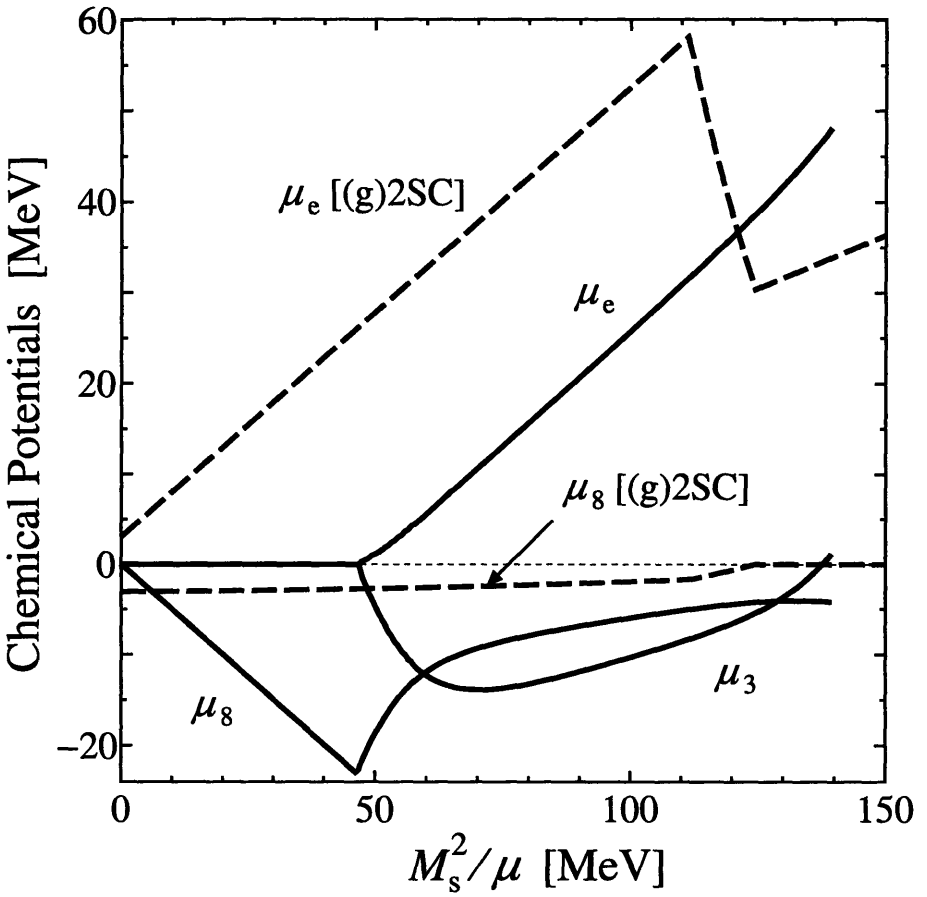

Figure 3-3: Chemical potentials μ_e, μ_3 and μ_8 as a function of M_s^2/μ at $T = 0$, for the (g)CFL and (g)2SC solutions of Fig. 3-2. ($\mu_3 = 0$ in the (g)2SC solution and so is not shown.) Beyond the M_s^2/μ at which the g2SC solution ends, the dashed curve shows the chemical potentials ($\mu_e \neq 0$ and $\mu_8 = 0$) for neutral unpaired quark matter.

shell in momentum space. There is a larger shell in momentum space, whose width grows with increasing M_s^2/μ in the gCFL phase, within which there are unpaired *bd*-quarks. This "blocking region" of momentum space does not contribute in the Δ_1 gap equation, and Δ_1 is consequently driven down. The gap equations and neutrality conditions are all coupled, and the consequences of the reduction in Δ_1 and the increase in μ_e are manifest in all the curves in Figs. 3-2 and 3-3.

As M_s^2/μ increases further, the gCFL solution eventually ceases to exist at $M_s^2/\mu = 139$ MeV. The gCFL solution to the gap equations is a minimum of Ω with respect to variation of the Δ's for $M_s^2/\mu < 139$ MeV, becomes an inflection point at

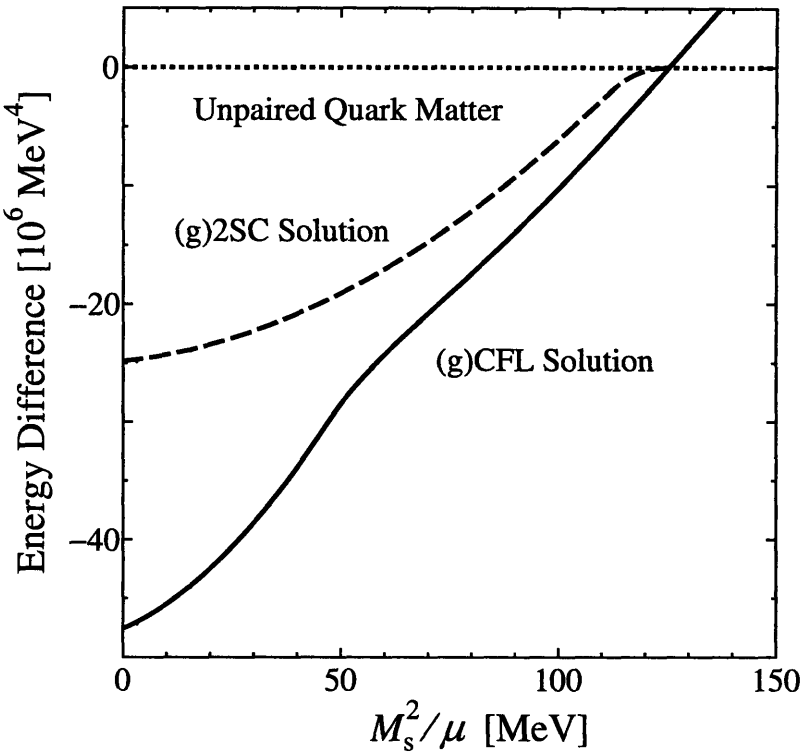

Figure 3-4: Free energies of the (g)CFL and (g)2SC solutions of Fig. 3-2 at $T = 0$, relative to that of neutral unpaired quark matter.

$M_s^2/\mu = 139$ MeV, and for larger M_s^2/μ there is no such solution. This is analyzed in greater detail in Chapter 2 and Refs. [24, 25]. The fact that the gCFL solution disappears indicates that there should be some other minimum with lower free energy, and indeed as shown in Fig. 3-4 we find that a first-order phase transition at which the gCFL free energy crosses above that of unpaired quark matter has occurred at $M_s^2/\mu = 125$ MeV, indicated in Fig. 3-2 by the vertical line. In Chapter 2, the first order phase transition and the termination of the gCFL phase at a point of inflection of the free energy occur at $M_s^2/\mu = 130$ MeV and $M_s^2/\mu = 144$ MeV respectively. Therefore, the errors in these quantities introduced by the small-M_s^2/μ^2 approximation, used in Chapter 2 but not here, are about 4% at these values of M_s^2/μ. As in Chapter 2, we find an additional neutral 2SC solution, whose gap parameter Δ_3 and free energy are shown in Figs. 3-2 and 3-4. At $M_s = 0$, the 2SC gap is $2^{1/3}\Delta_0$ [34–36, 63, 64, 104]. For M_s^2/μ below the 2SC→g2SC transition at $M_s^2/\mu = 112$ MeV,

rd-gu and *ru-gd* pairing occur at all momenta; above this transition, in the gapless 2SC phase [74, 85], there is a blocking region [56] in momentum space in which one finds unpaired *rd* and *gd* quarks, and Δ_3 drops precipitously. An analogue of the g2SC phase [83] (and in fact an analogue of the gCFL phase [84]) were first analyzed in contexts in which they were metastable, but it was shown in Ref. [74] that the g2SC phase could be stabilized in two-flavor quark matter by the constraints of neutrality. However, we see in Fig. 3-4 that in this three-flavor quark matter setting, the (g)2SC solution everywhere has a larger free energy than the (g)CFL solution at the same M_s^2/μ, and is therefore metastable. The value of M_s^2/μ at which $\Delta_3 \to 0$ in the g2SC solution is less than 1 MeV below the M_s^2/μ at which the gCFL phase becomes metastable. In contrast, in Chapter 2 the g2SC solution persists to an M_s^2/μ that is less than 1 MeV above that at which the gCFL phase free energy crosses that of unpaired quark matter. This is the one instance where the small-M_s^2/μ^2 approximation made in Chapter 2 leads one (slightly) astray, as it predicts a (very narrow) M_s^2/μ-window in which the g2SC phase is favored and we find no such window. However, we shall see below that the physics at values of M_s^2/μ that are this large compared to Δ_0 is anyway not robust, changing qualitatively with increasing Δ_0.

We now investigate how our zero temperature results change if we vary the strength of the coupling, and hence Δ_0. In Fig. 3-5, we show the gap parameters as a function of M_s^2/μ with $\Delta_0 = 40$ MeV. We have changed the scale on both the horizontal and vertical axes by the same factor of 40/25. We see that the CFL→gCFL transition again occurs at $M_s^2/\mu \simeq 2\Delta_1$, and that the shape of the curves in the gCFL region is qualitatively as before, when suitably rescaled. However, at large values of M_s^2/μ we now find a g2SC window: the gCFL free energy crosses above that of the g2SC phase whose gap parameter Δ_3 is also shown in Fig. 3-5 at the vertical line in the figure, and the g2SC gap vanishes only at a larger M_s^2/μ. (We have located the vertical line by comparing free energies, as we did in Fig. 3-4, but we shall not give the figure.)

If we reduce Δ_0 from 25 MeV, rather than increasing it, and rescale both axes of Fig. 3-2 by the same factor by which we reduce Δ_0, we obtain a figure that looks

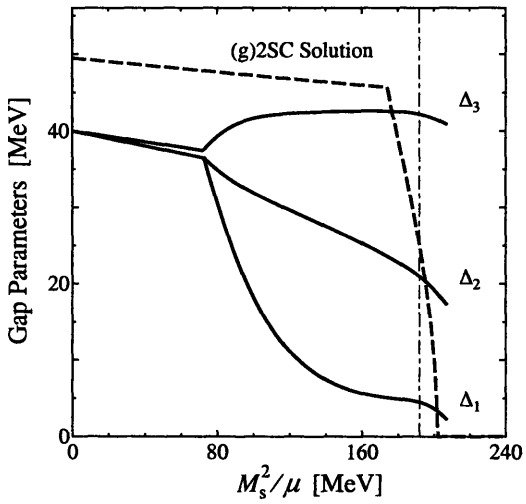

Figure 3-5: Gap parameters for a stronger interaction than that in Fig. 3-2, chosen such that $\Delta_0 = 40$ MeV for $M_s = 0$. As in Fig. 3-2, the CFL→gCFL transition occurs where $M_s^2/\mu \simeq 2\Delta_1$. Here, however, the gCFL phase becomes metastable (at the thin vertical line) at a value of M_s^2/μ above which there is a g2SC solution. There is a first order gCFL→g2SC transition at the thin vertical line, followed at a larger M_s^2/μ by a second order transition at which the g2SC gap Δ_3 vanishes.

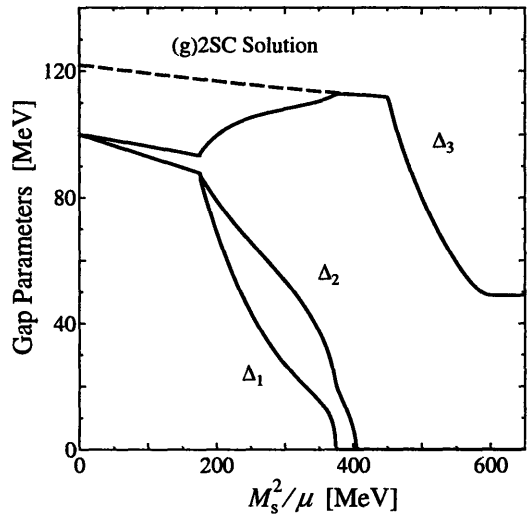

Figure 3-6: Gap parameters for a still stronger interaction, with $\Delta_0 = 100$ MeV for $M_s = 0$. As in Fig. 3-2, the CFL→gCFL transition occurs where $M_s^2/\mu \simeq 2\Delta_1$. At $M_s^2/\mu = 375$ MeV, Δ_1 vanishes at a second order gCFL→uSC transition. Then, at $M_s^2/\mu = 405$ MeV, Δ_2 vanishes at a second order uSC→2SC transition. At $M_s^2/\mu = 449$ MeV, there is a second order 2SC→g2SC transition. And finally, for $M_s^2/\mu > 598$ MeV, corresponding to $M_s > 547$ MeV, there are no more strange quarks present in the system, as shown explicitly in Fig. 3-7, and further increase in M_s changes nothing.

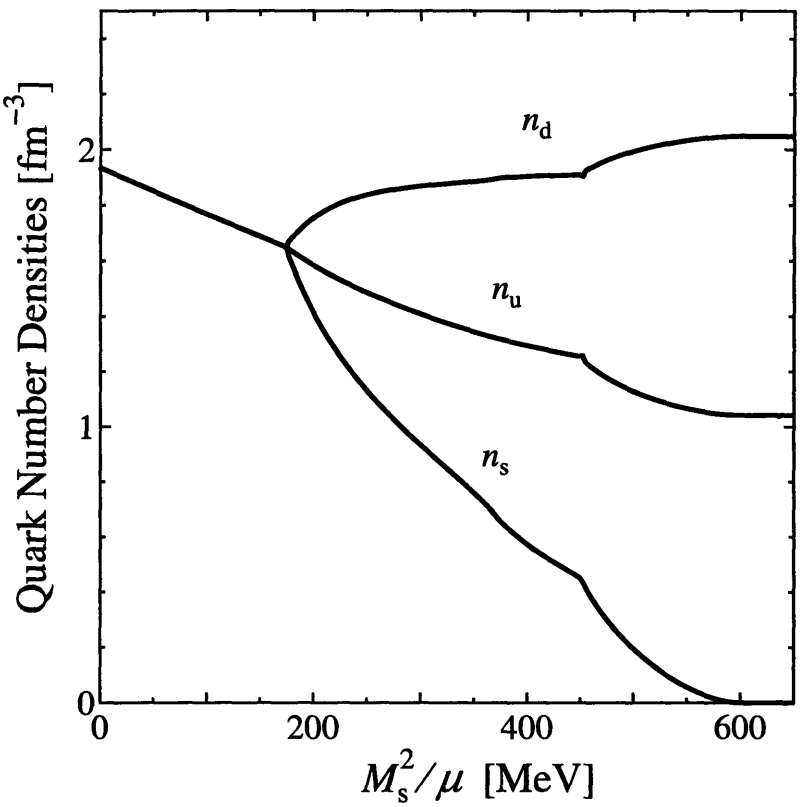

Figure 3-7: Number densities of quarks with flavors u, d and s (in each case summed over the three colors) as a function of M_s^2/μ. All parameters are as in Fig. 3-6, with $\Delta_0 = 100$ MeV. We see that the number densities are equal only in the CFL phase, and see that for $M_s^2/\mu > 598$ MeV there are no strange quarks present.

qualitatively like Fig. 3-2. We conclude that stronger interaction tends to favor a g2SC window at large values of M_s^2/μ, whereas weaker interaction disfavors it. The boundary between the two cases is at $\Delta_0 = 25$ MeV in our model.

It is interesting to ask what happens at still larger Δ_0. We show the gap parameters in our model with $\Delta_0 = 100$ MeV in Fig. 3-6. We see the CFL→gCFL transition at $M_s^2/\mu = 2\Delta_1$ once again. The physics at and beyond the large-M_s^2/μ boundary of the gCFL regime is now qualitatively different. This regime corresponds either to very large values of M_s, or else to such small values of μ that the hadronic phase will likely have taken over, making the right half of this plot somewhat academic. One reason it is of interest, however, is simply the fact that we can draw it: had we made a small M_s^2/μ^2 approximation as in Chapter 2 and Ref. [27], this regime would be inac-

cessible. The figure shows a sequence of phases as M_s^2/μ is increased above the gCFL phase: (i) the gCFL phase ends at a second order phase transition at which $\Delta_1 \to 0$, above which we find a uSC window in which both Δ_2 and Δ_3 remain nonzero; (ii) next, $\Delta_2 \to 0$ at a second order phase transition at which the uSC phase is succeeded by the 2SC phase; (iii) finally, there is a 2SC→g2SC transition. This sequence of phases agrees with that found in Ref. [27] at large Δ_0, in a calculation done using a small-M_s^2/μ^2 approximation pushed beyond its regime of validity. Our present calculation can be extended (within its model context) to arbitrarily large M_s. Indeed, as can be seen in Fig. 3-7 we find a transition to two-flavor quark matter, with zero strange quark density, at $M_s = 547$ MeV, corresponding to $M_s^2/\mu = 598$ MeV. Below this M_s, we find the g2SC phase with unpaired strange quarks. Above this value of M_s, we have two-flavor g2SC quark matter and further increase in M_s has no effect on the physics.

As Δ_0 is increased from 40 MeV to 100 MeV, going from Fig. 3-5 to Fig. 3-6, the first qualitative change to occur is that the gCFL phase ends at a second order transition at which $\Delta_1 \to 0$, instead of ending at a first order transition. Above this Δ_0, the phase diagram includes a uSC window separated from the (g)2SC phase by a first order phase transition. At a somewhat larger Δ_0, this first order phase transition becomes second order. At a still larger Δ_0, the interaction is strong enough to have g2SC pairing in the two flavor quark matter that our model describes for $M_s \to \infty$, and the physics is as in Fig. 3-6.

3.4 The Phase Diagram at Nonzero Temperature

We now explore the solutions to the gap equations and neutrality conditions at nonzero temperatures. As in the previous section, we begin with a coupling chosen so that $\Delta_0 = 25$ MeV. The phase diagram for this value of the coupling is given in Fig. 3-1, to which the reader should refer in this section. We constructed Fig. 3-1 by first making plots of the gap parameters and chemical potentials versus M_s^2/μ at many values of T, and versus T at many values of M_s^2/μ. In this Section, we

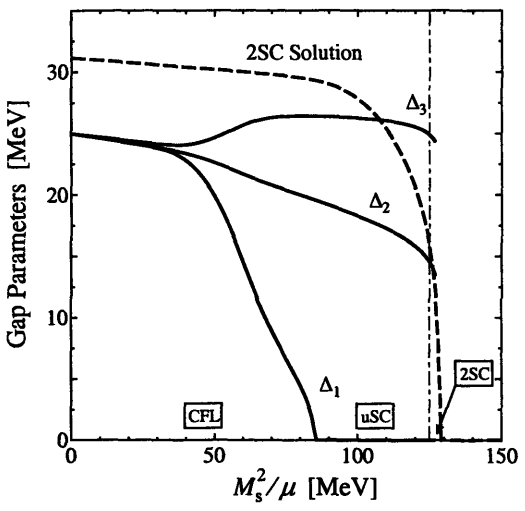

Figure 3-8: Gap parameters as a function of M_s^2/μ at $T = 2$ MeV, with all other parameters as in Fig. 3-2.

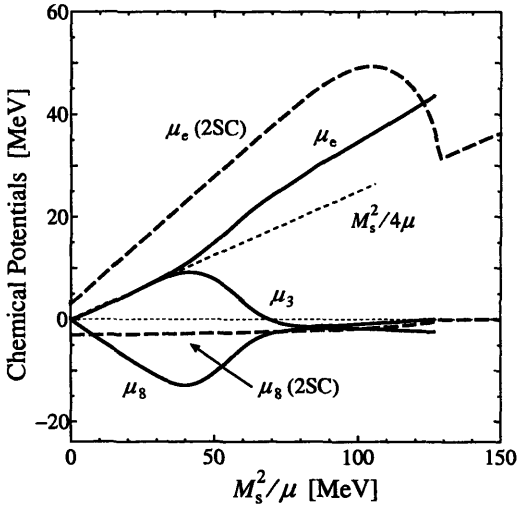

Figure 3-9: Chemical potentials as a function of M_s^2/μ at $T = 2$ MeV, with all other parameters as in Fig. 3-3. At small M_s^2/μ, μ_e and μ_3 are close to $M_s^2/4\mu$.

present and discuss several of these "sections" of Fig. 3-1, enough to understand the many features of the phase diagram. We then show phase diagrams for $\Delta_0 = 40$ and 100 MeV.

We start by turning on a small temperature, $T = 2$ MeV, and seeing how the plots of gaps and chemical potentials, shown in Figs. 3-8 and 3-9, change from those at zero temperature, Figs. 3-2 and 3-3. We see many interesting changes already at this relatively small temperature. The CFL→gCFL transition seen at zero temperature in Figs. 3-2 and 3-3 has become completely smooth at $T = 2$ MeV: there is no sharp difference between CFL and gCFL at nonzero T. Furthermore, note that the zero temperature transition from 2SC to g2SC is also washed out. This makes sense: at $T = 2$ MeV, it makes no physical difference whether a certain fermionic quasiparticle is gapless or has a gap that is nonzero but smaller than 2 MeV. So, although in Fig. 3-1 we have shown the values of M_s^2/μ where quark quasiparticles become gapless within the CFL, uSC and 2SC phases, these dashed lines have physical significance only where they intersect $T = 0$.

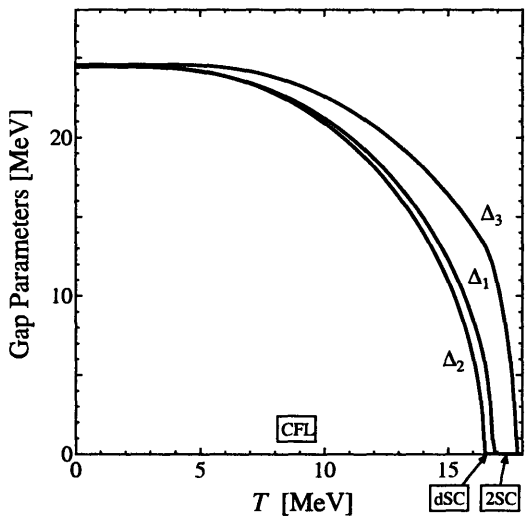

Figure 3-10: Gap parameters as a function of T at $M_s^2/\mu = 15$ MeV.

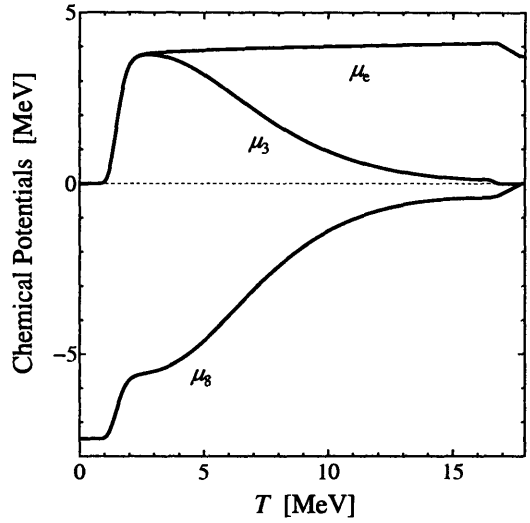

Figure 3-11: Chemical potentials as a function of T at $M_s^2/\mu = 15$ MeV.

We see in Fig. 3-8 that Δ_1 vanishes at a second order CFL→uSC transition at $M_s^2/\mu = 85.1$ MeV. Another way to say this is that for $M_s^2/\mu < 85.1$ MeV, the critical temperature at which Δ_1 vanishes upon heating must be greater than 2 MeV, whereas for $M_s^2/\mu > 85.1$ MeV, this critical temperature is less than 2 MeV. As at $T = 0$, there is a first order phase transition, denoted in Fig. 3-8 by a thin vertical line, but here it is a first order phase transition between the uSC phase at $M_s^2/\mu < 125$ MeV and the 2SC phase at $M_s^2/\mu > 125$ MeV. The 2SC phase ends at a second order phase transition where $\Delta_3 \to 0$ at $M_s^2/\mu = 129$ MeV. This means that there is a regime of M_s^2/μ at which there is 2SC pairing at $T = 2$ MeV, but no pairing at $T = 0$. We investigate this further below.

We see in Fig. 3-9 that at small M_s^2/μ, the chemical potentials μ_e and μ_3 are both close to $M_s^2/4\mu$ at $T = 2$ MeV. This is qualitatively different than their zero temperature behavior $\mu_e = \mu_3 = 0$. In comparison, μ_e takes on the value $M_s^2/4\mu$ in unpaired quark matter. Thus, already at a temperature of only 2 MeV there is no sense in which μ_e is small. We see that at larger M_s^2/μ, μ_e and μ_3 diverge as at zero temperature, but they do so smoothly and they diverge from $M_s^2/4\mu$, rather than from 0. Since we have found that the CFL phase has become a metal already

at $T = 2$ MeV, it is natural to ask at what temperature the insulator-metal crossover occurs. We answer this question at $M_s^2/\mu = 15$ MeV in Figs. 3-10 and 3-11. The latter figure shows a rapid insulator to metal crossover occurring between $T = 1$ MeV and $T = 2$ MeV, with μ_e, μ_3 and μ_8 all changing. We shall discuss this crossover at length in Section 3.5. It can be understood analytically, and we shall see in Section 3.5 that the reason that μ_e takes on the value $M_s^2/4\mu$ is quite different from that in unpaired quark matter. Above the crossover, μ_e changes little as T increases further but both μ_3 and μ_8 decrease in magnitude. This occurs because at larger temperatures the gap parameters decrease, as seen in Fig. 3-10, and as the gap parameters vanish color neutrality occurs with $\mu_3 = \mu_8 = 0$ [97] whereas electrical neutrality still requires a nonzero μ_e.

We see in Fig. 3-10 that the gap parameters change little at the low temperatures at which the CFL phase is undergoing its insulator to metal crossover. Although it is not really visible in the figure, we find that $\Delta_2 > \Delta_1$ for $0 < T < 6.28$ MeV, and $\Delta_1 > \Delta_2$ at higher temperatures. At $T = 16.46$ MeV, Δ_2 vanishes at a second order phase transition and we find the dSC phase. Then, at $T = 16.81$ MeV, Δ_1 vanishes, yielding the 2SC phase. The final phase transition, at which Δ_3 vanishes, occurs at $T = 17.73$ MeV. This ordering of phase transitions is in qualitative agreement with that found in Ref. [97] using a Ginzburg-Landau approximation, and is in disagreement with the results of Ref. [27], in which no dSC regime was found. In order to gain confidence in the accuracy of our calculation and in the existence of the dSC phase, in Section 3.6 we make a detailed and quantitative comparison between our results and those obtained via the Ginzburg-Landau approximation.

At larger values of M_s^2/μ, the ordering of phase transitions as a function of increasing temperature changes. For example, if we consider $M_s^2/\mu = 70$ MeV, in the gCFL phase at $T = 0$ with $\Delta_1 < \Delta_2 < \Delta_3$, we see in Fig. 3-12 that as the temperature is increased, Δ_1 vanishes first, then Δ_2 and then Δ_3, meaning that the phase which intervenes between CFL and 2SC is uSC, not dSC. This order of phase transitions is unsurprising, given that $\Delta_1 < \Delta_2 < \Delta_3$ at $T = 0$ in the gCFL phase. All three transitions are second order transitions in mean field theory. Fig. 3-13 shows the chemical

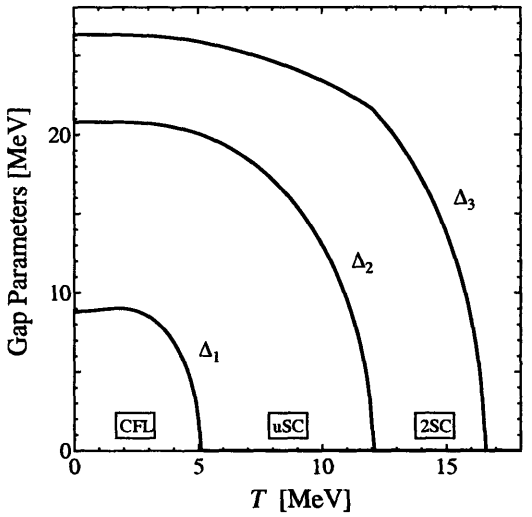

Figure 3-12: Gap parameters versus temperature at $M_s^2/\mu = 70$ MeV.

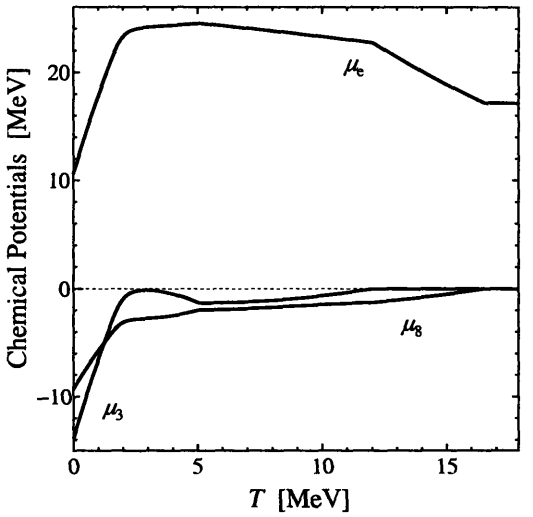

Figure 3-13: Chemical potentials versus temperature at $M_s^2/\mu = 70$ MeV.

potentials as a function of increasing temperature at $M_s^2/\mu = 70$ MeV. Whereas the $T = 0$ CFL phase undergoes an insulator to metal crossover as it is heated, the gCFL phase is already a metal at $T = 0$.

In both Figs. 3-10 and 3-12, we see a sequence of three second order phase transitions. The first of these, a transition from the CFL phase to either the dSC or the uSC phase, is likely not significantly affected by gauge field fluctuations, because the same gauge symmetries are unbroken (the $U(1)_{\tilde{Q}}$ symmetry) and broken (the other eight gauge symmetries) on both sides of the transition. It is therefore an interesting question for future work to consider the order parameter fluctuations at this transition, asking whether they render it first order or, if not, determining its universality class. The two mean field transitions occurring at higher temperatures in Figs. 3-10 and 3-12 will be qualitatively affected by gauge field fluctuations, as at each of them there are gauge symmetries that are broken on the low temperature side of the transition and restored above the transition. Gauge field fluctuations will presumably make these transitions first order, and shift their critical temperatures upward. These effects will be significant, because the relevant gauge fields are strongly coupled [95, 96].

We have found that at small M_s^2/μ, Δ_2 vanishes at a lower temperature than Δ_1

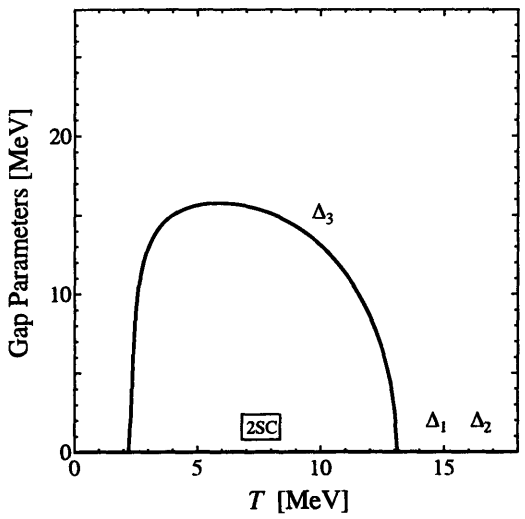

Figure 3-14: Gap parameters versus temperature at $M_s^2/\mu = 130$ MeV. At this large value of M_s^2/μ, both Δ_1 and Δ_2 are zero at all temperatures. $\Delta_3 = 0$ at $T = 0$, but this gap parameter is nonzero for 2.37MeV $< T <$ 13.08 MeV.

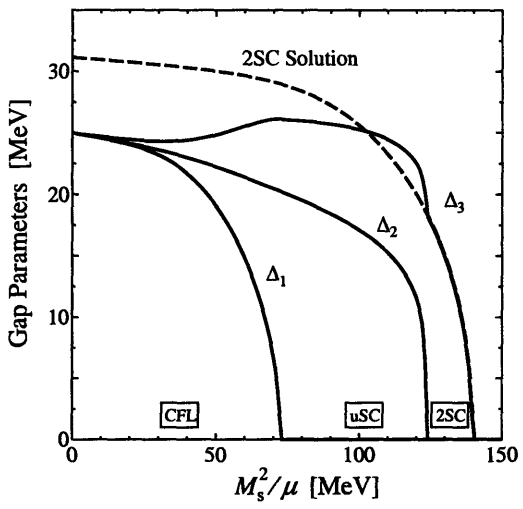

Figure 3-15: Gap parameters versus M_s^2/μ at $T = 4$ MeV.

whereas at larger M_s^2/μ, these two transitions occur in the opposite order. There must, therefore, be some M_s^2/μ at which both vanish at the same temperature. We see in Fig. 3-1 that this "doubly critical" point occurs at $T = 15.3$ MeV and $M_s^2/\mu = 29.4$ MeV.

Having followed what happens upon heating the CFL phase at $M_s^2/\mu = 15$ MeV and upon heating the gCFL phase at $M_s^2/\mu = 70$ MeV, in Fig. 3-14 we consider heating quark matter at $M_s^2/\mu = 130$ MeV, which is unpaired at $T = 0$. We see that Δ_3 becomes nonzero at a second order phase transition, and then vanishes at a higher temperature at a second order phase transition. This behavior has been described previously [74, 105], and can be understood as follows. At $T = 0$, the u and d Fermi surfaces in the unpaired quark matter are too far apart to allow 2SC pairing. However, as we increase T, we excite u quarks above the u Fermi surface, and d holes below the d Fermi surface. This smearing of the separated Fermi surfaces assists u-d pairing, and Δ_3 turns on at a nonzero temperature. Of course, at a still

higher temperature the Δ_3 condensate melts.

The final slice of the phase diagram of Fig. 3-1 that we shall show explicitly is a plot of the gap parameters as a function of M_s^2/μ at $T = 4$ MeV, shown in Fig. 3-15. By comparing this figure with Fig. 3-8, we see qualitative changes in the physics between $T = 2$ MeV and $T = 4$ MeV: the 2SC phase now takes over from the uSC phase not via a first order phase transition, but instead via a second order phase transition at $M_s^2/\mu = 123.2$ MeV at which $\Delta_2 \to 0$. This means that a line of first order phase transitions, present at lower temperatures, has turned into a second order transition at a tricritical point. This tricritical point is shown by a diamond in Fig. 3-1, and is located between $T = 3.9$ MeV and $T = 4.0$ MeV.

The results that we have presented up to this point in this section, plotted in Figs. 3-8 through 3-15, constitute a description of all of the features at $T \neq 0$ depicted in the phase diagram given in Fig. 3-1. We now ask how this phase diagram changes as we vary the strength of the interaction, and hence Δ_0. If we reduce Δ_0, there are no qualitative changes as long as we rescale the vertical and horizontal axes of the phase diagram by the same factor that we reduce Δ_0. As at $T = 0$, however, increasing Δ_0 leads to qualitative changes in the phase diagram at large M_s^2/μ, indicating that the details of the large M_s^2/μ regions of the phase diagram are not robust predictions of our model.

With $\Delta_0 = 40$ MeV, in Fig. 3-16, we see the same three special points as in Fig. 3-1: a quantum critical point separating the CFL and gCFL phases at $T = 0$, a doubly critical point at which the $\Delta_1 \to 0$ and $\Delta_2 \to 0$ transitions cross, and a tricritical point at large M_s^2/μ at which a line of first order phase transitions ends. Since both axes of Fig. 3-16 have been rescaled by 40/25 relative to Fig. 3-1, the two figures are qualitatively similar: the one qualitative change occurs at large M_s^2/μ, where the g2SC phase extends down to $T = 0$, as we have already seen in Fig. 3-5. (At $T = 0$, there is a sharp distinction between 2SC and g2SC, and in this instance the phase is g2SC.) The most interesting quantitative change is a change in the slopes of the $\Delta_1 \to 0$ and $\Delta_2 \to 0$ transitions on the phase diagram at small M_s^2/μ, which pushes the doubly critical point somewhat down in temperature. This effect is more clearly

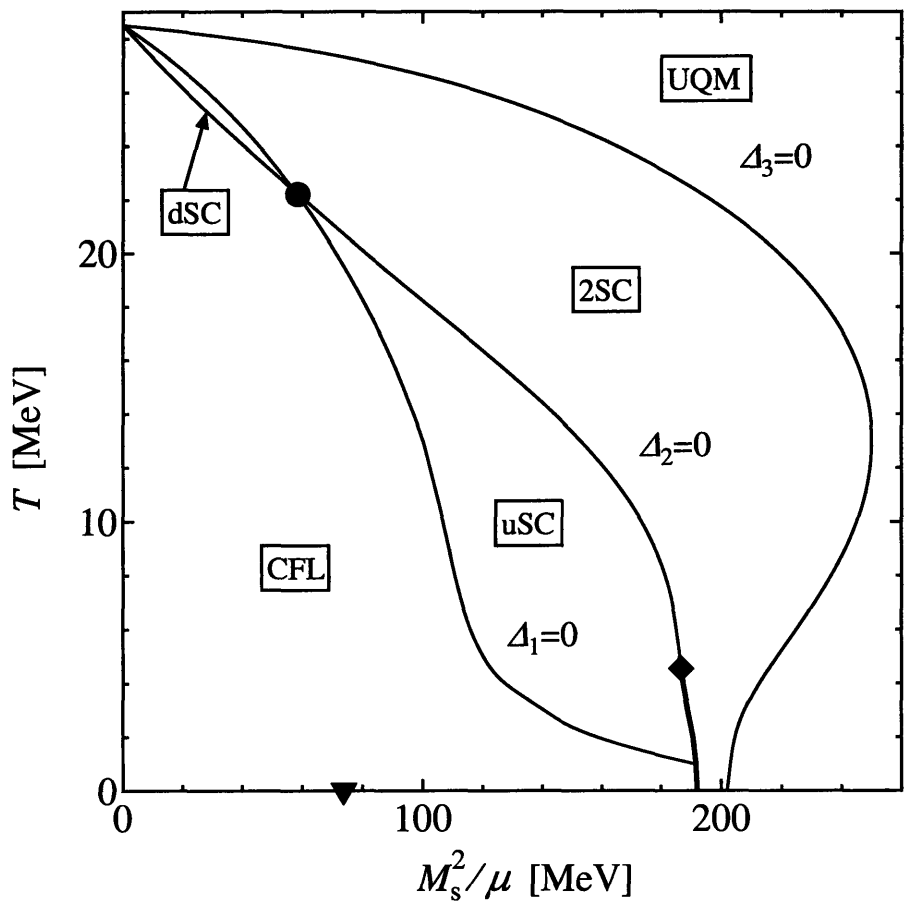

Figure 3-16: Phase diagram of dense neutral quark matter in the $(M_s^2/\mu, T)$ plane, with a coupling chosen such that $\Delta_0 = 40$ MeV. (All parameters except Δ_0 are the same as in Fig. 3-1.) Only phase transitions are shown — the analogues of the dashed and dotted lines in Fig 3-1 are not given.

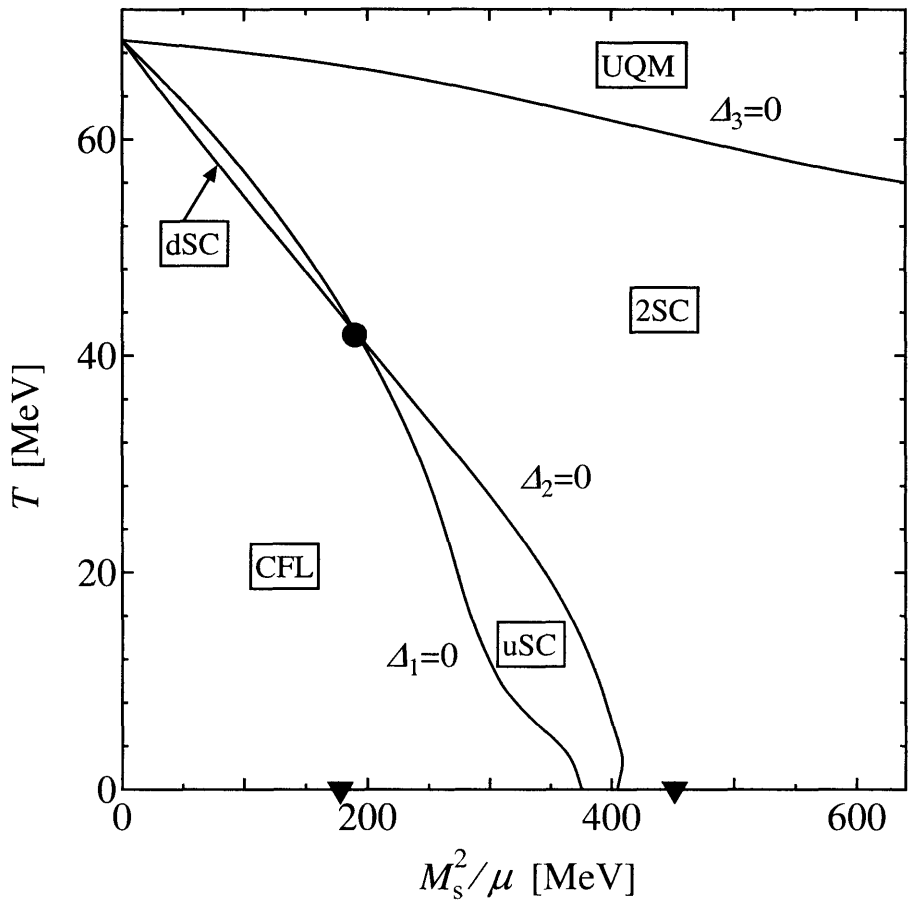

Figure 3-17: Phase diagram of dense neutral quark matter in the $(M_s^2/\mu, T)$ plane, with a coupling chosen such that $\Delta_0 = 100$ MeV. (All parameters except Δ_0 are the same as in Figs. 3-1 and 3-16.) The two triangles on the $T = 0$ axis indicate quantum critical points at which modes become gapless. The first, which separates the CFL and gCFL phases, is familiar. The second separates 2SC and g2SC phases, as shown in Fig. 3-6.

visible at stronger coupling, with $\Delta_0 = 100$ MeV, as shown in Fig. 3-17. We shall explain this quantitatively in Section 3.6.

With $\Delta_0 = 100$ MeV, in Fig. 3-17, we see further qualitative changes at large M_s^2/μ, corresponding to those at $T = 0$ shown in Fig. 3-6. Now, the uSC phase and the 2SC phase both extend to $T = 0$. And, at $T = 0$ there is a 2SC regime separated from g2SC by a quantum critical point, like that separating the CFL and gCFL phases at $T = 0$. If we start at $T = 0$ in the g2SC phase and heat the system, Δ_3 at first increases, before decreasing at higher temperature, eventually vanishing at the upper phase transition shown in Fig. 3-17. If we extended the phase diagram to $M_s^2/\mu \to \infty$, this critical temperature would become M_s-independent in the limit. The small remaining M_s-dependence at the largest M_s^2/μ we show is easily understood: even though there are no strange quarks present at $T = 0$ at these large values of M_s, meaning that the $T = 0$ physics has become M_s-independent, strange quarks can still be excited at nonzero temperature.

As Δ_0 is increased from 40 MeV to 100 MeV, the phase diagram changes continuously from that of Fig. 3-16 to that of Fig. 3-17. First, the uSC phase reaches the $T = 0$ axis. Next, the tricritical point indicated by the diamond in Fig. 3-16 retreats down to $T = 0$. All the while, the (g)2SC region is extending farther and farther to the right, eventually to $M_s \to \infty$ when the coupling is strong enough to allow ud pairing even once there are no strange quarks present.

We shall discuss the implications of the phase diagrams that we have found in the last section of this chapter. First, however, our investigation has raised several interesting questions that we have been able to address analytically, as we describe in Sections 3.5 and 3.6.

3.5 Heating the CFL phase: understanding the insulator to metal crossover

We have seen in Fig. 3-11 that as CFL quark matter is heated, it undergoes a crossover from an insulator, with μ_e exponentially small, to a metal, with $\mu_e \sim M_s^2/4\mu$. With $\Delta_0 = 25$ MeV and $M_s^2/\mu = 15$ MeV as in Fig. 3-11, the crossover occurs between $T = 1$ MeV and $T = 2$ MeV. This insulator to metal crossover has been seen previously in Ref. [27]; our goal here is to understand it analytically.

We see from Fig. 3-10 that the gap parameters change little between $T = 1$ MeV and $T = 2$ MeV, whereas the chemical potentials change dramatically. We shall explain the variation of the chemical potentials, treating the gap parameters as T-independent. We note from Fig. 3-11 that during the crossover, μ_e increases from near 0 to near $M_s^2/4\mu$, while μ_3 increases by the same amount and μ_8 increases by half as much. This tells us that the equations,

$$\mu_3 = \mu_e, \tag{3.12}$$

$$\mu_8 = -\frac{M_s^2}{2\mu} + \frac{\mu_e}{2}, \tag{3.13}$$

that hold at zero temperature neutral CFL matter [46], are maintained, and hence it is the combination $\mu_{\tilde{Q}}$ of (2.31) that is changing. We recall that at $T = 0$ the contribution of the quark matter to the free energy Ω is independent of $\mu_{\tilde{Q}}$, and this "plateau" is only curved by the small contribution of the electrons to the free energy, of order μ_e^4, which favors $\mu_e = 0$. Above the crossover we find $\mu_e \simeq M_s^2/4\mu$, which is on the plateau but away from the point on the plateau favored by the electron neutrality condition. In order to understand the crossover, then, there must be thermally excited $\tilde{Q}$-charged quasi-particles whose neutrality condition favors $\mu_e \neq 0$, and we must see the curvature of the free energy plateau due to these quasiparticles "take over" from that due to the electrons. We first show that the CFL quark quasiparticle excitations have the desired effect, and then in Section 3.5.1 we show that the thermally excited charged mesonic pseudo-Nambu-Goldstone boson excitations of the CFL phase play

a negligible role.

The quarks with nonzero $\tilde{Q}$ are the rs and bu which pair with gap parameter Δ_2, and the rd and gu which pair with gap parameter Δ_3. This means that in the CFL phase there are two quasiquarks with $\tilde{Q} = +1$ (one a linear combination of bu quarks and rs holes; the other a linear combination of gu quarks and rd holes) and two quasiquarks with $\tilde{Q} = -1$ (one a linear combination of rs quarks and bu holes; the other a linear combination of rd quarks and gu holes).

We now evaluate the dispersion relations of these excitations, and estimate the number density of thermally excited charged quasiquarks. In this Section, we shall follow Chapter 2 and include the nonzero strange quark mass only via its effect as a shift in the chemical potentials of the strange quarks. We have seen in Section 3.3 that this is a good approximation in the CFL phase. The dispersion relations of these four quasiparticles are given by [25]

$$\begin{aligned}
\varepsilon_{(rs\text{-}bu)}(p) &= \pm\tfrac{1}{2}\left(\mu_{rs} - \frac{M_s^2}{2\mu} - \mu_{bu}\right) \\
&\quad + \sqrt{\left(p - \bar{\mu}_{(bu\text{-}rs)} + \frac{M_s^2}{4\mu}\right)^2 + \Delta_2^2} \\
\varepsilon_{(rd\text{-}gu)}(p) &= \pm\tfrac{1}{2}(\mu_{gu} - \mu_{rd}) + \sqrt{(p - \bar{\mu}_{(rd\text{-}gu)})^2 + \Delta_3^2}
\end{aligned} \tag{3.14}$$

where $\bar{\mu}_{bu\text{-}rs} \equiv (\mu_{bu} + \mu_{rs})/2$ and $\bar{\mu}_{rd\text{-}gu} \equiv (\mu_{rd} + \mu_{gu})/2$. Upon substituting the definitions (3.9) and the relations (3.12) and (3.13), which are maintained through the crossover, these become

$$\varepsilon_{(rs\text{-}bu)}(p) = \pm\left(\mu_e - \frac{M_s^2}{2\mu}\right) + \sqrt{\left(p - \mu + \frac{M_s^2}{6\mu}\right)^2 + \Delta_2^2}$$
$$\varepsilon_{(rd\text{-}gu)}(p) = \pm\mu_e + \sqrt{\left(p - \mu + \frac{M_s^2}{6\mu}\right)^2 + \Delta_3^2}\,. \tag{3.15}$$

At the temperatures of interest, these excitation energies are all greater than T, and so only the lowest energy excitation with each $\tilde{Q}$ charge matters — the number density of the higher energy excitations is exponentially smaller. Labeling the quasiparticles by their $\tilde{Q}$ charge, the excitation energies of the lowest lying charged quasiquarks are

$$\varepsilon_{+1}(p) = \left(\mu_e - \frac{M_s^2}{2\mu}\right) + \sqrt{\left(p - \mu + \frac{M_s^2}{6\mu}\right)^2 + \Delta_2^2}$$
$$\varepsilon_{-1}(p) = -\mu_e + \sqrt{\left(p - \mu + \frac{M_s^2}{6\mu}\right)^2 + \Delta_3^2}\,, \tag{3.16}$$

corresponding to the $(rs\text{-}bu)$ quasiquark with $\tilde{Q} = +1$ and the $(rd\text{-}gu)$ quasiquark with $\tilde{Q} = -1$. We now evaluate the T-dependent contribution of these quasiquarks to the free energy Ω given by (3.3). Because the quasiquark energies are much larger than the temperatures of interest, the Boltzmann factors are small, the integral is dominated by p near the minimum of $\varepsilon(p)$, and we can use the saddle-point approximation. We find that, for example, the contribution of the $\tilde{Q} = +1$ quasiquark to Ω is given by

$$\begin{aligned} &-\frac{1}{\pi^2}\int_0^\Lambda dp\, p^2 T \ln\left(1 + \mathrm{e}^{-|\varepsilon_{+1}(p)|/T}\right) \\ &\simeq -\frac{1}{\pi^2}\int_0^\Lambda dp\, p^2 T\, e^{-|\varepsilon_{+1}(p)|/T} \\ &\simeq -\frac{1}{\pi^2}\sqrt{2\pi\Delta T}\bar{\mu}^2 T e^{-|\varepsilon_{+1}(\bar{\mu})|/T}\,, \end{aligned} \tag{3.17}$$

where $\bar{\mu} \equiv \mu - M_s^2/6\mu$. The contribution of the $\tilde{Q} = -1$ quasiparticle is analogous.

The contribution of these two quasiparticles to the $\tilde{Q}$-charge density is then

$$(\tilde{Q}=+1) \qquad \frac{\sqrt{2\pi\Delta T}\bar{\mu}^2}{\pi^2}e^{-(\Delta+\mu_e-M_s^2/2\mu)/T}, \tag{3.18}$$

$$(\tilde{Q}=-1) \qquad -\frac{\sqrt{2\pi\Delta T}\bar{\mu}^2}{\pi^2}e^{-(\Delta-\mu_e)/T}. \tag{3.19}$$

We have set $\Delta_3=\Delta_2\equiv\Delta$, a good approximation throughout the crossover as shown in Fig. 3-10. $\tilde{Q}$-neutrality is a balance between the charge densities of these two quark quasiparticles and the electrons.

We can now see that what drives the system to $\mu_e\neq 0$ is the fact that the lightest $\tilde{Q}=+1$ and $\tilde{Q}=-1$ quark quasiparticles have dispersion relations with different gaps when $M_s\neq 0$, and consequently contribute charge densities of different magnitudes when thermally excited. If we attempt to set $\mu_e=0$ at $T\neq 0$, there are more $\tilde{Q}=+1$ quasiparticles present than $\tilde{Q}=-1$ quasiparticles, and the system is not neutral. To achieve neutrality, μ_e must be increased as this increases the density of $\tilde{Q}=-1$ quasiparticles, decreases the density of $\tilde{Q}=+1$ quasiparticles, and adds electrons, which have $\tilde{Q}=-1$. This is described by the neutrality condition

$$\frac{2\sqrt{2\pi\Delta T}\bar{\mu}^2}{\pi^2}\mathrm{e}^{-(\Delta-M_s^2/4\mu)/T}\sinh\left(\frac{M_s^2/4\mu-\mu_e}{T}\right) - \frac{\mu_e^3}{3\pi^2}-\frac{\mu_e T^2}{3}=0\,, \tag{3.20}$$

which we can solve for $\mu_e(T)$ if we take Δ to be T-independent.

Let us now investigate the implications of this result. At very small T, the quark quasiparticles are exponentially rare, and those with $\tilde{Q}=-1$ are exponentially rarer than those with $\tilde{Q}=+1$. The $\tilde{Q}=+1$ quasiparticle density is balanced by the electron density, and μ_e is exponentially small. However, the quasiparticle densities are proportional to μ^2 whereas the electron density is not. This means that at the T at which μ_e starts to take off, the quasiparticle Boltzmann factors are still rather small. Once T is large enough that μ_e approaches $M_s^2/4\mu$, however, even though the individual Boltzmann factors continue to rise rapidly as T increases further, the sinh factor in (3.20) becomes small. Neutrality at this point is primarily a balance

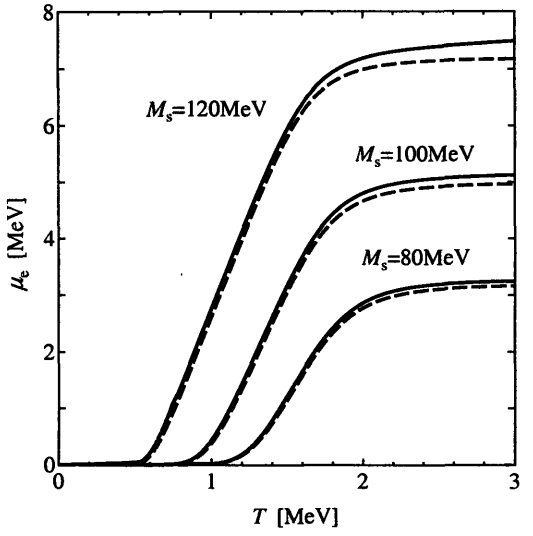

Figure 3-18: Comparison between the analytic results (dashed curves) and the numerical results (solid curves) for μ_e as a function of temperature with $\Delta_0 = 25$ MeV for several values of M_s in the CFL phase. The analytic results were obtained from (3.20), and the numerical results were obtained by solving the full coupled gap equations and neutrality conditions, as in previous Sections. In evaluating μ_e from (3.20) we have taken Δ to be the average of Δ_2 and Δ_3 at the midpoint of the crossover.

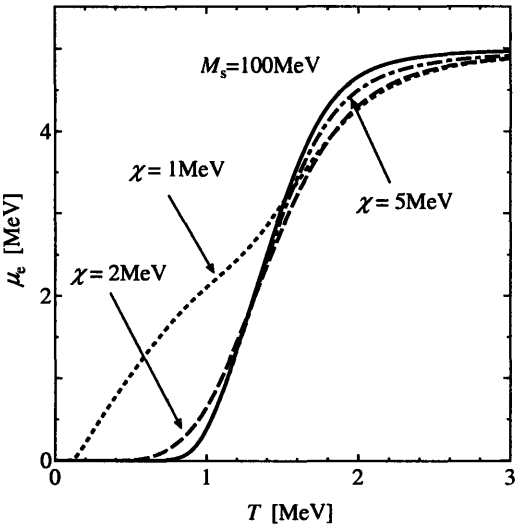

Figure 3-19: Comparison between the analytic estimate for μ_e versus T with and without charged meson contributions. The solid curve, with no meson contributions, is the same as the $M_s = 100$ MeV analytic estimate in Fig. 3-18. The dashed curves include the contribution of thermally excited charged pions and kaons, for three values of the parameter χ described in the text that parameterizes the instanton contribution to the meson masses.

between the densities of the $\tilde{Q} = +1$ and $\tilde{Q} = -1$ quasiparticles, with electrons cancelling only the small difference between their densities. The result, seen already in Fig. 3-11 and shown in greater detail in Fig. 3-18 is a crossover in which μ_e is at first exponentially small, then rises rapidly, and then saturates as it approaches $M_s^2/4\mu$. We see in Fig. 3-18 that the equation (3.20) for μ_e that we have derived, making approximations as described, gives a very good description of the numerical solution of the full coupled gap and neutrality equations. This demonstrates that (3.20) provides us with a good analytic description of the insulator to metal crossover that CFL quark matter experiences when heated.

We have set the electron mass to zero in Fig. 3-18 and throughout. Including it means that it takes a larger μ_e to achieve a given electron density, pushing all the curves in Fig. 3-18 very slightly upwards. With an electron mass as in nature, the effect on the curves is invisible on the scale of the plot.

3.5.1 Contribution of charged mesons

As described in Chapter 2, there are other charged excitations in the CFL phase. Among the pseudo-Nambu-Goldstone bosons, there are mesons with the quantum numbers of the $\pi^{\pm}$ and $K^{\pm}$. We have neglected the contribution of thermally excited charged mesons to the charge density in the derivation of (3.20). We now investigate this approximation.

The dispersion relations of the charged mesons, together with that for the K^0-meson which we shall also need below, are given by [41, 47, 99–102]

$$\begin{aligned}
\varepsilon_{\pi^{\pm}}(p) &= \pm\mu_e + \sqrt{v^2p^2 + M_{\pi^{\pm}}^2} \\
\varepsilon_{K^{\pm}}(p) &= \pm\mu_e \mp \frac{M_s^2}{2\mu} + \sqrt{v^2p^2 + M_{K^{\pm}}^2} \\
\varepsilon_{K^0}(p) &= -\frac{M_s^2}{2\mu} + \sqrt{v^2p^2 + M_{K^0}^2}\ ,
\end{aligned} \tag{3.21}$$

where $v^2 = 1/3$ at high density [47]. The meson masses in the CFL phase are given by

$$\begin{aligned}
M_{\pi^{\pm}}^2 &= a(M_u + M_d)M_s + \chi(M_u + M_d) \\
M_{K^{\pm}}^2 &= a(M_u + M_s)M_d + \chi(M_u + M_s) \\
M_{K^0}^2 &= a(M_d + M_s)M_u + \chi(M_d + M_s)\ .
\end{aligned} \tag{3.22}$$

Here, $a = 3\Delta^2/\pi^2 f_\pi^2$ with $f_\pi^2 = (21 - 8\log 2)\mu^2/36\pi^2$ at high density [47], which yields $a = 0.0175$ for $\Delta_0 = 25$ MeV at $\mu = 500$ MeV. And, χ parameterizes the contribution of $U(1)_A$-breaking instanton effects which generate $\langle\bar{q}q\rangle$ condensates and therefore contributions to meson masses in the CFL phase [100–102], via the 't Hooft

interaction which contributes couplings of the form $\Delta^2\langle\bar{q}q\rangle$. The magnitude of χ is not well known, as it depends on the instanton size distribution and instanton form factors at nonzero density. It has been estimated to lie in the range 1MeV $< \chi <$ 100 MeV [101, 102]. In Fig. 3-19, we include the contribution of all four charged mesons to the $\tilde{Q}$-charge neutrality condition, determining the density of thermally excited bosonic quasiparticles from the dispersion relations. The contribution to the charge density from the $K^{\pm}$ mesons is

$$\frac{1}{2\pi^2}\int_0^\infty dp\, p^2\left(\frac{1}{\exp\left[\varepsilon_{K^+}(p)/T\right]-1}-\frac{1}{\exp\left[\varepsilon_{K^-}(p)/T\right]-1}\right), \tag{3.23}$$

and that from the pions is analogous. We then solve for μ_e vs. T, taking $M_s =$ 100 MeV and $M_u = 5$ MeV and $M_d = 10$ MeV. We plot the results for $\chi = 1$, 2 and 5 MeV in Fig. 3-19.

Adding the charged mesons adds new charge carriers, and so the simplest expectation for their effects is that a smaller μ_e will be required in order to neutralize the imbalance in the fermionic quasiparticle sector. We see in Fig. 3-19 that this expectation is borne out above the crossover, but not below. Above the crossover, we see that μ_e is reduced relative to the results we obtained in Fig. 3-18, where we neglected the mesons. The mesonic contributions get less significant at larger values of χ, as the mesons get heavier. They are already small for $\chi = 1$ MeV and are negligible by $\chi = 5$ MeV. At low temperatures, and for the smallest values of χ, there is another effect to be understood. The dispersion relations for the $K^{\pm}$ in (3.21) indicate that the K^+ is easier to excite than the K^-. This means that they behave like the quasiquarks, in the sense that at a nonzero temperature they contribute a positive $\tilde{Q}$-charge density, which must be cancelled. If χ is very small, the K^+ charge density becomes significant at such a low temperature that its contribution can only be cancelled by electrons — the Boltzmann factors for all other excitations are still prohibitive. This means that if χ is very small, μ_e initially rises with temperature significantly more rapidly than in the absence of the mesons. We see this effect clearly in Fig. 3-19 for $\chi = 1$ MeV and still to a small degree for $\chi = 2$ MeV. For $\chi = 5$ MeV, $\mu_e(T)$ is

indistinguishable at low temperatures from that in the absence of the mesons.

We can summarize the results in Fig. 3-19 as follows. For $\chi \gtrsim 2$ MeV, the thermally excited charged mesons have no significant effects at any temperature. But, if $\chi \sim 1$ MeV, which is at the bottom end of the estimated allowed range 1MeV $< \chi <$ 100 MeV [101, 102], the K^+ excitations contribute significantly at very low temperatures.

At much larger temperatures, well above the insulator to metal crossover that we have analyzed, we come to the various critical temperatures that we have seen in Section 3.4 and will analyze further in Section 3.6. At these temperatures, at which gap parameters vanish, it is well understood that the fermionic quasiparticles are the most important degrees of freedom. What we have shown is that at low temperatures also, the charged mesons are less important than the charged fermions among the thermal excitations, as long as χ is not very small.

Mesons can nevertheless play an important role if they condense [41]. At $T = 0$, the CFL phase is stable against meson condensation as long as $\varepsilon_{K^0} > 0$ at $p = 0$. (K^0-condensation yields the most stringent constraint.) This requires $M_{K^0}^2 > M_s^4/4\mu^2$, corresponding to $\chi \gtrsim M_s^3/4\mu^2$. For $M_s = 100$ MeV, as in Fig. 3-19, this requires $\chi > 1$ MeV. We are therefore justified in our neglect of K^0-condensation in Fig. 3-19. If $\chi > 3.6$ MeV, there is no K^0-condensation in the CFL phase with $\Delta_0 = 25$ MeV for $M_s^2/\mu < 46.8$ MeV, meaning that there is no K^0-condensation at $T = 0$ for all values of M_s^2/μ below the CFL→gCFL transition. (K^0-condensation in the gCFL phase has yet to be analyzed.) It seems likely that $\chi > 3.6$ MeV at accessible densities, since χ is larger at lower densities and the analysis in Ref. [101] which yields the estimate 1MeV $< \chi <$ 100 MeV becomes more reliable at higher densities. If the coupling is stronger, however, K^0-condensation becomes more likely. For example, for $\Delta_0 = 100$ MeV, there is no K^0-condensation in the CFL phase only if $\chi > 26$ MeV. If K^0-condensation were to occur, it delays the CFL→gCFL transition, increasing the M_s^2 at which it occurs by a factor 4/3 if $\chi = 0$ [81]. Further work remains to be done, for example extending the analysis of Ref. [81] to nonzero χ and to the gCFL phase.

Another issue that remains to be investigated is the possibility of π^- condensation

at nonzero temperature. We have seen that above the insulator to metal transition, $\mu_e \approx M_s^2/4\mu$. At zero temperature, this would lead to π^- condensation if $\chi < M_s^4/(16\mu^2(M_u + M_d))$, but this μ_e only arises at $T \neq 0$, and nonzero T acts to stabilize against meson condensation.

Finally, all these issues should be investigated in an expanded model in which the 't Hooft interaction is included from the beginning in the free energy and hence in the gap and neutrality conditions, and the quark masses are also solved for dynamically.

3.6 The Ginzburg-Landau approximation

In the $M_s^2/\mu \to 0$ limit, the three critical temperatures at which the gap parameters vanish become one. Near this critical temperature, where all gap parameters are small, a Ginzburg-Landau approximation can be employed. The Ginzburg-Landau free energy was analyzed at $M_s = 0$ in Refs. [69, 98], and was extended to small but nonzero M_s^2/μ in Ref. [97]. We wish to compare our results at small but nonzero M_s^2/μ to those obtained in the Ginzburg-Landau approximation, and to compare the coefficients in the Ginzburg-Landau potential (actually, ratios of coefficients) in our model to those calculated in QCD at asymptotic densities and thus at weak coupling in Refs. [69, 97].

The Ginzburg-Landau potential is parameterized as [97]

$$\begin{aligned}\Omega =& \alpha\left(\Delta_1^2 + \Delta_2^2 + \Delta_3^2\right) \\ &+ \epsilon\left(\Delta_1^2 + \Delta_2^2\right) + \tfrac{1}{3}\eta\left(-2\Delta_1^2 + \Delta_2^2 + \Delta_3^2\right) \\ &+ \beta_1\left(\Delta_1^2 + \Delta_2^2 + \Delta_3^2\right)^2 + \beta_2\left(\Delta_1^4 + \Delta_2^4 + \Delta_3^4\right),\end{aligned} \tag{3.24}$$

where $\alpha = \alpha_0(T - T_c)/T_c$ and where the coefficients ϵ and η are proportional to M_s^2 and μ_e respectively and are therefore present only if $M_s \neq 0$. The form of the ϵ and η terms was derived in Ref. [97] for QCD at asymptotic densities. In the Ginzburg-Landau limit, in which all gap parameters are small, color neutrality occurs with μ_3 and μ_8 vanishingly small [97], and electrical neutrality requires a nonzero μ_e, of

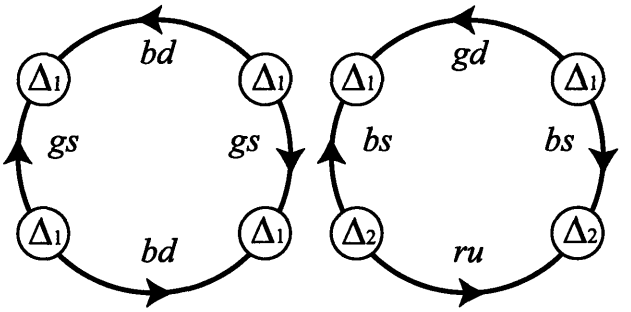

Figure 3-20: Diagrams contributing to the Δ_1^4 and $\Delta_1^2\Delta_2^2$ terms in the Ginzburg Landau potential (3.24).

order $M_s^2/4\mu$ as in unpaired quark matter. At low temperatures, the most important consequences of M_s and μ_e (and also μ_3 and μ_8) derive from the stress they put on pairing, as they (seek to) push Fermi momenta apart. Near T_c, $T \gg \Delta$. And, we are working at $M_s^2/\mu \ll T_c$, where the thermal smearing of the Fermi distributions is much greater than the splittings between Fermi momenta. In this regime, the effects of M_s^2 or μ_e on the pairing of two quarks do not arise from the splitting between their Fermi momenta, as this is negligible. The effects of M_s^2 or μ_e arise from the change in the *average* Fermi momenta of the two quarks, and hence in the density of states, that M_s^2 or μ_e induces. For example, M_s^2 depresses the average Fermi momenta of u-s and d-s pairs, but does not affect u-d pairs. This explains the form of the ϵ term in (3.24). On the other hand, $\mu_e > 0$ increases the average Fermi momenta of d-s pairs, while decreasing that of u-d and u-s pairs. This explains the form of the η term.

The quartic coefficients β_1 and β_2 are nonzero at $T = T_c$, meaning that unlike in the case of the quadratic terms we can safely neglect corrections to the quartic terms proportional to M_s^2 and μ_e [97]. We shall find that (3.24) describes our results very well, confirming the validity of this approximation. In Ref. [69] it is shown that the quartic coefficients simplify further in the weak coupling regime, satisfying $\beta_1 = \beta_2$. This result is valid beyond weak coupling, however, as all that is required to demonstrate it is the pairing ansatz (2.2) and the mean field approximation. The quarks in the 2×2 blocks contribute through diagrams like the first in Fig. 3-20, leading to a contribution proportional to $\Delta_1^4 + \Delta_2^4 + \Delta_3^4$. The quarks in the 3×3 block

contribute through diagrams like both the first and second in Fig. 3-20, leading to a contribution proportional to $\Delta_1^4 + \Delta_2^4 + \Delta_3^4 + 2\Delta_1^2\Delta_2^2 + 2\Delta_2^2\Delta_3^2 + 2\Delta_1^2\Delta_3^2$. Adding all the diagrams, we conclude that $\beta_1 = \beta_2$.

We now wish to confirm that (3.24) correctly describes the M_s-dependent physics in our model. We do so by extracting the ratio

$$\zeta \equiv \frac{\epsilon}{\eta} \tag{3.25}$$

from our results in three independent ways. If (3.24) is correct — that is if there are no M_s-dependent terms missed — the three extractions of ζ should agree. We see in the phase diagrams of Figs. 3-1, 3-16 and 3-17 that the slopes of the three transition temperatures (i.e. $dT_c/d(M_s^2/\mu)$ at $M_s^2/\mu = 0$) are different, with that for the $\Delta_3 \to 0$ critical temperature the shallowest and that for the $\Delta_2 \to 0$ critical temperature the steepest. The ratios of these slopes can be extracted from the Ginzburg-Landau free energy Ω of (3.24) and are given by

$$1 : (6\zeta - 5) : (6\zeta + 4) \tag{3.26}$$

where we have used $\beta_1 = \beta_2$. We can also read the slopes directly from our phase diagrams. The $\Delta_0 = 25$ MeV phase diagram of Fig. 3-1 yields the ratios

$$1 : 10.1 : 19.1 \tag{3.27}$$

which can be used to obtain two independent extractions of ζ, one from $1 : (6\zeta - 5) = 1 : 10.1$ and the other from $1 : (6\zeta + 4) = 1 : 19.1$. The two are in perfect agreement, with both yielding $\zeta = 2.52$ for $\Delta_0 = 25$ MeV.

A third extraction can be obtained from Fig. 3-21 upon realizing that, according to (3.24), in the CFL phase where all three gap parameters are nonzero ζ is given by the ratio

$$\frac{\Delta_3^2 - \Delta_2^2}{\Delta_1^2 - \Delta_2^2} \,. \tag{3.28}$$

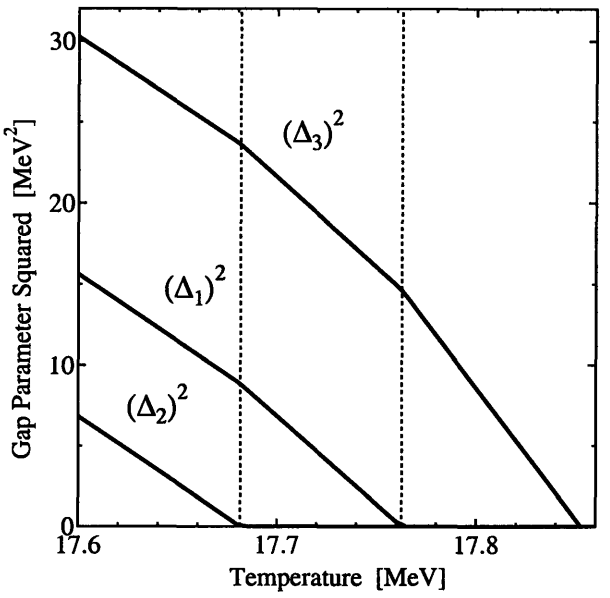

Figure 3-21: Gap parameters squared versus T at $M_s = 30$ MeV, namely $M_s^2/\mu = 1.8$ MeV. This figure should be compared to the "schematic illustration" given in Fig. 2 of [97]. We see the three phase transitions separating the CFL, dSC, 2SC and unpaired phases.

This ratio can be extracted at $M_s^2/\mu = 1.8$ MeV from Fig. 3-21. We have done this extraction at a number values of M_s^2/μ and fitted the results as

$$\frac{\Delta_3^2 - \Delta_2^2}{\Delta_1^2 - \Delta_2^2} = 2.52 + 36.2\left(\frac{M_s}{\mu}\right)^2 + 1.02\times 10^3\left(\frac{M_s}{\mu}\right)^4 \tag{3.29}$$

which leads us to conclude for the third time that $\zeta = 2.52$ for $\Delta_0 = 25$ MeV. In (3.29) we have extracted the M_s^2/μ^2 and M_s^4/μ^4 corrections to the ratio (3.28), in addition to extracting ζ. The coefficients we have obtained confirm that these higher order terms are negligible as long as $M_s^2/\mu^2 \ll T_c/\mu$ or, equivalently given (3.1), $M_s^2/\mu \ll \Delta_0$. This indicates yet again that the Ginzburg-Landau free energy (3.24) provides a good approximation to our results in the regime where it should be valid.

Upon comparing our Fig. 3-21 with the schematic illustration given in Fig. 2 of Ref. [97], there can already be little doubt that the Ginzburg-Landau potential (3.24) correctly describes the results that we have obtained by solving the full gap and neutrality equations numerically, for $T \sim T_c$ and for $M_s^2/\mu^2 \ll T_c/\mu$. The agreement

between our three extractions of ζ makes this point quantitatively.

We can also use Fig. 3-21 to check that our numerical results are consistent with $\beta_1 = \beta_2$. The Ginzburg-Landau potential (3.24) can first be used to show that in the CFL (and dSC) phases in Fig. 3-21 the slopes of the lines for the three (two) nonzero gap parameters are the same. Our results clearly satisfy this. Next, the Ginzburg-Landau potential (3.24) can be used to show that the ratio of the slopes of the gap parameters in the CFL phase in Fig. 3-21 to those in the dSC phase is $(2\beta_1 + \beta_2)/(3\beta_1 + \beta_2)$, and the ratio of those in the dSC phase to that in the 2SC phase is $(\beta_1 + \beta_2)/(2\beta_1 + \beta_2)$. These ratios cannot be extracted very accurately from Fig. 3-21, given the narrow windows within which the dSC and 2SC phases are found. However, they are consistent with 3/4 and 2/3, corresponding to $\beta_1 = \beta_2$.

In Ref. [97], the ratio ζ is calculated using weak coupling methods, valid at asymptotic densities. The weak coupling result is $\zeta = 2$. From our numerical results, we have found $\zeta = 2.52$ at $\Delta_0 = 25$ MeV. We also find $\zeta = 2.69$ at $\Delta_0 = 40$ MeV and $\zeta = 3.87$ at $\Delta_0 = 100$ MeV, extracting ζ from the ratio (3.28) as in (3.29). At weak coupling, $\zeta = 2$ and the Δ_3^2 and Δ_2^2 lines are equidistant from the Δ_1^2 line in the CFL phase region of Fig. 3-21. As the coupling gets stronger, the Δ_1^2 and Δ_2^2 lines move downward/leftward, further away from the Δ_3^2 line, and the ratio ζ increases.

Now that we are convinced that the ϵ and η terms fully describe the M_s-dependent physics in our model at small M_s, we calculate ϵ and η, from diagrams like those in Fig. 3-22.

After some calculation, the result is

$$\epsilon = \frac{M_s^2}{4\pi^2\mu}\int_0^\Lambda dp\, p^2 \Bigg\{ \frac{1}{(p-\mu)^2}\tanh\left(\frac{p-\mu}{2T_c}\right) - \frac{1}{(p+\mu)^2}\tanh\left(\frac{p+\mu}{2T_c}\right) - \frac{\mu}{2T_c\, p(p-\mu)}\left[\cosh\left(\frac{p-\mu}{T_c}\right)\right]^{-2} - \frac{\mu}{2T_c\, p(p+\mu)}\left[\cosh\left(\frac{p+\mu}{T_c}\right)\right]^{-2}\Bigg\} \tag{3.30}$$

$$\eta = \frac{\mu_e}{2\pi^2}\int_0^\Lambda dp\, p^2 \Bigg\{ \frac{1}{(p-\mu)^2}\tanh\left(\frac{p-\mu}{2T_c}\right) - \frac{1}{(p+\mu)^2}\tanh\left(\frac{p+\mu}{2T_c}\right) - \frac{1}{2T_c(p-\mu)}\left[\cosh\left(\frac{p-\mu}{T_c}\right)\right]^{-2} + \frac{1}{2T_c(p+\mu)}\left[\cosh\left(\frac{p+\mu}{T_c}\right)\right]^{-2}\Bigg\}. \tag{3.31}$$

In the weak-coupling limit, $T_c \ll \mu$ and the integrals are dominated by p within T_c of μ. In this limit, it is easy to check that $\zeta = \epsilon/\eta = M_s^2/2\mu\mu_e$, which yields $\zeta = 2$ since $\mu_e = M_s^2/4\mu$. At non-infinitesimal coupling, for example taking $\Delta_0 = 25$ MeV and reading the corresponding T_c from Fig. 3-1, we can evaluate ϵ and η. We find $\zeta = 2.55$ if we use $\mu_e = M_s^2/4\mu$, and if instead we obtain μ_e from our numerical results, we find $\zeta = 2.52$. Taking T_c and μ_e from our numerical results and evaluating ζ using (3.30,3.31) we find $\zeta = 2.52$, 2.65, 3.84 for $\Delta_0 = 25$, 40, 100 MeV respectively. From our numerical results, we have found $\zeta = 2.52$, 2.69, 3.87 at these values of Δ_0, extracting ζ from the ratio (3.28) as in (3.29). The agreement between these determinations is a confirmation of the accuracy of our numerical methods.

It is nice to see how quantitatively well the Ginzburg-Landau approximation describes the physics near T_c in our model, as we have demonstrated. Furthermore, the value of one of the two ratios of coefficients that we have investigated, $\beta_1/\beta_2 = 1$, is the same in our model and in QCD at asymptotic densities. And, the value of the other ratio $\zeta = \epsilon/\eta$ is comparable in our model to its value in QCD at asymptotic densities for $\Delta_0 = 25$ and 40 MeV, becoming significantly larger only for quite strong coupling, as at $\Delta_0 = 100$ MeV.

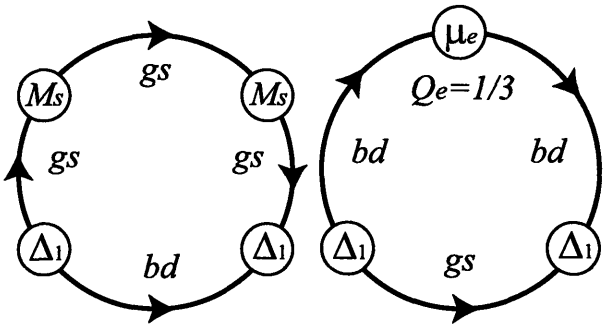

Figure 3-22: Diagrams contributing to the ϵ and η terms in the Ginzburg Landau potential (3.24).

3.7 Implications and Open Questions

The phase diagrams shown in Figs. 3-1, 3-16 and 3-17 constitute the central results of this chapter. They could be used in one of two different ways. If future theoretical advances constrain the μ-dependent values of Δ_0 and M_s more tightly than at present, these phase diagrams (and those that interpolate between them for other values of Δ_0) could be used to construct the phase diagram of nature. Or, if future astrophysical observations teach us that the phase diagram of nature must have certain features, for example must or must not include a certain phase, then the phase diagrams we have constructed could be used to draw inferences about the magnitudes of Δ_0 and M_s.

In thinking about the future phenomenological use of the phase diagrams that we have found, their complexity raises concerns. However, in most astrophysical contexts compact stars have temperatures much less than 1 MeV. At such low temperatures, which can be thought of as $T = 0$ in a QCD context, the phase diagrams are more manageable. We have the CFL phase at asymptotic densities, with the gCFL phase taking over at lower densities, when $\mu < M_s^2/2\Delta$. If Δ_0 lies at the large end of its estimated range 10 MeV$< \Delta_0 <$ 100MeV, it seems likely that hadronic matter will take over from gCFL (or even from CFL) meaning that the complexities that we have found in our phase diagrams at larger M_s^2/μ will likely be superseded by the transition to the hadronic phase.

If Δ_0 lies at the lower end of its allowed range, then in Fig. 3-1 we find a straightforward transition to "unpaired" quark matter as the density is decreased further and M_s^2/μ increases beyond the gCFL window. If we extend our pairing ansatz, we will certainly find some pairing in this regime at sufficiently low temperature. For example, perhaps weak pairing between quarks with the same flavor plays a role [52, 93], or perhaps it is the crystalline color superconducting phase [56, 91] that takes over from gapless CFL at lower densities. Recent developments [91] make the crystalline color superconducting phase look like the most viable contender [25].

The one astrophysical context in which the full complexity of the phase diagrams that we have analyzed must be faced head-on is the physics of the proto-neutron star formed during a supernova, and in particular of the propagation of neutrinos therein. Phenomena encoded in the phase diagrams that we have analyzed could ultimately result in observable consequences in the time-of-arrival distribution of the neutrinos detected from a future supernova [102, 106, 107]. The phenomenological implications of the complexity of the phase diagrams (with many phase transition lines, the doubly critical point, the tricritical point and the insulator to metal transition as the CFL phase is heated) will have to be thought through in this context. The analytic treatment of the insulator to metal crossover and the Ginzburg-Landau analysis of the physics near T_c for small $M_s^2/\mu T_c$ that we have presented in Sections 3.5 and 3.6 could prove valuable in this context.

Our analysis leaves many open avenues of investigation that must still be followed to their conclusions. The effects if gauge field fluctuations must be investigated, as must those of K^0-condensation in the gapless CFL phase. The effects of the 't Hooft interaction should be included, and the quark masses should be treated as dynamical condensates to be solved for, rather than as parameters. The pairing ansatz should be generalized, for example to allow for a comparison between the free energies of the gapless CFL and crystalline phases in three-flavor QCD.

Finally, the stability of the gapless CFL phase needs to be investigated further, along the lines of Ref. [108–110]. The authors of Ref. [108] find that in the g2SC phase, the gluons that correspond to the broken generators of the $SU(3)_c$ develop an

imaginary Meissner mass, which is indication of instability. The authors of Refs. [109, 110] get similar results for the gCFL phase, although with some disagreements. The g2SC phase might be unstable to a mixed phase of charged components [87], or to the crystalline color superconducting phase, or to some inhomogeneous phase yet to be discovered. The gCFL phase, as we showed in Chapter 2 is stable with respect to mixed phases, except perhaps at the largest values of M_s^2/μ where it is found in our phase diagram. It seems likely that at these large values of M_s^2/μ the gCFL phase may anyway be superseded by the crystalline phase [25, 91]. The appearance of the instability in the gCFL case might reflect the existence of some inhomogeneous phase, as in 2SC, or even gluon condensation. However, it is not clear that the Meissner masses in the gCFL phase have been calculated correctly. The calculations of the Meissner masses of the gluons that exist in the literature so far do not consider the modification of the neutral solution due to the presence of the gluons. Gluons can carry non-zero $\tilde{Q}$ charge and therefore it is expected that as they propagate through the gCFL matter, they change locally the solution. The "blocking" bu quarks and the electrons (whose $\tilde{Q}$ charge cancelled in the absence of the gluons), now must have a non-zero net $\tilde{Q}$ charge in order to cancel the $\tilde{Q}$ charge of the gluons.These readjustments of the gCFL solution in response to a gluonic excitation will contribute to the effective masses of the gluons, and may remove the instability.

Chapter 4

Applications in Neutron Stars

It has often been suggested that the core of a neutron star may contain quark matter in one of the color-superconducting phases. The densest predicted phase on the QCD phase diagram is the color-flavor locked (CFL) phase, which is a color superconductor but an electromagnetic insulator [10, 34–36, 63, 64]. The second-densest phase is the gapless CFL (gCFL) phase of Chapters 2 and 3, which is a conductor with a nonzero density of electrons [24–27]. It also has gapless quark quasiparticles, one of which has an almost-quadratic dispersion relation, arising without fine-tuning because it is enforced by the requirement that the matter be electrically neutral [24, 25]. We show in this chapter that this characteristic feature of the gCFL phase means that if quark matter in this phase is present in a neutron star, it dominates the heat capacity and neutrino luminosity, and therefore controls the cooling of the star. At late times this produces a unique signature, as the large heat capacity keeps the star anomalously warm. A neutron star that is tens of millions of years old will be an order of magnitude or more warmer if it contains a region of gCFL quark matter than if it does not.

In any speculation about the phases of matter that occur inside a neutron star, the main challenge is to provide observable signatures of the presence of these phases. Since we are proposing such a signature, albeit one that presents significant observational challenges, we first set the stage with a quick survey of previous proposals.

- Mass-radius relation. If we could measure the mass and radius of several neutron

stars to a reasonable accuracy, mapping out the mass-radius relationship, we would have a strong constraint on the equation of state of dense matter. However, although such measurements would dramatically reduce the current uncertainties in our knowledge of the equation of state of the nuclear matter "mantle" of neutron stars, and could yield evidence of some sort of exotic phase in the core, they would not provide specific evidence of the presence of quark matter [111, 112].

• Double pulsar timing. There is a good prospect that the long term analysis of the recently discovered binary double pulsar [113, 114] may yield a measurement of the moment of inertia of a neutron star [115]. This would provide information about the density profile that is complementary to that obtained from a mass-radius relation, as it would constrain the "compactness" of a star.

• Gravitational waves from collisions. If we could detect gravity waves from neutron stars spiraling into black holes in binary systems, we could perhaps analyze them for information about the density profile of the neutron star, in particular the presence of an interface separating a denser quark core from a less-dense nuclear mantle [90].

• Spinning out a quark matter core. If conditions are "just so", rapidly spinning oblate neutron stars may not have quark matter in their cores even though more slowly rotating spherical neutron stars do. This could be detected either by anomalies in braking indices of stars that are "spinning down" [116] or by anomalous population statistics of stars that are being "spun up" by accretion [117]. Recent observations show no sign of such an effect in the histogram of spin-frequencies of stars in the act of being spun up [118], indicating that if quark matter is present, spinning the star and making it oblate does not get rid of it. If there is a quark matter core, it must therefore occupy a reasonable fraction of the star.

• r-modes. A rapidly spinning neutron star will quickly slow down if it is unstable with respect to bulk flows known as r-modes, which transfer the star's angular momentum into gravitational radiation. This phenomenon will only occur if damping is sufficiently small, so it provides a probe of the viscosity of the interior of the star. Such arguments have been used to rule out the possibility that pulsars are made entirely of CFL quark matter [42], in which viscous damping is negligible [42, 43], but

their implications for the possibility of CFL quark matter localized within the core of a neutron star have not yet been analyzed. Since gCFL quark matter is expected to have a large viscosity, its presence is unlikely to be constrained by r-mode arguments.

• Core glitches. If the third-densest phase on the QCD phase diagram is not nuclear matter, it must be a form of quark matter with less pairing than in the gCFL phase. A leading candidate is the crystalline color superconducting phase [56]. If this form of quark matter occurs within the core of a neutron star, because it is both superfluid and crystalline it may be a locus for pulsar glitches. This proposal has not yet been worked out sufficiently quantitatively to determine whether such core glitches are observable and if so whether they are consistent with (some) observed glitches.

• Direct neutrino detection. Neutrinos have a long mean free path even in nuclear matter, so they can potentially carry information about the core directly to the outside world. Not coincidentally, neutrinos are very hard to detect, and the only time when a neutron star emits enough neutrinos to be detectable on earth is during the first few seconds after the supernova explosion. The time-of-arrival distribution of supernova neutrinos could teach us about possible phase transitions to and in quark matter [106, 119], but analysis of this proposal requires a better understanding of both the supernova itself and of the properties of quark matter at MeV temperatures, where the phase diagram of QCD is more baroque than at zero temperature [26, 27].

• Cooling. A much better prospect is the indirect detection of neutrino emission, which is the dominant heat loss mechanism for the first million years or so, and can therefore be inferred from measurements of neutron star temperature as a function of age. Moreover, because both neutrino emission rates and heat capacity generally rise with density, neutron star cooling is likely to be preferentially sensitive to the properties of matter in the core of a neutron star.

The qualitative distinction among cooling behaviors that may be discerned from the measurement of temperatures of stars that are 10^{3-6} years old is between stars in which direct Urca processes are allowed (which yields a neutrino emissivity $\varepsilon_\nu \sim T^6$), leading to rapid cooling, and stars in which direct Urca processes are forbid-

den [111, 120–128]. Ordinary nuclear matter is unusual in that its direct Urca processes $n \to p + e + \bar{\nu}$ and $p + e \to n + \nu$ are kinematically forbidden, meaning that neutrino emission relies upon slower reactions ($\varepsilon_\nu \sim T^8$). Direct Urca processes are allowed in sufficiently dense nuclear matter, nuclear matter with nonzero hyperon density [129], pion condensation [130] or kaon condensation [131], and in all proposed phases of quark matter except CFL [132, 133]. In the CFL phase, there are no direct Urca processes because thermally excited quark quasiparticles are exponentially rare. There are neutrino emission processes involving collective excitations that lead to $\varepsilon_\nu \sim T^{15}$ [119], but in reality any CFL quark matter within a star will cool by conduction, not by neutrino emission [134]. Indeed, because all forms of dense matter are good thermal conductors, the cooling of a star tends to be dominated by whichever phase has the highest neutrino emissivity. Hence, the discovery of fast cooling would only tell us that some part of the star consists of one of the many phases that allow direct Urca. Discovery of stars that cool slowly would be an indication that they contain only medium-density nuclear matter and perhaps CFL quark matter.

To date, none of the schemes listed above has provided an unambiguous signature of the presence of quark matter, although all are the subject of ongoing observational effort, which in turn drives improvements on the theoretical side. In this chapter, we argue that recent theoretical advances in our understanding of the properties of quark matter offer the prospect of an unambiguous detection, if it is possible to measure the temperatures of neutron stars that are old enough that their cooling is no longer dominated by neutrino emission. Admittedly, this presents an observational challenge. However, it is a challenge that has not been closely studied prior to our work, since all forms of dense matter *except* gCFL quark matter result in neutron stars that cool comparably (and very) rapidly in their old age. We show that quark matter in the gCFL phase keeps aged neutron stars (those significantly older than a million years) much warmer than is predicted by any other assumed dense matter physics.

Younger neutron stars containing gCFL quark matter have a faster-than-standard direct Urca neutrino emissivity $\varepsilon_\nu \sim T^{5.5}$, but this does not lead to faster-than-

standard-direct-Urca cooling because of the correspondingly enhanced gCFL specific heat.

In Section 4.1, we introduce the relevant properties of the gapless CFL phase of quark matter, and in Sections 4.2 and 4.3 we present the calculations of its specific heat c_V and neutrino emissivity ε_ν, respectively. These are our central calculational results. We do not provide a state-of-the-art calculation of the cooling of a neutron star containing gCFL quark matter. Instead, in Section 4.4, we provide an introduction to the physics of neutron star cooling that suffices to illustrate the qualitative consequences of the quantitative results for the gCFL c_V and ε_ν. The astrophysically inclined reader interested in our results and their implications but not in their derivation can find c_V in Eq. (4.8) and ε_ν in (4.31) and, more conveniently, Fig. 4-2 and should read the text around these results and then turn to Section 4.4.

4.1 Introduction to the Gapless CFL Phase of Quark Matter

At any densities that are high enough that nucleons are crushed into quark matter, the quark matter that results at sufficiently low temperatures is expected to be in one of a family of color superconducting phases, with Cooper pairing of quarks near their Fermi surfaces [34–36, 63, 64]. The QCD quark-quark interaction is strong and is attractive between quarks that are antisymmetric in color. If there is quark matter in the cores of neutron stars, we therefore expect it to be color superconducting. The phenomenon persists to asymptotically high densities, where the interaction becomes weak and *ab initio* calculations of properties of color superconducting matter become rigorous. As we have seen in Chapter 3, the QCD phase diagram exhibits a rich structure of color superconducting phases as a function of temperature and density [26, 27, 34–36, 63, 64], but in this chapter we can simplify it by working at zero temperature. This is reasonable because we will be discussing neutron stars with temperatures in the keV range, which is orders of magnitude colder than the vari-

ous critical temperatures at which phase transitions between different quark matter phases occur.

4.1.1 The CFL phase under stress

At asymptotically high densities, where the up, down and strange quarks can be treated on an equal footing and the disruptive effects of the strange quark mass can be neglected, quark matter is in the color-flavor locked (CFL) phase, in which quarks of all three colors and all three flavors form Cooper pairs [10]. The CFL phase is a color superconductor but is an electromagnetic insulator, with zero electron density. In real-world quark matter, as may exist in the cores of compact stars, the density is not asymptotically high. The quark chemical potential μ is of order 500 MeV at most, making it important to include the effects of the strange quark mass M_s, which is expected to be density dependent, lying somewhere between the current mass $\sim$ 100 MeV and the vacuum constituent quark mass $\sim$ 500 MeV. To describe macroscopic regions of quark matter, we must also impose electromagnetic and color neutrality [46, 69, 135] and allow for equilibration under the weak interactions. The CFL pairing pattern is antisymmetric in flavor, color, and spin, so it involves pairing between different flavors. For this reason, the effect of a relatively large M_s, combined with weak equilibration and the neutrality constraints, is to put a stress on the CFL pairing pattern: these effects would all act to pull apart the Fermi momenta of the different flavors by an amount of order M_s^2/μ in the absence of CFL pairing. (This can be seen by an analysis of neutral unpaired quark matter in which the Fermi momenta of the d, u and s quarks are split by $\simeq M_s^2/4\mu$.) In the CFL phase, Fermi momenta do not separate [78] but the consequence of the stress is that the excitation energies of those fermionic quasiparticles whose excitation would serve to ease the stress by breaking pairs and separating Fermi surfaces is reduced, again by of order M_s^2/μ [24]. When the density becomes low enough, some of the quasiparticles become gapless, the CFL pairing pattern is disrupted, and we enter the gapless CFL (gCFL) phase, the second-densest phase on the QCD phase diagram, as we described in detail in Chapters 2 and 3. Since the strength of the CFL pairing is measured by the gap

parameter Δ_{CFL}, and the stress on it is of order M_s^2/μ, the CFL pattern "breaks" and the CFL→gCFL transition occurs when the density is low enough that $M_s^2/\mu \sim \Delta_{CFL}$. Making this argument quantitative results in the prediction of a $T = 0$ second-order insulator-metal transition separating the CFL and gCFL phases at $M_s^2/\mu \simeq 2\Delta_{CFL}$ [24, 25]. An analogous zero temperature metal insulator transition has been analyzed in Ref. [82]. (If the CFL phase is augmented by a K^0-condensate [41, 80], the CFL→gCFL transition is delayed to a value of M_s^2/μ that is higher by a factor of 4/3 [81] or less [80].)

4.1.2 The nature of gCFL pairing

In the gCFL phase the pairing is still antisymmetric in flavor as well as color and spin, so as in CFL there are diquark condensates (gap parameters) $\Delta_1 \sim \langle ds \rangle$, $\Delta_2 \sim \langle us \rangle$, $\Delta_3 \sim \langle ud \rangle$. But unlike the CFL phase, where the gap parameters are very similar, $\Delta_1 = \Delta_2 \simeq \Delta_3$, in gCFL the pairing involving strange quarks is suppressed: very strongly for $\langle ds \rangle$, and quite strongly for $\langle us \rangle$, so that $\Delta_1 < \Delta_2 < \Delta_3$, as shown in Figs. 2-1, 3-2 and 3-5. The result is that while quarks of all three colors and all three flavors still form Cooper pairs, there are regions of momentum space in which there is no $\langle ds \rangle$ pairing, and other (very narrow) regions in which there is no $\langle us \rangle$ pairing, and these regions are bounded by momenta at which the relevant fermionic quasiparticles are gapless.

The gCFL phase is an electromagnetic conductor: unlike the CFL phase, it contains electrons, as discussed in Section 2.3.2. As seen in Figs. 2-2 and 3-3, the electron chemical potential μ_e increases as M_s^2/μ is increased, rising from zero at the CFL→gCFL transition to values which are comparable to or even larger than its typical values in unpaired quark matter, which has $\mu_e \simeq M_s^2/4\mu$.

4.1.3 The gCFL domain

To discuss the range of densities over which gCFL is expected to occur, we shall parametrize the strength of the attractive interaction between quarks by Δ_0, which

we define as the value of the CFL gap parameter at $M_s = 0$ in quark matter with $\mu = 500$ MeV. (We shall quote all numerical results at $\mu = 500$ MeV, corresponding to baryon densities between 8.8 n_0 and 9.1 n_0 depending on the value of Δ_0 that we choose, where $n_0 = 0.17$ fm^{-3} is the baryon density in nuclear matter.) Because asymptotic-density calculations are not quantitatively valid at this μ, Δ_0 is not known precisely, with estimates ranging from 10 to 100 MeV [34–36, 63, 64].

The gCFL phase extends over a range of M_s^2/μ from the continuous CFL→gCFL transition at $M_s^2/\mu = 2\Delta_1 \simeq 2\Delta_0$ up to a first order phase transition where gCFL gives way to some phase with even less pairing. In model calculations, this transition occurs at $M_s^2/\mu \simeq 5\Delta_0$, although this is only quantitatively determined within particular models [24–27]. To give a sense of the scales involved, for $\Delta_0 = 25$ MeV and $M_s = 250$ MeV, the gCFL window $2\Delta_0 \lesssim M_s^2/\mu \lesssim 5\Delta_0$ corresponds to 320 MeV $\lesssim \mu \lesssim$ 800 MeV. At the lower end of this range in μ (upper end in M_s^2/μ) hadronic matter would be more favorable than any form of quark matter. And, the upper end of this range in μ (lower end in M_s^2/μ) corresponds to densities much higher than those achievable in neutron stars. Hence, with these choices of parameters all the quark matter within neutron stars would be in the gCFL phase. For larger Δ_0 or smaller M_s, the gCFL window shifts to lower μ, and neutron stars with a CFL core surrounded by a gCFL layer become possible. In reality, both Δ_0 and M_s are μ-dependent, making these estimates illustrative only.

4.1.4 Gapless quasiparticles in the gCFL phase

In the CFL phase, all nine fermionic quasiparticles are gapped. In the gCFL phase, two dispersion relations are gapless, as shown in Fig. 4-1, which is similar to Fig. 2-4. We label the three quark colors as r,g,b, and make the by now conventional choice for which colors pair with which flavors in the CFL phase. In this notation one of the gapless branches describes quasiparticle excitations that are superpositions of bd particles and gs holes. These excitations are gapless at two momenta p_1^{bd} and p_2^{bd}

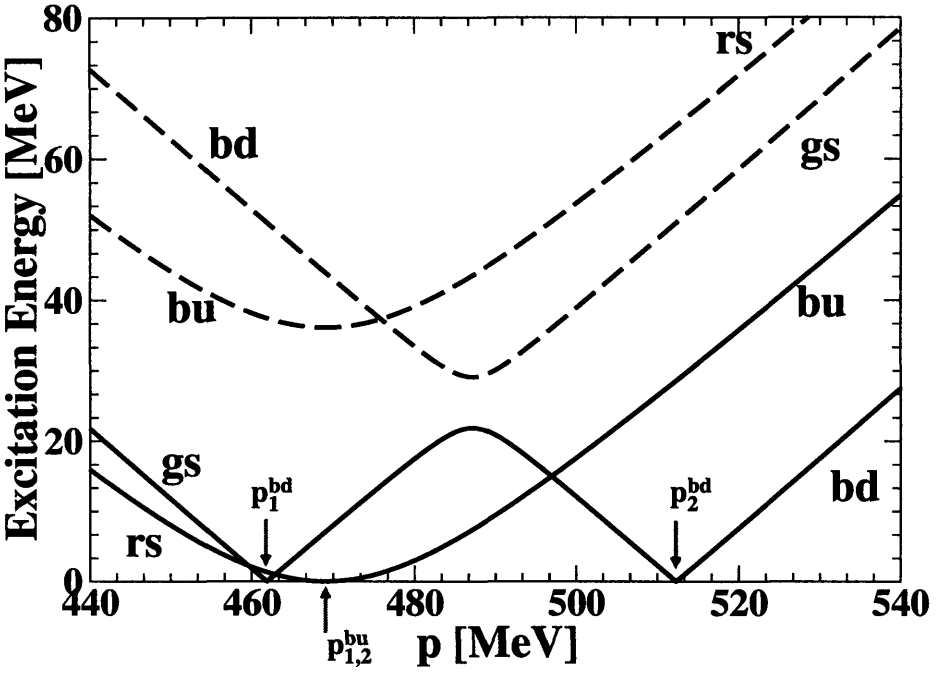

Figure 4-1: Dispersion relations for quasiquarks with *gs-bd* pairing ($\Delta_1 = 3.6$ MeV) and *bu-rs* pairing ($\Delta_2 = 18.5$ MeV), in the model calculation of Chapters 2 and 3 done at $\mu = 500$ MeV, $M_s^2/\mu = 100$ MeV, with $\Delta_0 = 25$ MeV. We find gapless *gs-bd* modes at $p_1^{bd} = 461$ MeV and $p_2^{bd} = 512$ MeV. One *bu-rs* mode is gapless with an almost exactly quadratic dispersion relation. Actually it is gapless at two momenta p_1^{bu} and p_2^{bu}, but these are too close together to be resolved until the temperature drops below the eV scale, meaning we can treat them as a single zero at $p_{1,2}^{bu} = 469$ MeV. The five quark quasiparticles not plotted are all fully gapped in the CFL and gCFL phases.

shown in Fig. 4-1 and given, as we discussed in Chapter 2, by

$$\tfrac{1}{2}(\mu_{gs} + \mu_{bd}) \pm \sqrt{\left[\tfrac{1}{2}\left(\mu_{gs} - \mu_{bd}\right)\right]^2 - \Delta_1^2}\,, \tag{4.1}$$

where μ_{gs} and μ_{bd} are determined by the (nontrivial) requirements of color and electric neutrality. They are defined in Section 2.2, and their values as a function of M_s^2/μ at various Δ_0 can be determined from Figs. 2-2 and 3-3. The gapless excitations at p_1^{bd} are predominantly *gs*, with *bd* contributing only a small component in the superposition. Those at p_2^{bd} are predominantly *bd*. In Section 4.3 we shall focus on this dispersion relation in the vicinity of p_1^{bd}, where it takes the form

$$\epsilon_{bd}(p) = v_{bd}|p - p_1^{bd}|\,, \tag{4.2}$$

where

$$v_{bd} = \sqrt{1 - \frac{\Delta_1^2}{\left[\frac{1}{2}\left(\mu_{gs} - \mu_{bd}\right)\right]^2}} \tag{4.3}$$

is the Fermi velocity of the gapless quasiparticles. The *bd* states with momenta between p_1^{bd} and p_2^{bd} are filled, whereas the *gs* states in this momentum range are empty. This means that there is no *gs-bd* pairing in the ground state wave function in this region of momentum space, although (as the dispersion relations show) there is still pairing among the excitations. The width $p_2^{bd} - p_1^{bd}$ of this "blocking region" wherein pairing is "breached" is zero at the CFL→gCFL phase transition, and grows steadily with increasing M_s^2/μ throughout the gCFL phase. These dispersion relations behave similarly to those describing the gapless modes in the two-flavor gapless 2SC phase [74], and in a metastable three-flavor phase discovered in an early analysis in which the constraints imposed by neutrality were not considered [84].

The physics of the gapless *bu-rs* dispersion relation is interestingly different. As above these excitations are gapless at two momenta p_1^{bu} and p_2^{bu} given by

$$\tfrac{1}{2}(\mu_{bu} + \mu_{rs}) \pm \sqrt{\left[\tfrac{1}{2}\left(\mu_{bu} - \mu_{rs}\right)\right]^2 - \Delta_2^2}\,, \tag{4.4}$$

but in this instance $[\frac{1}{2}(\mu_{bu} - \mu_{rs})]^2 - \Delta_2^2$ is *very* small, making the dispersion relation in Fig. 4-1 look quadratic with a single zero at $p_{1,2}^{bu} = \frac{1}{2}(\mu_{bu} + \mu_{rs})$. For the parameters of Fig. 4-1, $p_2^{bu} - p_1^{bu} = 0.026$ MeV and the height of the dispersion relation half way between these very nearby gapless points is only about 5 eV. Since this is much smaller than the temperatures that will be of interest to us, we can safely treat the dispersion relation as quadratic, with a dispersion relation in the vicinity of its gapless point given approximately by

$$\epsilon_{bu}(p) = \frac{\left(p - p_{1,2}^{bu}\right)^2}{2\Delta_2}\,, \tag{4.5}$$

with the velocity v_{bu}, defined analogously to v_{bd} of (4.3), vanishing at the gapless point. The gap parameter Δ_2 and the chemical potentials that determine $p_{1,2}^{bu}$ are plotted as functions of M_s^2/μ at several values of Δ_0 in Chapters 2 and 3.

As described in Section 2.3.2, this near-quadratic dispersion relation is not a result of fine tuning. It occurs at all μ in the gCFL phase, and arises from the fact that bulk matter must be electrically and color neutral. In both the CFL and gCFL phase, there is an unbroken gauge symmetry, denoted $U(1)_{\tilde{Q}}$, generated by a linear combination of the generators of electromagnetic and color symmetry [10]. Among the neutrality constraints, it is the imposition of $\tilde{Q}$-neutrality that has the implication of interest. The quarks in the gCFL phase are almost $\tilde{Q}$-neutral by themselves, but not quite: their small excess positive $\tilde{Q}$ charge is cancelled by a small admixture of electrons, which have $\tilde{Q} = -1$. The excess of unpaired *bd*-quarks, occurring in a broad band of momenta $p_1^{bd} < p < p_2^{bd}$, does not contribute to the $\tilde{Q}$ imbalance because these quarks have $\tilde{Q} = 0$. It is the unpaired *bu*-quarks with $p_1^{bu} < p < p_2^{bu}$ that matter, because they have $\tilde{Q} = +1$. They contribute a positive $\tilde{Q}$-charge density of order $\mu^2(p_2^{bu} - p_1^{bu})$, balanced by the electron number density, of order μ_e^3. Since $\mu_e \ll \mu$ throughout the gCFL phase, $p_2^{bu} - p_1^{bu}$ is forced (by the dynamics of the gauge fields that maintain neutrality) to remain extremely small, parametrically of order μ_e^3/μ^2, throughout the gCFL phase.

As described above, the dispersion relations for the *gs-bd* quasiparticles are linear about their gapless momenta p_1^{bd} and p_2^{bd}, as in Eq. (4.2), at generic values of M_s^2/μ in the gCFL phase. However, this dispersion relation is fine-tuned to be quadratic precisely at the CFL→gCFL transition, where $p_1^{bd} = p_2^{bd}$ and the Fermi velocity $v_{bd} = 0$. For values of M_s^2/μ that are in the gCFL regime but are close to the CFL→gCFL transition, therefore, the simplified linear expression in Eq. (4.2) cannot be used. Indeed, if we are interested in those excitations with energies of order T or less, the linear expression in Eq. (4.2) is a good approximation as long as $v_{bd} \gtrsim \sqrt{2T/\Delta_1}$. And, close enough to the transition that $v_{bd} \ll \sqrt{2T/\Delta_1}$ the *gs-bd* dispersion relation can be approximated as quadratic, as is appropriate for the *bu-rs* dispersion relation throughout the gCFL phase.

The gapless excitations of the gCFL phase whose dispersion relations we have described determine the specific heat and neutrino emissivity of this phase of matter. In the next two sections, we calculate these quantities in turn.

4.2 Specific Heat of Gapless CFL Quark Matter

The specific heat of any phase of matter is essentially a count of the number of possible excitations with excitation energies of order T or smaller. Precisely, the contribution of quasiparticle excitations with dispersion relation $\epsilon(p)$ to the specific heat (heat capacity per unit volume) at temperature T is given by

$$\begin{aligned} c_V &= 2\int \frac{d^3p}{(2\pi)^3}\,\epsilon(p)\frac{d}{dT}\left(\frac{1}{e^{\epsilon(p)/T}+1}\right) \\ &= \frac{2}{T^2}\int \frac{d^3p}{(2\pi)^3}\,\frac{\epsilon(p)^2}{\left(e^{\epsilon(p)/T}+1\right)\left(e^{-\epsilon(p)/T}+1\right)} \end{aligned} \tag{4.6}$$

where the prefactor 2 assumes that the quasiparticle is doubly degenerate by virtue of its spin. Clearly, only those excitations with $\epsilon \lesssim T$ are important. For the gapless quasiparticle with quadratic dispersion relation, ϵ is near zero for p near $p_{1,2}^{bu}$ and in this regime the dispersion relation can be approximated as in (4.5). Approximating the dispersion relation in this way will give us the specific heat in the small T limit, and so although it is straightforward to obtain an "exact" result upon assuming (4.5), we simply quote the leading result in the small T limit:

$$\begin{aligned} c_V &= \frac{3(\sqrt{2}-1)\zeta\left(\frac{3}{2}\right)}{4\pi^{3/2}}\left(p_{1,2}^{bu}\right)^2\Delta_2^{1/2}T^{1/2} \\ &\simeq 0.146\left(p_{1,2}^{bu}\right)^2\Delta_2^{1/2}T^{1/2}\,. \end{aligned} \tag{4.7}$$

As expected, this is proportional to the number of excitations with energy less than T, given a quadratic dispersion relation (4.5). For quasiparticles with conventional linear dispersion relations, namely $\epsilon(p) = v|p-p_F|$ for some p_F and v, the expression (4.6) yields the familiar $c_V = \frac{1}{3}p_F^2T/v$. Hence, the specific heat of the gCFL phase is given by

$$c_V = \frac{k_B}{(\hbar c)^3}\left[0.146\left(p_{1,2}^{bu}c\right)^2\Delta_2^{1/2}(k_BT)^{1/2} + \frac{c}{3v_{bd}}\left(p_1^{bd}c\right)^2k_BT + \frac{c}{3v_{bd}}\left(p_2^{bd}c\right)^2k_BT + \tfrac{1}{3}\mu_e^2k_BT\right], \tag{4.8}$$

where we have restored factors of $\hbar$, c and Boltzmann's constant k_B and where the last term comes from the electrons and is negligible because all the quark Fermi momenta are of order μ, and $\mu_e \ll \mu$. As long as $T \ll \Delta_2$, the contribution from the quasiparticle with quadratic dispersion relation dominates. We shall describe reasonable values of Δ_2 and T in subsequent sections; it suffices here to say that Δ_2/T is of order hundreds or thousands.

Note that close enough to the CFL→gCFL transition that $v_{bd} \lesssim \sqrt{2T/\Delta_1}$, the *gs-bd* dispersion relation cannnot be treated as linear, and the expression (4.8) is modified. Indeed, if $v_{bd} \ll \sqrt{2T/\Delta_1}$ the *gs-bd* dispersion relation can be treated as quadratic, making their contribution to the specific heat comparable to that of the *bu-rs* quasiparticles.

The gCFL phase also has light bosonic excitations, for example that associated with superfluidity, but their contribution to the specific heat is of order T^3 and so can be neglected. The specific heat may be enhanced by logarithimc corrections analogous to those in unpaired quark matter [136], but we leave their analysis to future work.

4.3 Neutrino Emissivity of Gapless CFL Quark Matter

The presence of gapless quark quasiparticles in the gCFL phase raises the possibility of neutrino emission by direct Urca processes. Because the gapless modes are superpositions of *gs* and *bd* quarks, and *bu* and *rs* quarks, and because weak interactions cannot change the color of a quark, the direct Urca processes that we must consider are

$$bd \to bu + e^- + \bar{\nu} \tag{4.9}$$

and

$$bu + e^- \to bd + \nu \ . \tag{4.10}$$

Momentum conservation in these reactions requires that the momenta of the two quarks and the electron form a triangle [132, 133]. (The argument is that these

three fermions must all have energies of order T and hence must all be close to the momenta at which their dispersion relations are gapless. The neutrinos escape from the star, and hence have zero Fermi momentum. By energy conservation, the escaping neutrino therefore has energy, and hence momentum, of order T. This is negligible compared with the momenta of the other fermions.) Momenta of the two quarks and the electron satisfying the triangle constraint can only be found if $|p^{bu} - p^{bd}| \leq \mu_e$, where p^{bu} and p^{bd} are the magnitudes of the momenta at which the bu and bd quarks are gapless. The only momentum at which gapless quasiparticles with a bu component are found is $p^{bu}_{1,2}$. Gapless bd quarks occur at two momenta. For the parameters in Fig. 4-1, the electron Fermi momentum is $\mu_e = 25.9$ MeV, meaning that the triangle constraint can be satisfied if we choose bd quarks with momenta near p^{bd}_1, but cannot be satisfied for those near p^{bd}_2. Indeed, we find that direct Urca processes involving the quasiparticles at p^{bd}_2 are forbidden throughout the gCFL regime of M_s^2/μ, whereas those involving quasiparticles at p^{bd}_1 are allowed throughout all of the gCFL regime, with the available phase space vanishing at the CFL→gCFL transition and opening up with increasing M_s^2/μ.

The calculation of the neutrino emissivity due to direct Urca processes in unpaired quark matter was first done by Iwamoto in Refs. [132, 133], and we shall follow his analysis, leaving the calculation of any logarithmic enhancement analogous to that in unpaired quark matter [137] to future work. There are two essential differences between Iwamoto's calculation for unpaired quark matter and ours for the gCFL phase. First, although the quasiparticles near p^{bd}_1 have a conventional linear dispersion relation $\epsilon_{bd}(p)$ given in (4.2), as in unpaired quark matter, the quasiparticles near $p^{bu}_{1,2}$ have a quadratic dispersion relation $\epsilon_{bu}(p)$ given in (4.5). Analogous to its effect on the specific heat, this unusual dispersion relation increases the available phase space for the direct Urca reactions by a factor of order $\sqrt{\Delta_2/T}$ relative to that in the standard calculation, resulting in a neutrino emissivity $\varepsilon_\nu \sim T^{5.5}$ rather than $\sim T^6$. Second, the quasiparticles near p^{bd}_1 and $p^{bu}_{1,2}$ with dispersion relations ϵ_{bd} and ϵ_{bu} are *not* purely bd and bu quarks. They are superpositions of bd and gs quarks, and bu and rs quarks, respectively. Only the bd and bu components of the quasiparticles

participate, meaning that the neutrino emissivity is proportional to the probabilities that each quasiparticle is blue. These probabilities are the squares of the Bogoliubov coefficients B_{bu} and B_{bd}, specified as follows [10]. B_{bu} is given by

$$B_{bu}(p)^2 = \frac{1}{2}\left(1 + \frac{p - p_{1,2}^{bu}}{\sqrt{(p - p_{1,2}^{bu})^2 + \Delta_2^2}}\right) \tag{4.11}$$

where $p_{1,2}^{bu} = \frac{1}{2}(\mu_{bu} + \mu_{rs})$ and where Δ_2 is the gap parameter for the pairing between bu and rs quarks. To simplify the calculation we Taylor expand the coefficient around $p_{1,2}^{bu}$ and get

$$B_{bu}(p)^2 = \frac{1}{2}\left(1 + \frac{p - p_{1,2}^{bu}}{\Delta_2}\right) . \tag{4.12}$$

The bd Bogoliubov coefficient is given by

$$B_{bd}(p)^2 = \frac{1}{2}\left(1 + \frac{p - \bar{\mu}}{\sqrt{(p - \bar{\mu})^2 + \Delta_1^2}}\right) \tag{4.13}$$

where $\bar{\mu} = \frac{1}{2}(\mu_{bd} + \mu_{gs})$ and where Δ_1 is the gap parameter for the pairing between bd and gs quarks. Because the dispersion relation is linear, the quarks that contribute to the emissivity lie in a band about p_1^{bd} whose width is only of order T, and we shall replace $B_{bd}(p)$ by $B_{bd}\left(p_1^{bd}\right)$. This coefficient can be quite small. For example, with parameters as in Fig. 4-1, meaning in particular $M_s^2/\mu = 100$ MeV, the probability that the gapless quasiparticles at p_1^{bd} are in fact bd is only $B_{bd}\left(p_1^{bd}\right)^2 = 0.00479$.

We now present the calculation of ε_ν, following Refs. [132, 133]. The transition rate for the process (4.9) is

$$W = \frac{V(2\pi)^4 \delta^{(4)}(p_{bd} - p_\nu - p_{bu} - p_e)}{\prod_{i=1}^4 2E_i V} |M|^2 \tag{4.14}$$

where the index i runs over the four species that participate in the interaction. V is the normalization volume, which will drop out by the end of the calculation, and the

squared amplitude $|M|^2$ is given by

$$|M|^2 = 64 G_F^2 \cos^2\theta_c (p_{bd} \cdot p_\nu)(p_{bu} \cdot p_e) \ , \tag{4.15}$$

where we have averaged over the spin of the initial down quark and summed over the spin of the final up quark. Here, G_F is the Fermi constant and θ_c is the Cabibbo angle.

The neutrino emissivity is the rate of energy loss per unit volume due to neutrino emission. It is obtained by multiplying the transition rate by the neutrino energy and integrating over the available phase space, weighted by the Bogoliubov coefficients. The expression can be written as

$$\varepsilon_\nu = \frac{2}{V}\left[\prod_{i=1}^{4} V \int \frac{d^3p_i}{(2\pi)^3}\right] E_\nu \, W \, n(p_{bd})(1-n(p_{bu}))(1-n(p_e)) B_{bu}(p_{bu})^2 B_{bd}(p_1^{bd})^2 \ . \tag{4.16}$$

Here, the Fermi distribution functions $n(p_{bd})(1-n(p_{bu}))(1-n(p_e))$ state that in order for the process to occur we have to have an occupied down state and unoccupied up and electron states. In thermal equilibrium (which is maintained by strong and electromagnetic processes occurring on timescales much faster than neutrino emission via weak interactions) the distribution functions are given by

$$n(p_i) = \frac{1}{1+\exp x_i} \tag{4.17}$$

where

$$x_e = \frac{p_e - \mu_e}{T} \ , \tag{4.18}$$

where

$$x_{bd} = \pm \frac{\epsilon_{bd}(p_{bd})}{T} \ , \tag{4.19}$$

with the $\pm$ serving in effect to undo the absolute value in (4.2), and where

$$x_{bu} = \pm \frac{\epsilon_{bu}(p_{bu})}{T} \tag{4.20}$$

with the $\pm$ chosen positive for $p_{bu} > p_{1,2}^{bu}$ and negative for $p_{bu} < p_{1,2}^{bu}$. In defining x_{bd} we have used (4.2), meaning that this derivation is valid at generic values of M_s^2/μ in the gCFL regime where $v_{bd} \gtrsim \sqrt{2T/\Delta_1}$, but not close to the CFL→gCFL transition, where both the *bd* and *bu* branches should be treated as quadratic. We shall discuss this further below. For later use, we also define

$$x_\nu = \frac{p_\nu}{T} \ . \tag{4.21}$$

It is possible to set the calculation up directly in terms of the positive quasiparticle excitation energies, but introducing the $\pm$ as we have done allows us to follow Iwamoto's calculation more closely.

We combine Eqs. (4.14), (4.15), (4.16), (4.17) and multiply by a factor of 2 in order to include the emissivity due to the second process (4.10), whose contribution proves to be the same as that above. We write the integration element $d^3p_i = p_i^2 dp_i d\Omega_i$, where $d\Omega_i$ is the infinitesimal solid angle. The complete expression for the emissivity then takes the form [132, 133]

$$\varepsilon_\nu = \frac{G_F^2}{16\pi^8} \cos^2\theta_c (1 - \cos\theta_{ue}) \mathcal{A}\mathcal{B} \ . \tag{4.22}$$

Here, $\mathcal{A}$ is an angular integral defined as

$$\mathcal{A} = \left(\prod_{i=1}^{4} \int d\Omega_i \right) \delta(\mathbf{p}_{bd} - \mathbf{p}_{bu} - \mathbf{p}_e) \ , \tag{4.23}$$

where we have eliminated certain terms that vanish identically upon angular integration. $\mathcal{A}$ is identical to that in Refs. [132, 133] and upon evaluation yields

$$\mathcal{A} = \frac{32\pi^3}{p_1^{bd} p_{1,2}^{bu} \mu_e} \ , \tag{4.24}$$

where we have taken $|\mathbf{p}_{bd}| = p_1^{bd}$, $|\mathbf{p}_{bu}| = p_{1,2}^{bu}$, $|\mathbf{p}_e| = \mu_e$, knowing that these are the values at which the $\mathcal{B}$ integral is dominated. The integral $\mathcal{B}$ is defined as

$$\mathcal{B} = \int_0^\infty p_{bd}^2 dp_{bd} \int_0^\infty p_{bu}^2 dp_{bu} \int_0^\infty p_e^2 dp_e \int_0^\infty p_\nu^3 dp_\nu n(p_{bd})(1-n(p_{bu}))(1-n(p_e)) \\ \times \frac{1}{T}\delta\left(x_{bd} - x_\nu - x_{bu} - x_e\right) B_{bu}(p_{bu})^2 B_{bd}(p_1^{bd})^2. \quad (4.25)$$

Finally, the angle θ_{ue} in (4.22) is the angle between the momentum of the bu-quark and that of the electron, when the two quark momenta and the electron momentum are arranged in a momentum conserving triangle. A little trigonometry shows that $\theta_{ue} = \theta_{de} + \theta_{du}$ where

$$\cos\theta_{de} = \frac{(p_1^{bd})^2 + \mu_e^2 - (p_{1,2}^{bu})^2}{2p_1^{bd}\mu_e} \quad (4.26)$$

and

$$\cos\theta_{du} = \frac{(p_1^{bd})^2 - \mu_e^2 + (p_{1,2}^{bu})^2}{2p_1^{bd}p_{1,2}^{bu}}\ . \quad (4.27)$$

Now, all that remains is the evaluation of $\mathcal{B}$.

The integral $\mathcal{B}$ is dominated by p_{bd} near p_1^{bd}, by p_{bu} near $p_{1,2}^{bu}$, and by p_e near μ_e so we can pull the factor $p_{bd}^2 p_{bu}^2 p_e^2$ out of the integrand and replace it by $(p_1^{bd})^2(p_{1,2}^{bu})^2\mu_e^2$. Next, we change variables of integration from the p's to the x's and obtain

$$\mathcal{B} = (p_1^{bd})^2(p_{1,2}^{bu})^2\mu_e^2 T^6 \frac{B_{bd}(p_1^{bd})^2}{2} \int_{-\infty}^\infty \frac{dx_{bd}}{v_{bd}} \int_{-\infty}^\infty dx_e \int_0^\infty dx_\nu x_\nu^3 \int_{-\infty}^\infty dx_{bu} \\ \times \frac{\sqrt{\Delta_2}}{\sqrt{2T\left|x_{bu}\right|}} \frac{1}{e^{x_{bd}}+1} \frac{1}{e^{x_{bu}}+1} \frac{1}{e^{x_e}+1} \delta(x_{bd} + x_{bu} + x_e - x_\nu) \quad (4.28)$$

where, as in the calculation of the specific heat, the enhanced density of states $dp_{bu}/dx_{bu} = (\Delta_2 T/2\left|x_{bu}\right|)^{1/2}$ for the quasiparticle with the quadratic dispersion relation is crucial. In (4.28) we have made the approximation $B_{bu}(p_{1,2}^{bu})^2 \simeq \frac{1}{2}$, since the other term in (4.12) leads to a contribution proportional to T^6 and we are keeping

only the leading contribution, proportional to $T^{5.5}$. We now rewrite (4.28) as

$$\mathcal{B} = \frac{1}{2\sqrt{2}}(p_1^{bd})^2(p_{1,2}^{bu})^2\mu_e^2\frac{T^{5.5}\sqrt{\Delta_2}B_{bd}(p_1^{bd})^2}{v_{bd}}\int_{-\infty}^{\infty}dx_{bd}\int_{-\infty}^{\infty}dx_e\int_0^{\infty}dx_\nu x_\nu^3\int_{-\infty}^{\infty}dx_{bu}$$
$$\times\frac{1}{\sqrt{|\,x_{bu}\,|}}\frac{1}{e^{x_{bd}}+1}\frac{1}{e^{x_{bu}}+1}\frac{1}{e^{x_e}+1}\delta(x_{bd}+x_{bu}+x_e-x_\nu)\ , \quad (4.29)$$

use the delta function to perform one of the integrations, and then perform the remaining dimensionless triple integral numerically. The result is

$$\mathcal{B} = 31.18\,(p_1^{bd})^2(p_{1,2}^{bu})^2\mu_e^2\frac{T^{5.5}\sqrt{\Delta_2}B_{bd}(p_1^{bd})^2}{v_{bd}}\ . \quad (4.30)$$

Combining this with the result (4.24) for $\mathcal{A}$ and substituting into (4.22) we obtain the final result for the neutrino emissivity of the gCFL phase

$$\varepsilon_\nu = \frac{62.36\,G_F^2\cos^2\theta_c}{\pi^5}\frac{}{\hbar^{10}c^7}(1-\cos\theta_{ue})p_1^{bd}p_{1,2}^{bu}\mu_e\frac{(k_BT)^{5.5}\sqrt{\Delta_2}B_{bd}(p_1^{bd})^2}{v_{bd}}\ , \quad (4.31)$$

where we have restored the factors of $\hbar$, c and k_B. This result is valid as long as $v_{bd} \gtrsim \sqrt{2T/\Delta_1}$, meaning that the *gs-bd* dispersion relation can be treated as linear with slope v_{bd}. At any nonzero temperature, there is a region just on the gCFL side of the CFL $\to$ gCFL transition where this approximation breaks down. Indeed, in the region so close to the transition that $v_{bd} \ll \sqrt{2T/\Delta_1}$, the *gs-bd* and *bu-rs* dispersion relations can both be treated as quadratic, and an analysis similar to that we have presented above yields

$$\varepsilon_\nu = \frac{42.70\,G_F^2\cos^2\theta_c}{\pi^5}\frac{}{\hbar^{10}c^7}(1-\cos\theta_{ue})p_1^{bd}p_{1,2}^{bu}\mu_e(k_BT)^5\sqrt{\Delta_2\Delta_1}B_{bd}(p_1^{bd})^2\ . \quad (4.32)$$

We shall see below that for temperatures of interest in neutron star physics, this expression is valid only in a very narrow window of parameter space. It is (4.31) that is relevant to neutron star phenomenology.

The gCFL emissivity (4.31) can be compared to the neutrino emissivity of nonin-

teracting quark matter [132, 133]

$$\begin{aligned}\varepsilon_\nu^{\text{unpaired}} &= \frac{457\pi}{1680}\frac{G_F^2\cos^2\theta_c}{\hbar^{10}c^4}M_s^2 p_F (k_B T)^6 \\ &= (3.6\times 10^{14}\ \text{erg cm}^{-3}\,\text{s}^{-1})\times \\ &\quad \left(\frac{(M_s^2/\mu)}{100\ \text{MeV}}\right)\left(\frac{\mu}{500\ \text{MeV}}\right)^2\left(\frac{T}{10^7\ \text{K}}\right)^6\end{aligned} \tag{4.33}$$

where $p_F \simeq \mu$ is the up quark Fermi momentum and where μ_e has been replaced by $M_s^2/4\mu$, appropriate for neutral unpaired quark matter. The gCFL emissivity (4.31) is enhanced by a factor of $\sqrt{\Delta_2/T}$ relative to that of noninteracting quark matter, but the full comparison between the two rates is more involved.

We have obtained our result (4.31) in a form which makes the dependence of ε_ν on T manifest, but which obscures the dependence on M_s and μ because Δ_2, $B_{bd}(p_1^{bd})$, μ_e, v_{bd}, p_1^{bd} and $p_{1,2}^{bu}$ all change with M_s and μ. The most important μ dependence is straightforward: $p_1^{bd} \sim p_{1,2}^{bu} \sim \mu$ and hence $\varepsilon_\nu \sim \mu^2$. The remaining dependence on M_s and μ is dominated by the dependence on M_s^2/μ, which is nontrivial because Δ_2, $B_{bd}(p_1^{bd})$, μ_e and v_{bd} and $p_2^{bd} - p_1^{bd}$ all depend nontrivially on M_s^2/μ. The result also depends on Δ_0, through this same set of quantities. The reader who wishes to obtain numerical values of ε_ν would need numerical values for the gap parameters and chemical potentials in the gCFL phase given in plots in Chapters 2 and 3, which are used in the specification of many of the quantities occurring in (4.31). Given all these implicit dependences, we provide Fig. 4-2 for the convenience of the reader who wishes to use our result (4.31) for the gCFL neutrino emissivity, for example in order to calculate its effects on neutron star cooling.

The most important dependences of ε_ν are straightforward: $\varepsilon_\nu \sim T^{5.5}$ and $\varepsilon_\nu \sim \mu^2$. All the remaining dependences are best described as dependence on M_s^2/μ and Δ_0, and hence are described by Figure 4-2 which shows $\varepsilon_\nu/T^{5.5}$ as a function of M_s^2/μ for two values of Δ_0. For each Δ_0, we see nonzero neutrino emissivity in the corresponding gCFL regime, with ε_ν negligible at lower M_s^2/μ in the CFL phase. We do not plot ε_ν at values of M_s^2/μ that are larger than the gCFL regime, because it is not known what phase of quark matter would be favored there, with what T-dependence for its

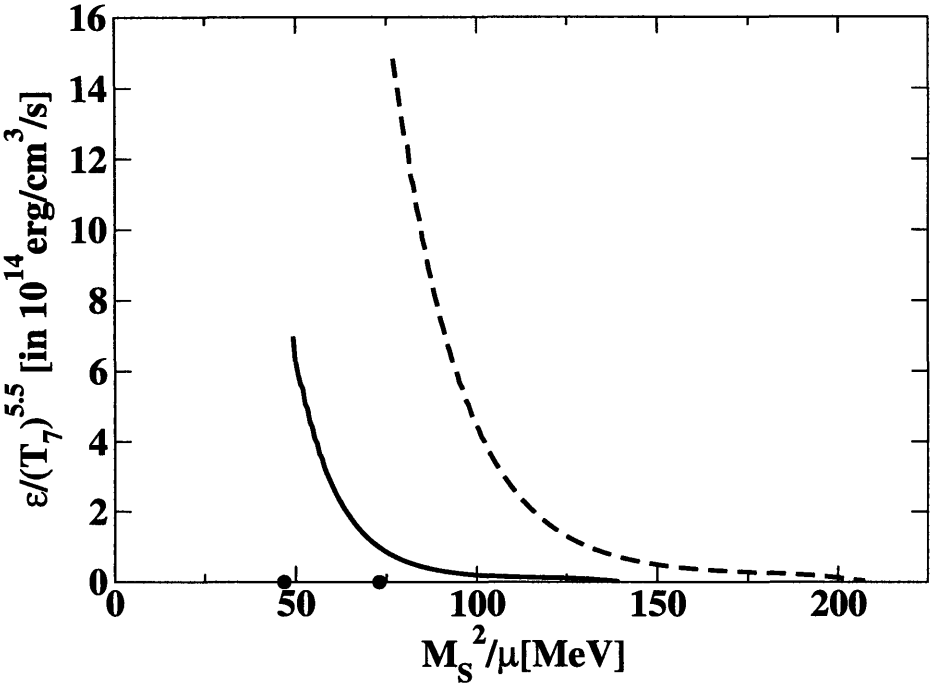

Figure 4-2: Neutrino emissivity ε_ν of gCFL quark matter from (4.31) divided by $(T/10^7\mathrm{K})^{5.5}$, plotted versus M_s^2/μ. The two curves are drawn for two different values of the strength of the interaction between quarks, corresponding to CFL gap parameters $\Delta_0 = 25$ (solid curve) and $\Delta_0 = 40$ MeV (dashed). The location of the CFL $\rightarrow$ gCFL transitions for $\Delta_0 = 25$ and 40 MeV are indicated by dots on the horizontal axis, at $M_s^2/\mu = 46.8$ and 73.0 MeV respectively. To the left of these dots, ε_ν is negligible in the CFL phase. As discussed in the text we begin the curves a small interval to the right of the transition, at the M_s^2/μ where $v_{bd} = 0.15$. (The $\Delta_0 = 25$ MeV and $\Delta_0 = 40$ MeV curves begin 2.5 MeV and 3.9 MeV to the right of their respective transitions.) The baryon chemical potential is $\mu = 500$ MeV, corresponding to a density about nine times that of ordinary nuclear matter. The effect of changing μ while keeping M_s^2/μ and Δ_0 fixed can be approximated by scaling ε_ν with μ^2.

ε_ν. (Crystalline color superconducting quark matter [56] is a leading candidate for the third-densest phase on the QCD phase diagram, and its neutrino emissivity has not been calculated.) Also, at these low densities quark matter may well have already been superseded by nuclear matter. Note that a reasonable estimate of the range of M_s^2/μ of interest to describe possible quark matter in neutron stars is 50 MeV $< M_s^2/\mu <$ 250 MeV, corresponding roughly to 350 MeV $< \mu <$ 500 MeV and 150 MeV $< M_s <$ 300 MeV. If Δ_0 is large, say $\Delta_0 = 100$ MeV, the curve on Fig. 4-2 shifts far to the right, and any quark matter that occurs is likely CFL, with negligible ε_ν. We see from the figure that for $\Delta_0 = 25$ MeV, the highest density quark matter that can be

reached is likely in the gCFL phase. For intermediate values of Δ_0, it is possible to obtain a CFL core surrounded by a gCFL layer.

The shape of the curves in Fig. 4-2 arises from the combination of many effects. As M_s^2/μ increases through the gCFL regime, μ_e rises monotonically and $(1-\cos\theta_{ue})$ initially rises rapidly as phase space for neutrino emission opens up, and then varies little. These effects are overwhelmed by the fact that as M_s^2/μ increases through the gCFL regime, Δ_2, $1/v_{bd}$, and the Bogoliubov coefficient $B_{bd}(p_1^{bd})$ all decrease monotonically.

Close to the CFL $\rightarrow$ gCFL transition, the most important contribution to the steep decrease of ε_ν with increasing M_s^2/μ seen in Fig. 4-2 is the factor $1/v_{bd}$ occurring in (4.31), since after all $v_{bd} = 0$ at the transition. However, one must recall that the expression (4.31) plotted in Fig. 2 is only valid for $v_{bd} \gtrsim \sqrt{2T/\Delta_1}$. Indeed, for any nonzero T there is a region close to the transition where $v_{bd} \ll \sqrt{2T/\Delta_1}$ and the emissivity is given by (4.32) with $\varepsilon_\nu \sim T^5$, not by (4.31) with $\varepsilon_\nu \sim T^{5.5}$ as plotted in Fig. 2. In Fig. 4-2, we have begun the gCFL curves at the value of M_s^2/μ at which $v_{bd} = 0.15$, meaning that the curves can be trusted as long as $T \lesssim \Delta_1/100 \simeq \Delta_0/100$. (Note that $\Delta_1 \simeq \Delta_0$ near the CFL $\rightarrow$ gCFL transition.) For typical neutron star temperatures of order keV, $\varepsilon_\nu \sim T^{5.5}$ as given by (4.31) (and the curves of Fig. 4-2 are therefore valid) even closer to the transition than where we stopped the curves in the Fig 2. The curves can safely be used in neutron star cooling calculations, as we shall do in Section 4.4.

Further to the right in Fig. 4-2, well away from the transition, v_{bd} approaches 1 and the factor $1/v_{bd}$ ceases to control the shape of the curves. In this regime, the most important contribution to the decline in ε_ν is the rapidly falling Bogoliubov coefficient: as M_s^2/μ increases p_1^{bd} and p_2^{bd} in Fig. 4-1 separate and the bd-component of the gapless quasiparticle at p_1^{bd}, namely $B_{bd}(p_1^{bd})$, drops faster than μ_e rises.

In Section 4.4 we shall sketch the implications of our results for the specific heat and neutrino emissivity of gCFL quark matter for neutron star cooling. The most important dependence of ε_ν in this context is its T-dependence. In all plots in Section 4.4, we show two curves, both with $M_s^2/\mu = 100$ MeV, one with $\Delta_0 = 25$ MeV and

one with $\Delta_0 = 40$ MeV. We choose these values because we see from Fig. 4-2 that they correspond to a small, but reasonable, and a larger, but still reasonable, value of $\varepsilon_\nu/T^{5.5}$. Were we to choose values of parameters that happened to land very close to the CFL $\rightarrow$ gCFL transition, all the conclusions that we draw in the next section would become stronger.

4.4 Implications for the Cooling of Neutron Stars

The central results of this chapter are the specific heat and neutrino emissivity, calculated in Sections 4.2 and 4.3. We shall not attempt a state-of-the-art neutron star cooling calculation here, preferring instead to provide a calculation that is better thought of as illustrative, not quantitative. The effect that we wish to highlight is both large and qualitative, arising from the T-dependence of c_V and ϵ_ν, and we expect that even our crude treatment will persuade the reader of its significance.

We analyze the cooling of a "toy star" consisting of a volume of "nuclear matter" at a constant density $1.5n_0$ and a volume of denser quark matter with a constant density specified by $\mu = 500$ MeV. As nuclear matter we take an electrically neutral gas of noninteracting neutrons, protons and electrons in weak equilibrium. We investigate three different possibilities for the quark matter, all electrically and color neutral and in weak equilibrium, and all with $\mu = 500$ MeV and $M_s^2/\mu = 100$ MeV. We consider two possibilities for quark matter in the gCFL phase, with $\Delta_0 = 40$ MeV and $\Delta_0 = 25$ MeV. And, we consider noninteracting quark matter. These three options have densities of 9.1, 8.9 and 8.8 times normal nuclear matter density n_0, respectively. By treating the quark matter core as having a constant density, our calculation neglects the possibility of a thin spherical gCFL-CFL interface region, in which there would be an enhancement in both the specific heat (by a factor of two, see end of Sect. 4.2) and the neutrino emissivity (see Eq. (4.32)) relative to the gCFL expressions (4.8) and (4.31) that we shall use. Such a shell would be very thin because these enhancements occur only within a very narrow window in M_s^2/μ, but a quantitative investigation of how small its effects are is not possible in our "toy

star calculation". We choose the quark matter and nuclear matter volumes V_{qm} and V_{nm} such that the total mass of the star is 1.4 solar masses. If we set the quark matter volume to zero, this corresponds to choosing a nuclear matter "star" that is a sphere with radius $R = 12$ km. If we include a dense quark matter core with radius $R_{\rm core}$ while keeping the total mass fixed, the star shrinks as we increase $R_{\rm core}$. With $R_{\rm core} = 5$ km the stellar radius is $R = 10$ km. A gCFL core with radius 5 km has the same volume as a gCFL layer extending from $r = 4.5$ km to $r = 6$ km. Since such a layer would surround a CFL quark matter core, and since CFL matter plays no role in neutron star cooling, the estimates that we quote for $R_{\rm core} = 5$ km can equally well be taken as a guide to this scenario. Our final toy-model assumption is that our "star" is a black body. The work that needs to be done to turn our illustrative "toy star calculation" into a quantitative calculation of neutron star cooling includes the investigation of realistic density profiles, realistic nuclear matter, and realistic atmospheres. We defer this, as our calculation suffices to make our qualitative point.

Our "star" loses heat by neutrino emission from its entire volume and by black body emission of photons from its surface. The heat loss due to neutrino emission is

$$L_\nu = V_{nm}\varepsilon_\nu^{nm} + V_{qm}\varepsilon_\nu^{qm} \ . \tag{4.34}$$

The quark matter neutrino emissivity ε_ν^{qm} is given either by (4.31) or (4.33), depending on whether we are considering a gCFL core or an unpaired quark matter core. The nuclear matter emits neutrinos via modified Urca processes like $n+X \to p+X+e+\bar{\nu}$, with X either a neutron or a proton that serves to carry away some recoil momentum, in order that momentum and energy can both be conserved in the process. The resulting emissivity is [125, 130]

$$\varepsilon_\nu^{nm} = \left(1.2 \times 10^4 \,\mathrm{erg\ cm^{-3} s^{-1}}\right) \left(\frac{n}{n_0}\right)^{2/3} \left(\frac{T}{10^7\ \mathrm{K}}\right)^8 \ . \tag{4.35}$$

In evaluating the nuclear matter and quark matter emissivities, we shall assume that the entire interior of the star is at a common temperature T. Both nuclear matter

and quark matter are good conductors of heat, and neutron stars older than a few years are well approximated as isothermal.

Because $\varepsilon_\nu \sim T^{5.5}$ in the gCFL phase, L_ν will be dominated by neutrino emission from the gCFL matter, unless the gCFL volume is very small. We include cooling curves for cores made of "unpaired quark matter" even though this is not expected to be present on the phase diagram of QCD at neutron star temperatures because it serves as a representative example of the large class of phases of dense matter in which $\varepsilon_\nu \sim T^6$ and $c_V \sim T$. This class includes all quark and nuclear phases that cool by direct Urca processes, except for gCFL.

The surface of real neutron stars is colder than their interiors, with the temperature gradients occurring only in the outer envelope of the star within of order 100 meters of the surface. The heat transport within this envelope has been analyzed [138, 139], and the result is well approximated by a phenomenological relationship between the interior temperature T and the surface temperature $T_{\rm surface}$ given by [127, 138, 139]

$$T_{\rm surface} = (0.87 \times 10^6 \text{ K}) \left(\frac{g_s}{10^{14}\text{cm/s}^2}\right)^{1/4} \left(\frac{T}{10^8\text{K}}\right)^{0.55} , \tag{4.36}$$

where $g_s \equiv G_N M/R^2$ is the surface gravity. This means that the rate of heat loss from the surface of the star, which for a black body is

$$L_\gamma = 4\pi R^2 \sigma T_{\rm surface}^4 \tag{4.37}$$

with σ the Stefan-Boltzmann constant, is given by

$$L_\gamma = 4\pi R^2 \sigma (0.87 \times 10^6 \text{ K})^4 \left(\frac{g_s}{10^{14}\text{cm/s}^2}\right) \left(\frac{T}{10^8\text{K}}\right)^{2.2} . \tag{4.38}$$

We shall use this expression for L_γ, even though we are not treating other aspects of the problem realistically, because the fact that $L_\gamma \sim T^{2.2}$ will play an important qualitative role.

The cooling of our "star" is described by the differential equation

$$\frac{dT}{dt} = -\frac{L_\nu + L_\gamma}{V_{nm}c_V^{nm} + V_{qm}c_V^{qm}} = -\frac{V_{nm}\varepsilon_\nu^{nm} + V_{qm}\varepsilon_\nu^{qm} + L_\gamma}{V_{nm}c_V^{nm} + V_{qm}c_V^{qm}} \tag{4.39}$$

which equates the heat lost ($\sim Ldt$) to the change in the heat energy of the star ($\sim -Vc_V dT$). We have all the ingredients needed to evaluate the right hand side of this equation in place, with the exception of the specific heat of nuclear matter and of unpaired quark matter. For a gas of several species of nointeracting fermions, the specific heat is given by

$$c_V = \frac{k_B^2 T}{3\hbar^3 c}\sum_i p_F^i \sqrt{m_i^2 c^2 + (p_F^i)^2}\ , \tag{4.40}$$

where the sum runs over all the species. In the case of noninteracting nuclear matter, the sum runs over $i = n, p, e$ and the Fermi momenta for neutral matter in weak equilibrium are given by [125]

$$\begin{aligned} p_F^n &= (340\ \text{MeV})\left(\frac{n}{n_0}\right)^{1/3} \\ p_F^p &= p_f^e = (60\ \text{MeV})\left(\frac{n}{n_0}\right)^{2/3}\ . \end{aligned} \tag{4.41}$$

We are taking non-interacting nuclear matter with density $n = 1.5n_0$ for the mantle of our "stars". In the case of neutral unpaired quark matter in weak equilibrium, the sum on i runs over the nine quarks and the Fermi momenta are independent of color and are given by [46]

$$\begin{aligned} p_F^d &= \mu + \frac{M_s^2}{12\mu} \\ p_F^u &= \mu - \frac{M_s^2}{6\mu} \\ p_F^s &= \mu - \frac{5M_s^2}{12\mu}\ , \end{aligned} \tag{4.42}$$

up to corrections of order M_s^4/μ^3. We are using matter with $\mu = 500$MeV in the core

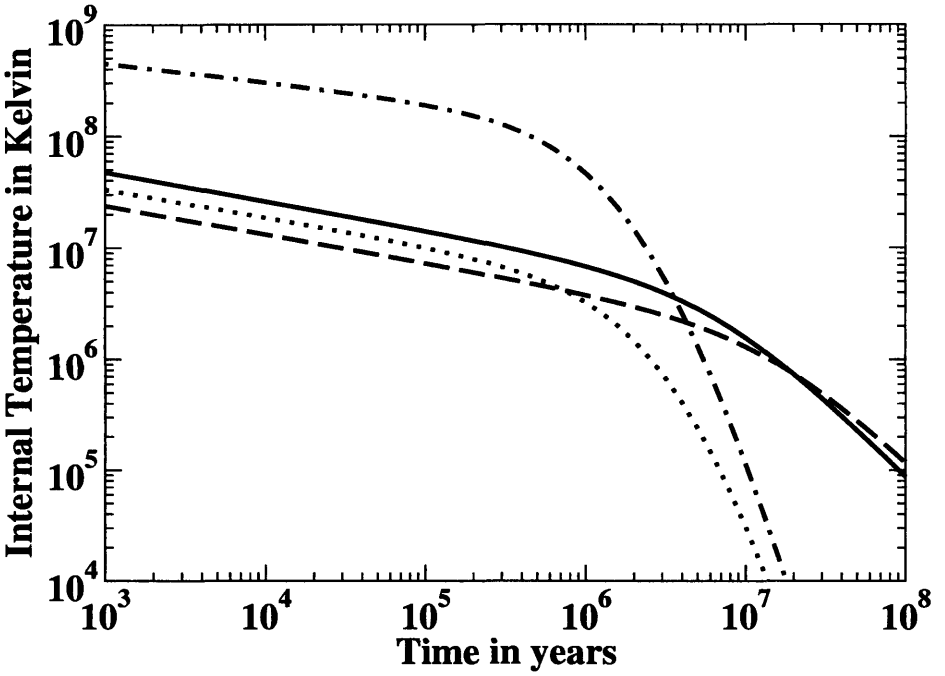

Figure 4-3: Solutions to the cooling equation (4.39) for 1.4 solar mass "toy stars" (described in the text) of four different compositions. The curves show internal temperature as a function of time. The dot-dashed curve is for a star with radius $R = 12$ km made entirely of nuclear matter with a density $1.5n_0$, with no quark matter core. The other three curves describe stars with radii $R = 10$ km that have quark matter cores with radii $R_{\rm core} = 5$ km. For all three curves, the quark matter has $\mu = 500$ MeV and $M_s^2/\mu = 100$ MeV, with densities $\simeq 9n_0$. For the dotted curve, the quark matter is noninteracting. For the solid (dashed) curve, it is in the gCFL phase with $\Delta_0 = 25$ MeV ($\Delta_0 = 40$ MeV).

of our "stars".

Fig. 4-3 shows the cooling curves obtained by solving (4.39) for the four toy stars we have described, plotted on a log-log plot. Each curve has an early time power law during the period when cooling by neutrino emission dominates, namely the first 10^5 or so years. At early times, $L_\gamma \ll L_\nu$ because $L_\gamma \sim R^2$ whereas $L_\nu \sim R^3$. Because L_ν drops much more rapidly than L_γ as T decreases, at late times L_γ dominates and a new power law is seen.

It is easy to see why power law solutions arise. In any temperature regime in which the numerator and the denominator of the right hand side of (4.39) are each

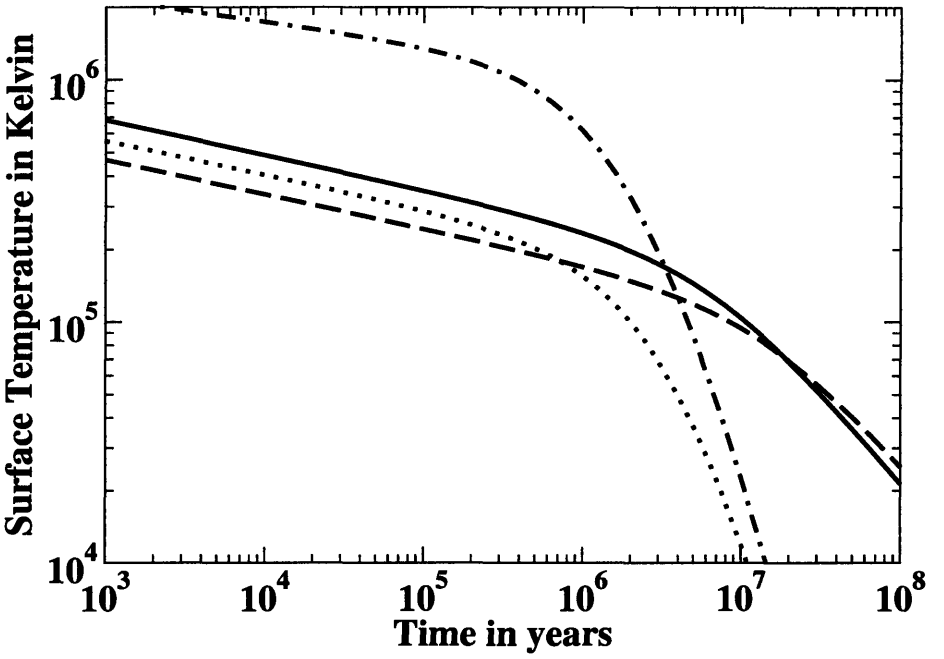

Figure 4-4: Same as Fig. 4-3, except that here we plot T_{surface}, related to the interior temperatures plotted in Fig. 4-3 by Eq. (4.36).

dominated by one of their component terms, the cooling equation takes the form

$$\frac{dT}{dt} = -aT^p \tag{4.43}$$

for some p and a. For example, for a star that is made entirely of nuclear matter, during the epoch when $L_\nu \gg L_\gamma$ we have $p = 7$, coming from $L_\nu \sim T^8$ and $c_V^{nm} \sim T$. For $p > 1$, (4.43) has a power-law solution

$$T = [a(p-1)\,t]^{-\frac{1}{p-1}} \ . \tag{4.44}$$

There are no arbitrary constants in this solution. We initialize the differential equation with some temperature T_0 at a time $t_0 = 1$ year, chosen because by that time the interior star can reasonably be treated as isothermal. The initial condition $T_0(t_0)$ does not appear in the power law solution: it only affects how the power law solution is reached, if $T_0(t_0)$ does not lie on it. Once the power law solution is reached, the form

of the solution to the differential equation is independent of the initial condition. We begin all our plots at $t = 1000$ years, by which time the solution is on the power law (4.44) for any reasonable choice of $T_0(t_0)$.

During the epoch when $L_\nu \gg L_\gamma$, a star made entirely of nuclear matter has $p = 7$ and $T \sim t^{-1/6}$. For the stars with unpaired quark matter, or gCFL quark matter, $p = 5$ and $T \sim t^{-1/4}$ during this epoch. This explains how similar the three quark matter core curves are during the first 10^5 years, and why all three stars with quark matter cores are colder than the nuclear matter star. Note that the gCFL quark matter has $L_\nu \sim T^{5.5}$ and $c_V \sim T^{0.5}$, both enhanced by $1/T^{0.5}$ relative to that of unpaired quark matter, and indeed relative to any phase of nuclear or quark matter in which direct Urca processes occur that has been considered previously. But, the effect of these enhancements cancel in the cooling curve during the epoch when $L_\nu \gg L_\gamma$. There are now a number of indications [140] that some neutron stars with ages of order 10^3 to 10^5 years (presumably the heavier ones, although this is certainly not demonstrated) are significantly colder than would be expected in the absence of direct Urca neutrino emission, whereas other (presumably less massive) stars have temperatures consistent with theoretical cooling curves calculated upon assuming nuclear matter composition. Were this to be confirmed, the discovery of direct Urca emission with $T \sim t^{-1/4}$, instead of the slower $T \sim t^{-1/6}$, could indicate the presence of any number of dense matter phases, including gCFL quark matter but also including nuclear matter leavened with either hyperons, kaons or pions.

At late times, when $L_\gamma \gg L_\nu$ all stars except those containing gCFL quark matter have $p = 2.2 - 1 = 1.2$ because $L_\gamma \sim T^{2.2}$ and $c_V \sim T$, and hence cool with $T \sim t^{-1/0.2} = t^{-5}$. This explains the rapidly dropping temperatures at late times for the stars without gCFL quark matter in Fig. 4-3. If the volume of gCFL matter is sufficient (more on this below) it dominates the heat capacity of the star, yielding $p = 2.2 - 0.5 = 1.7$ because $c_V \sim T^{0.5}$, and hence the star cools with $T \sim t^{-1/0.7} = t^{-1.4}$ at late times. The gCFL matter keeps the aging star warm by virtue of its large heat capacity.

We show the surface temperatures of our toy stars in Fig. 4-4. It is tempting to

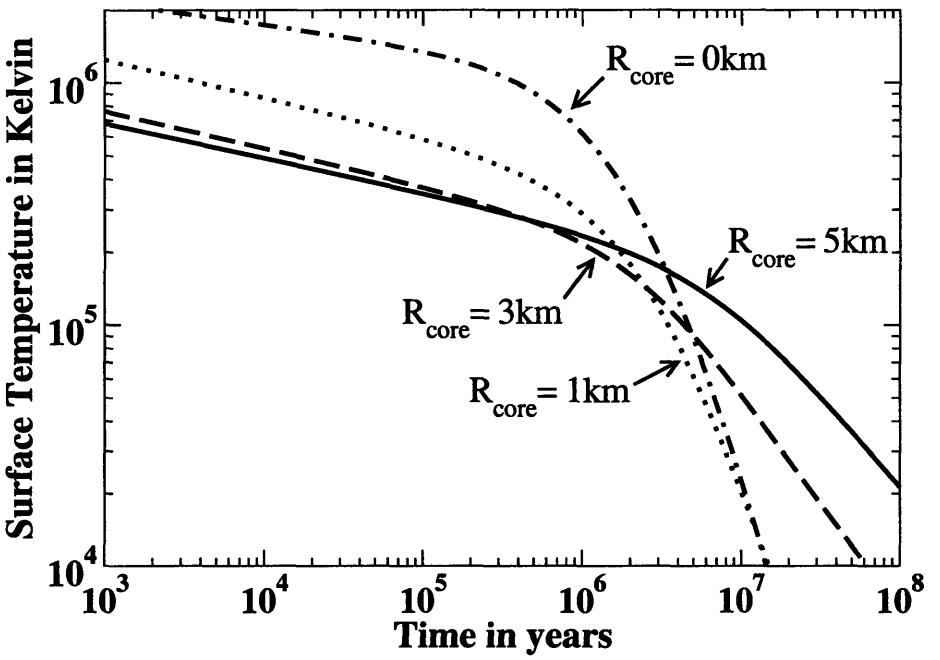

Figure 4-5: Cooling curves showing the surface temperature of stars with gCFL cores with $\Delta_0 = 25$ MeV for $R_{\text{core}} = 5$ km (solid; same as solid curve in Fig. 4-4), $R_{\text{core}} = 3$ km (dashed), $R_{\text{core}} = 1$ km (dotted), $R_{\text{core}} = 0$ km (dot-dashed; same as dot-dashed curve in Fig. 4-4).

put data obtained from the observation of real stars on this plot, but we resist the temptation given that our "stars" are not realistic. The qualitative impact of gCFL quark matter is, however, clear: stars which are old enough that they cool by photon emission stay much warmer if they contain a gCFL hot water bottle. In our Fig. 4-4, which should be taken as illustrative and not yet as a quantitative prediction, the effect is a full order of magnitude for 10^7-year old stars, and gets much larger for older stars, as the cooling curves of all stars except those containing gCFL quark matter drop rapidly.

In Fig. 4-5, we investigate the dependence of the cooling curves on the volume of gCFL quark matter present in the core of the star. We see that the "hot water bottle effect" is present for $R_{\text{core}} = 3$ km, but reduced in magnitude. For $R_{\text{core}} = 1$ km, no effect is visible: the effect does occur, but only at even lower temperatures than we have plotted. (Because its heat capacity is $c_V \sim T^{0.5}$, if any gCFL quark matter is present it will eventually dominate the heat capacity of the entire star, no matter how small its volume fraction. For $R_{\text{core}} = 1$ km, this occurs at temperatures below those

we have plotted.) Note that what we are referring to as $R_{\rm core} = 5$ km could equally well describe a star with a shell of gCFL quark matter extending between radii of 4.5 and 6 km.

4.5 Outlook

We hope that our results challenge observers to constrain the temperature of neutron stars that are 10 million years old or older. Prior to our work, all proposed cooling curves for these old stars drop so fast into unobservability that there has been little motivation to make the effort to obtain the best constraints possible on their temperatures. Given that we know of isolated neutron stars that are younger than a million years old and closer than 200 parsecs, it is reasonable to expect that there are 10^7-year old isolated neutron stars closer than 100 parsecs to earth. At first we were concerned that if such old nearby stars had temperatures of order 10^5 K, as Fig. 4-4 suggests will be the case if they contain gCFL hot water bottles, they should already have been detected. However, initial estimates suggest that they will in fact be quite a challenge to find, since the peak of a 10^5 K black body spectrum lies in the far ultraviolet, where the interstellar medium is opaque, and since they will be quite faint in the accessible UV and visible wavelengths [141]. Another option, perhaps easier than finding these stars without knowing where to look, is to study nearby old pulsars, already detected by their nonthermal emission, and to constrain their thermal emission hence putting an upper bound on their temperature. This has been done for PSR 0950+08, whose spin-down age is $10^{7.2}$ years, yielding the bound $T < 10^{5.2}$ K [142]. This limit is quite promising, as it is close to the curves in Fig. 4-4 describing the cooling of our toy star with a gCFL core. And, we are confident that we have not thought of the best way of looking for aging but still warm neutron stars. We are therefore hopeful that the opportunity to make an unambiguous discovery of the presence of quark matter within neutron stars or to rule out the presence of gCFL quark matter in the entire region of the QCD phase diagram sampled by neutron stars will stimulate observers to rise to the challenge.

Much theoretical work remains to be done. Interesting microphysical questions about the gCFL phase remain, and have been enumerated in Refs. [25, 26]. Phases with some features in common with the gCFL phase can be unstable with respect to inhomogeneous mixed phases [87], and although the gCFL phase is stable with respect to all straightforward mixed phase possibilities [25, 61], an exhaustive investigation has not yet been performed. Perhaps the most interesting open questions are the possibilities of K^0-condensation [80, 81] or gluon condensation [108] in the gCFL phase. Either could change our quantitative results for its c_V and ε_ν, but neither is likely to change their unusual T-dependence: $c_V \sim T^{0.5}$ and $\varepsilon_\nu \sim T^{5.5}$. (Neither K^0-mesons nor gluons [46, 135] would affect the $\tilde{Q}$-charge balance, which is responsible for the existence of the gapless quasiparticle with a quadratic dispersion relation in Fig. 4-1, whose consequence in turn is the unusual T-dependence of the gCFL c_V and ε_ν.) As far as theoretical astrophysical work, our results for c_V and ε_ν must be incorporated into calculations of cooling curves for stars with realistic atmospheres and density profiles before plots like those in Figs. 4-4 and 4-5 can be compared quantitatively to data. Nonetheless, our conclusion that gCFL quark matter within a neutron star will keep the star warm in its old age relies only on the unusual T-dependence of the gCFL specific heat, and is therefore expected to be robust.

Bibliography

[1] D. J. Gross and F. Wilczek, Phys. Rev. **D8**, 3633 (1973).

[2] H. D. Politzer, Phys. Rev. Lett. **30**, 1346 (1973).

[3] B. C. Barrois, Nucl. Phys. **B129**, 390 (1977).

[4] D. Bailin and A. Love, Phys. Rept. **107**, 325 (1984).

[5] M. G. Alford, K. Rajagopal, and F. Wilczek, Phys. Lett. **B422**, 247 (1998), `hep-ph/9711395`.

[6] R. Rapp, T. Schafer, E. V. Shuryak, and M. Velkovsky, Phys. Rev. Lett. **81**, 53 (1998), `hep-ph/9711396`.

[7] J. Bardeen, L. N. Cooper, and J. R. Schrieffer, Phys. Rev. **106**, 162 (1957).

[8] J. Pochodzalla, Prog. Part. Nucl. Phys. **39**, 443 (1997).

[9] M. Iwasaki and T. Iwado, Phys. Lett. **B350**, 163 (1995).

[10] M. G. Alford, K. Rajagopal, and F. Wilczek, Nucl. Phys. **B537**, 443 (1999), `hep-ph/9804403`.

[11] M. G. Alford, K. Rajagopal, and F. Wilczek, Nucl. Phys. **A638**, 515c (1998), `hep-ph/9802284`.

[12] D. T. Son, Phys. Rev. **D59**, 094019 (1999), `hep-ph/9812287`.

[13] R. D. Pisarski and D. H. Rischke, Phys. Rev. Lett. **83**, 37 (1999), `nucl-th/9811104`.

[14] R. Rapp, T. Schafer, E. V. Shuryak, and M. Velkovsky, Annals Phys. **280**, 35 (2000), hep-ph/9904353.

[15] T. Schafer and F. Wilczek, Phys. Rev. **D60**, 114033 (1999), hep-ph/9906512.

[16] J. Berges and K. Rajagopal, Nucl. Phys. **B538**, 215 (1999), hep-ph/9804233.

[17] M. A. Halasz, A. D. Jackson, R. E. Shrock, M. A. Stephanov, and J. J. M. Verbaarschot, Phys. Rev. **D58**, 096007 (1998), hep-ph/9804290.

[18] M. A. Stephanov, Phys. Rev. Lett. **76**, 4472 (1996), hep-lat/9604003.

[19] M. Oertel and M. Buballa (2002), hep-ph/0202098.

[20] Z. Fodor and S. D. Katz, JHEP **03**, 014 (2002), hep-lat/0106002.

[21] C. R. Allton et al., Phys. Rev. **D66**, 074507 (2002), hep-lat/0204010.

[22] P. de Forcrand and O. Philipsen, Nucl. Phys. **B642**, 290 (2002), hep-lat/0205016.

[23] M. G. Alford, J. Phys. **G30**, S441 (2004), nucl-th/0305097.

[24] M. Alford, C. Kouvaris, and K. Rajagopal, Phys. Rev. Lett. **92**, 222001 (2004), hep-ph/0311286.

[25] M. Alford, C. Kouvaris, and K. Rajagopal, Phys. Rev. **D71**, 054009 (2005), hep-ph/0406137.

[26] K. Fukushima, C. Kouvaris, and K. Rajagopal, Phys. Rev. **D71**, 034002 (2005), hep-ph/0408322.

[27] S. B. Ruster, I. A. Shovkovy, and D. H. Rischke, Nucl. Phys. **A743**, 127 (2004), hep-ph/0405170.

[28] D. J. Gross, R. D. Pisarski, and L. G. Yaffe, Rev. Mod. Phys. **53**, 43 (1981).

[29] L. D. McLerran, Rev. Mod. Phys. **58**, 1021 (1986).

[30] J. C. Collins and M. J. Perry, Phys. Rev. Lett. **34**, 1353 (1975).

[31] E. V. Shuryak, Z. Phys. **C38**, 141 (1988).

[32] F. Karsch, Nucl. Phys. **A698**, 199 (2002), hep-ph/0103314.

[33] E. Laermann, Nucl. Phys. Proc. Suppl. **63**, 114 (1998), hep-lat/9802030.

[34] K. Rajagopal and F. Wilczek (2000), hep-ph/0011333.

[35] M. G. Alford, Ann. Rev. Nucl. Part. Sci. **51**, 131 (2001), hep-ph/0102047.

[36] T. Schafer (2003), hep-ph/0304281.

[37] T. Schafer and F. Wilczek, Phys. Lett. **B450**, 325 (1999), hep-ph/9810509.

[38] M. G. Alford, J. Berges, and K. Rajagopal, Nucl. Phys. **B558**, 219 (1999), hep-ph/9903502.

[39] T. Schafer, Phys. Rev. Lett. **85**, 5531 (2000), nucl-th/0007021.

[40] D. B. Kaplan and S. Reddy, Phys. Rev. **D65**, 054042 (2002), hep-ph/0107265.

[41] P. F. Bedaque and T. Schafer, Nucl. Phys. **A697**, 802 (2002), hep-ph/0105150.

[42] J. Madsen, Phys. Rev. Lett. **85**, 10 (2000), astro-ph/9912418.

[43] C. Manuel, A. Dobado, and F. J. Llanes-Estrada (2004), hep-ph/0406058.

[44] N. Bogoliubov, N, Zh. Eksperim. i Teor. Fiz. **34**, 58 (1958), engl. transl.:Soviet Phys.–JETP 7,41 (1958).

[45] J. Valatin, Nuovo Cimento **7**, 843 (1958).

[46] M. Alford and K. Rajagopal, JHEP **06**, 031 (2002), hep-ph/0204001.

[47] D. T. Son and M. A. Stephanov, Phys. Rev. **D61**, 074012 (2000), hep-ph/9910491.

[48] R. D. Pisarski and D. H. Rischke, Phys. Rev. **D61**, 074017 (2000), nucl-th/9910056.

[49] R. D. Pisarski and D. H. Rischke, Phys. Rev. **D61**, 051501 (2000), nucl-th/9907041.

[50] T. Schafer, Phys. Rev. **D62**, 094007 (2000), hep-ph/0006034.

[51] A. Schmitt (2004), nucl-th/0412033.

[52] M. G. Alford, J. A. Bowers, J. M. Cheyne, and G. A. Cowan, Phys. Rev. **D67**, 054018 (2003), hep-ph/0210106.

[53] M. Buballa, J. Hosek, and M. Oertel, Phys. Rev. Lett. **90**, 182002 (2003), hep-ph/0204275.

[54] A. I. Larkin and Y. N. Ovchinnikov, Zh. Eksp. Teor Fiz. **47**, 1136 (1964), translation: Sov. Phys. JETP **20**, 762 (1965).

[55] P. Fulde and R. A. Ferrell, Phys. Rev. **135**, A550 (1964).

[56] M. G. Alford, J. A. Bowers, and K. Rajagopal, Phys. Rev. **D63**, 074016 (2001), hep-ph/0008208.

[57] J. A. Bowers, J. Kundu, K. Rajagopal, and E. Shuster, Phys. Rev. **D64**, 014024 (2001), hep-ph/0101067.

[58] A. K. Leibovich, K. Rajagopal, and E. Shuster, Phys. Rev. **D64**, 094005 (2001), hep-ph/0104073.

[59] R. Casalbuoni, R. Gatto, M. Mannarelli, and G. Nardulli, Phys. Lett. **B511**, 218 (2001), hep-ph/0101326.

[60] J. A. Bowers and K. Rajagopal, Phys. Rev. **D66**, 065002 (2002), hep-ph/0204079.

[61] M. Alford, C. Kouvaris, and K. Rajagopal (2004), hep-ph/0407257.

[62] M. Alford, P. Jotwani, C. Kouvaris, J. Kundu, and K. Rajagopal (2004), astro-ph/0411560.

[63] G. Nardulli, Riv. Nuovo Cim. **25N3**, 1 (2002), hep-ph/0202037.

[64] S. Reddy, Acta Phys. Polon. **B33**, 4101 (2002), nucl-th/0211045.

[65] I. Arsene et al. (BRAHMS) (2004), nucl-ex/0410020.

[66] K. Adcox et al. (PHENIX) (2004), nucl-ex/0410003.

[67] B. B. Back et al. (2004), nucl-ex/0410022.

[68] J. Adams et al. (STAR) (2005), nucl-ex/0501009.

[69] K. Iida and G. Baym, Phys. Rev. **D63**, 074018 (2001), hep-ph/0011229.

[70] T. Schafer and F. Wilczek, Phys. Rev. **D60**, 074014 (1999), hep-ph/9903503.

[71] M. Buballa and M. Oertel, Nucl. Phys. **A703**, 770 (2002), hep-ph/0109095.

[72] A. W. Steiner, S. Reddy, and M. Prakash, Phys. Rev. **D66**, 094007 (2002), hep-ph/0205201.

[73] F. Neumann, M. Buballa, and M. Oertel, Nucl. Phys. **A714**, 481 (2003), hep-ph/0210078.

[74] I. Shovkovy and M. Huang, Phys. Lett. **B564**, 205 (2003), hep-ph/0302142.

[75] M. Huang and I. Shovkovy, Nucl. Phys. **A729**, 835 (2003), hep-ph/0307273.

[76] P. Amore, M. C. Birse, J. A. McGovern, and N. R. Walet, Phys. Rev. **D65**, 074005 (2002), hep-ph/0110267.

[77] A. Gerhold and A. Rebhan, Phys. Rev. **D68**, 011502 (2003), hep-ph/0305108.

[78] K. Rajagopal and F. Wilczek, Phys. Rev. Lett. **86**, 3492 (2001), hep-ph/0012039.

[79] J. Kundu and K. Rajagopal, Phys. Rev. **D65**, 094022 (2002), hep-ph/0112206.

[80] M. M. Forbes (2004), hep-ph/0411001.

[81] A. Kryjevski and T. Schafer, Phys. Lett. **B606**, 52 (2005), hep-ph/0407329.

[82] W. V. Liu, F. Wilczek, and P. Zoller, Phys. Rev. **A70**, 033603 (2004), cond-mat/0404478.

[83] G. Sarma, Phys. Chem. Solid. **24**, 1029 (1963).

[84] M. G. Alford, J. Berges, and K. Rajagopal, Phys. Rev. Lett. **84**, 598 (2000), hep-ph/9908235.

[85] E. Gubankova, W. V. Liu, and F. Wilczek, Phys. Rev. Lett. **91**, 032001 (2003), hep-ph/0304016.

[86] W. V. Liu and F. Wilczek, Phys. Rev. Lett. **90**, 047002 (2003), cond-mat/0208052.

[87] P. F. Bedaque, H. Caldas, and G. Rupak, Phys. Rev. Lett. **91**, 247002 (2003), cond-mat/0306694.

[88] M. M. Forbes, E. Gubankova, W. V. Liu, and F. Wilczek, Phys. Rev. Lett. **94**, 017001 (2005), hep-ph/0405059.

[89] S. Reddy and G. Rupak (2004), nucl-th/0405054.

[90] M. G. Alford, K. Rajagopal, S. Reddy, and F. Wilczek, Phys. Rev. **D64**, 074017 (2001), hep-ph/0105009.

[91] R. Casalbuoni et al., Phys. Rev. **D70**, 054004 (2004), hep-ph/0404090.

[92] H. Muther and A. Sedrakian, Phys. Rev. **D67**, 085024 (2003), hep-ph/0212317.

[93] A. Schmitt, Q. Wang, and D. H. Rischke, Phys. Rev. **D66**, 114010 (2002), nucl-th/0209050.

[94] B. i. Halperin, T. C. Lubensky, and S.-k. Ma, Phys. Rev. Lett. **32**, 292 (1974).

[95] T. Matsuura, K. Iida, T. Hatsuda, and G. Baym, Phys. Rev. **D69**, 074012 (2004), hep-ph/0312042.

[96] I. Giannakis, D.-f. Hou, H.-c. Ren, and D. H. Rischke, Phys. Rev. Lett. **93**, 232301 (2004), hep-ph/0406031.

[97] K. Iida, T. Matsuura, M. Tachibana, and T. Hatsuda, Phys. Rev. Lett. **93**, 132001 (2004), hep-ph/0312363.

[98] K. Iida and G. Baym, Phys. Rev. **D66**, 014015 (2002), hep-ph/0204124.

[99] D. K. Hong, T. Lee, and D.-P. Min, Phys. Lett. **B477**, 137 (2000), hep-ph/9912531.

[100] C. Manuel and M. H. G. Tytgat, Phys. Lett. **B479**, 190 (2000), hep-ph/0001095.

[101] T. Schafer, Phys. Rev. **D65**, 094033 (2002), hep-ph/0201189.

[102] S. Reddy, M. Sadzikowski, and M. Tachibana, Nucl. Phys. **A714**, 337 (2003), nucl-th/0203011.

[103] J. M. Cornwall, R. Jackiw, and E. Tomboulis, Phys. Rev. D **10**, 2428 (1974).

[104] T. Schafer, Nucl. Phys. **B575**, 269 (2000), hep-ph/9909574.

[105] A. Sedrakian and U. Lombardo, Phys. Rev. Lett. **84**, 602 (2000), nucl-th/9907076.

[106] G. W. Carter and S. Reddy, Phys. Rev. **D62**, 103002 (2000), hep-ph/0005228.

[107] J. Kundu and S. Reddy, Phys. Rev. **C70**, 055803 (2004), nucl-th/0405055.

[108] M. Huang and I. A. Shovkovy, Phys. Rev. **D70**, 051501 (2004), hep-ph/0407049.

[109] R. Casalbuoni, R. Gatto, M. Mannarelli, G. Nardulli, and M. Ruggieri, Phys. Lett. **B605**, 362 (2005), hep-ph/0410401.

[110] M. Alford and Q.-h. Wang (2005), hep-ph/0501078.

[111] J. M. Lattimer and M. Prakash (2004), astro-ph/0405262.

[112] M. Alford, M. Braby, M. W. Paris, and S. Reddy (2004), nucl-th/0411016.

[113] M. Burgay, Nature **426**, 531 (2003).

[114] A. G. Lyne, Science **303**, 1153 (2004).

[115] M. Kramer et al. (2004), astro-ph/0405179.

[116] N. K. Glendenning, S. Pei, and F. Weber, Phys. Rev. Lett. **79**, 1603 (1997), astro-ph/9705235.

[117] N. K. Glendenning and F. Weber, Astrophys. J. **559**, L119 (2001), astro-ph/0003426.

[118] D. Chakrabarty (2004), astro-ph/0408004.

[119] P. Jaikumar, M. Prakash, and T. Schafer, Phys. Rev. **D66**, 063003 (2002), astro-ph/0203088.

[120] G. Baym and C. J. Pethick, Ann. Rev. Astron. Astrophys. **17**, 415 (1979).

[121] C. J. Pethick, Rev. Mod. Phys. **64**, 1133 (1992).

[122] J. G. Hirsch and D. Page, Prakash, M., in Nuclear and Particle Astrophysics, eds. **64**, 153 (Cambridge: Cambridge University Press,1998).

[123] D. G. Yakovlev, A. D. Kaminker, O. Y. Gnedin, and P. Haensel, Phys. Rept. **354** (2001).

[124] D. G. Yakovlev and C. J. Pethick, Ann. Rev. Astron. Astrophys. **42**, 169 (2004).

[125] S. L. Shapiro and S. A. Teukolsky, **Black Holes, White Dwarfs and Neutron Stars** (New York: Wiley, 1983).

[126] D. Page, M. Prakash, J. M. Lattimer, and A. Steiner, Phys. Rev. Lett. **85**, 2048 (2000), hep-ph/0005094.

[127] D. Page, J. M. Lattimer, M. Prakash, and A. W. Steiner (2004), astro-ph/0403657.

[128] D. G. Yakovlev et al. (2004), astro-ph/0409751.

[129] N. K. Glendenning, Astrophys. J. **293**, 470 (1985).

[130] J. N. Bahcall and R. A. Wolf, Phys. Rev. B **140**, 1452 (1965).

[131] D. B. Kaplan and A. E. Nelson, Phys. Lett. **B175**, 57 (1986).

[132] N. Iwamoto, Phys. Rev. Lett. **44**, 1637 (1980).

[133] N. Iwamoto, Annals Phys. **141**, 1 (1982).

[134] I. A. Shovkovy and P. J. Ellis, Phys. Rev. **C66**, 015802 (2002), hep-ph/0204132.

[135] A. Gerhold, Phys. Rev. **D71**, 014039 (2005), hep-ph/0411086.

[136] A. Ipp, A. Gerhold, and A. Rebhan, Phys. Rev. **D69**, 011901 (2004), hep-ph/0309019.

[137] T. Schafer and K. Schwenzer, Phys. Rev. **D70**, 114037 (2004), astro-ph/0410395.

[138] C. J. Gundmundsson, E. H. and Pethick and R. I. Epstein, Astrophys. J. **259**, L19 (1982).

[139] C. J. Gundmundsson, E. H. and Pethick and R. I. Epstein, Astrophys. J. **272**, 286 (1983).

[140] P. Slane, D. J. Helfand, and S. S. Murray (2002), astro-ph/0204151.

[141] D. L. Kaplan (2004), private communication.

[142] V. E. Zavlin and G. G. Pavlov, Astrophys. J. **616**, 452 (2004).